TRANSPORT PROPERTIES OF QUANTUM DOT MOLECULES AND ELECTRONIC STRUCTURE OF GRAPHENE QUANTUM DOT QUBITS

BY

CHIH-CHIEH CHEN

DISSERTATION

Submitted in partial fulfillment of the requirements
for the degree of Doctor of Philosophy in Physics
in the Graduate College of the
University of Illinois at Urbana-Champaign, 2015

Urbana, Illinois

Doctoral Committee:

Professor Michael Stone, Chair
Professor Yia-Chung Chang, Director of Research
Research Assistant Professor Lucas K. Wagner
Professor Alexey Bezryadin

Abstract

Coupled Quantum dots systems, or quantum dot molecules (QDMs), have been suggested as good candidates for nanoelectronics, spintronics, thermoelectrics, and quantum computing applications. The knowledge in the transport and electronic properties of QDMs is important in making progress toward practical devices. We use many-body equation of motion method for Hubbard-Anderson model to study non-equilibrium charge and thermal transport properties of QDMs connected to metallic electrodes in the Coulomb blockade regime. An exterior algebra method is developed to construct the equation of motion computationally, taking into account all correlation functions. The quantum interference (QI) effect of triangular quantum dot molecule (TQDM) resulting from electron coherent tunneling between quantum dots is revealed. The spectra of electrical conductance of TQDM with charge filling from one to six electrons clearly depict the many-body and topological effects. The calculated charge stability diagram for conductance and total occupation numbers match well with the recent experimental measurements. We also demonstrate that the destructive QI effect on the tunneling current of TQDM is robust with respect to temperature variation, making the single electron QI transistor feasible at higher temperatures. The thermoelectric properties of QDMs with high figure of merit are also illustrated.

Graphene nanoribbon quantum dot qubits have been proposed as promising candidates for quantum computing applications to overcome the spin-decoherence problems associated with GaAs quantum dot qubits. We perform theoretical studies of the electronic structures of graphene nanoribbon quantum dots by solving the Dirac equation with appropriate boundary conditions. We then evaluate the exchange splitting based on an unrestricted Hartree-Fock method for the Dirac particles. The electronic wave function and long-range exchange coupling due to the Klein tunneling and the Coulomb interaction are calculated for various gate configurations. It is found that the exchange coupling between qubits can be significantly enhanced by the Klein tunneling effect. The implications of our results for practical qubit construction and operation are discussed.

To friends and family.

Acknowledgments

I would like to express my deepest gratitude to my advisor Yia-Chung Chang, for his guidance, support, and encouragement. This work would not have been possible without his help.

I would like to thank John Stack and Lance Cooper. Without their support, it would be impossible for me to survive the graduate study.

I would like to thank the committee members Michael Stone, Lucas K. Wagner, Alexey Bezryadin, and prelim committee member David M Ceperley for their valuable comments and help.

I would like to thank our collaborator David Ming-Ting Kuo, for his essential contribution in our works.

I would like to thank following people for their kindly help and support in academy and life during these years: RCAS Sinica: Zhenhua Ning, Shiue-Yuan Shiau, Shu-Wei Chang, Tung-Han Hsieh, Ming-Yaw Ng, Minfeng Chen, Ching-Hang Chien, Fu-Chen Hsiao, Shang-Hsuan Wu, Mohammad Tariq Yaseen, Trong Huynh-Buu Ngo, Mai Khaleel, Yu-Da Chen, Ching-Tarng Liang, Ching-Hsiang Chan, Chih-Ya Tsai, Huai-Yi Xie, Chao-Cheng Kaun, Jingxuan Su, Jen-Mao Wang, Yi-Tsun Lin, Wei-Cen Lin, Kelly Tsai, Po-Chieh Huang, Min-Hui Liao, Chi-Ti Hsieh. UIUC Physics: Jason Chang, Yun Liu, Alexander Weiss, Po-Yao Chang, Wen-Pin Hsieh, Mayukh Khan, Gordon Baym, Rob Leigh, Juan I. Jottar, Xianhao Xin, Xiaoqian Chen, Ching-Kai Chiu, Shinsei Ryu, Anthony J Leggett, Nigel Goldenfeld, Benjamin Wandelt, Melodee Schweighart, Wendy Wimmer, En-Chuan Huang, Chang-Tse Hsieh, Xueda Wen, AtMa Chan, Philip C Chang, Mao-Chuang Yeh, Shiying Dong, Pei-Wen Tsai, Kuei Sun, Tyler Earnest, Yoshitsugu Oono, John Jeffrey A Damasco, Mohammad Edalati, Tyler R Naibert, Nam Nguyen Hoang, Philip Phillips, Eduardo Fradkin. UIUC Astronomy: Hsiang-Yi Karen Yang, Katherine I. Lee, Hotaka Shiokawa, Kuo-Chuan Pan, Paul Ricker, You-Hua Chu. UIUC CS: Kai-Wei Chang, PoLiang Wu. NTU Physics: Yu-Cheng Su, Ping-Chun Li, Jen-Chien Chang, Yuan-Fu Shao, Yen-Ting Hwang, Pei-Ming Ho. UIUC other: Felice Cheng, Jason Feng, Jim Wu, Peter Lu, Irene Lin, Li Qiu, Cindy Hsu, Eunice Chen. Other: Guifre Vidal, Susan Coppersmith, Yuting Hung, Weichao Peng, Yi-Hua Hung, Yu-chen Karen Chen-Wiegart.

I would like to thank my family, for their everlasting support.

Table of Contents

List of Tables

List of Figures

List of Abbreviations

EOM	Equation of Motion
h.c.	Hermitian Conjugate
QD	Quantum Dot
QDM	Quantum Dot Molecule

List of Symbols

$\mathbb{I}$	Identity matrix
$\mathbb{1}$	Identity map
σ_i	Pauli matrices
$\mathbb{C}$	Complex number
$\Im$	Taking imaginary part
$\bar{A}$	Taking the complex conjugate of A
$\beta(V)$	A basis for vector space V

Chapter 1

Introduction

Making smaller and more efficient electronic devices with novel applications is one of the main challenges in the contemporary technology. Quantum dot, [1, 2] a kind of nano-scale semiconductor structure which exhibits zero-dimensional quantum confinement effect, provides an possible solution. Coupled Quantum dots systems, [3, 4] or quantum dot molecules (QDMs), have been suggested as good candidates for various applications in nanoelectronics, [5, 6] spintronics, [4, 7] thermoelectrics, [8, 9] and quantum computation. [4, 10] The knowledge in the transport and electronic properties of QDMs is important in making progress toward practical devices. We use many-body equation of motion method for Hubbard-Anderson model to study non-equilibrium charge and thermal transport properties of QDMs connected to metallic electrodes in the Coulomb blockade regime. [11, 12] An exterior algebra method is developed to construct the equation of motion computationally, taking into account all correlation functions. The quantum interference (QI) effect of triangular quantum dot molecule (TQDM) resulting from electron coherent tunneling between quantum dots is revealed. The spectra of electrical conductance of TQDM with charge filling from one to six electrons clearly depict the many-body and topological effects. The calculated charge stability diagram for conductance and total occupation numbers match well with the recent experimental measurements. We also demonstrate that the destructive QI effect on the tunneling current of TQDM is robust with respect to temperature variation, making the single electron QI transistor feasible at higher temperatures. The thermoelectric properties of QDMs with high figure of merit are also illustrated.

To overcome the spin-decoherence problems associated with GaAs quantum dot qubits, Graphene nanoribbon quantum dot qubits have been proposed as promising candidates for quantum computing applications.[13] We perform theoretical studies of the electronic structures of graphene nanoribbon quantum dots by solving the Dirac equation with appropriate boundary conditions.[14] We then evaluate the exchange splitting based on an unrestricted Hartree-Fock method for the Dirac particles. The electronic wave function and long-range exchange coupling due to the Klein tunneling and the Coulomb interaction are calculated for various gate configurations. It is found that the exchange coupling between qubits can be significantly enhanced by the Klein tunneling effect. The implications of our results for practical qubit construction and operation are discussed.

1.1 Charge and energy transport through quantum dot molecules

Molecule transistors (MTs) provide a brightened scenario of nanoelectronics with low power consumption.[15–17] To date, the implementation of MTs remains challenging, and a good theoretical understanding of their characteristics is essential for advancing the technology. The current-voltage (I-V) curves of MTs are typically predicted by calculations based on the density functional theory (DFT).[17] However, the DFT approach cannot fully capture the correlation effect in the transport behavior of MTs in the Coulomb-blockade regime. A theoretical framework to treat adequately the many-body problem of a molecular junction remains elusive due to the complicated quantum nature of such devices. Experimental studies of a artificial molecule with simplified structures are important not only for the advances of novel nanoelectronics, but also for providing a testing ground of many body theory. For example, the coherent tunneling between serially coupled double quantum dots (DQDs) was studied and demonstrated for application as a spin filter in the Pauli spin blockade regime.[4] Recent experimental studies have been extended to serially coupled triple quantum dots (SCTQDs) for studying the effect of long distance coherent tunneling (LDCT) in electron transport.[18–20] Triangular quantum dot molecule (TQDM) provides the simplest topological structure with quantum interference (QI) phenomena.[21–23] The QI effect in the coherent tunneling process of TQDM junctions has been studied experimentally.[24, 25]

It was suggested that the tunneling currents through benzene molecules can also show a destructive QI behavior.[17, 22] The tunneling current through a single benzene molecule was theoretically studied by DFT.[22] However, the influence of the strong correlation on the QI effect remains unclear due to the limitation of DFT. Many theoretical works have pointed out that electron Coulomb interactions have strong influence not only on the electronic structures of TQDM,[26, 27] but also on the probability weights of electron transport paths.[28–31] When both the intradot and interdot Coulomb interactions in a TQDM are included, the transport behavior involving multiple electrons becomes quite complicate. The setup for the TQDM junction of interest is depicted in Fig.2.1. Here we present a full many-body solution to the tunneling current of TQDM, which can well illustrate the Pauli spin blockade effect of DQDs,[4] LDCT of SCTQDs[18–20] and QI of TQDMs[24] for both equilibrium and nonequilibrium cases. Thus, our theoretical work can provide useful guidelines for the design of future molecular electronics and the realization of large scale quantum registers built by multiple QDs.[32]

We adopt the equation of motion method (EOM), which is a powerful tool for studying electron transport, taking into account electron Coulomb interactions.[28–31] This method has been applied to reveal the transport behaviors of a single QD with multiple energy levels[29] and DQDs.[30, 31] For a TQDM with one level per QD, there are 64 configurations for electrons to transport between electrodes.[33] Previous theoretical works have ignored the high-order Green functions resulting from electron Coulomb interactions to simplify the calculation.[33] To have a full

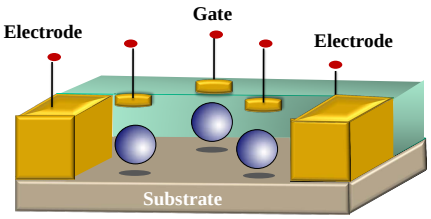

Figure 1.1: Illustration of the TQDM junction system of interest. Figure borrowed from Chen *et al.* [11].

solution becomes crucial for depicting the charge transport involving a few electrons. We solve the EOM of Green functions up to six electrons, taking into account all correlations caused by electron Coulomb interactions and electron hopping between TQDM. This involves solving 4752 Green's functions and 923 correlation functions self-consistently. We also apply this theory to study thermoelectric effect of double QD and TQDM, leading to the possibility of high thermoelectric figure of merit devices.[12]

1.2 Graphene nanoribbon quantum dot qubits

Despite rapid progress in computer technology, there are still computational problems that are difficult to solve for any known algorithm that uses modern computers. However, the theory that describes physics on atomic length-scales, quantum mechanics, suggests a new way to attack hard computational problems in a more efficient way. A computer using operations involving quantum states is known as a quantum computer. [34] A number of algorithms proposed for quantum computers are expected to solve many classically hard problems. [35] For example, Shor's algorithm [36] can efficiently solve the prime factorization problem, which is difficult to solve even with state-of-the-art classical algorithms and computers. The quantum analog of the bit – the fundamental information storage unit in classical computers – is called the qubit. Many physical realizations of qubits for quantum computers are being developed, including semiconductor, superconductor, nuclear, and optical qubit systems. The mature semiconductor manufacturing industry today offers several advantages in the construction of semiconductor qubits. In particular, the nanoscale semiconductor structure known as the quantum dot has been proposed as a possible semiconductor realization of the qubit. [37]

Semiconductor qubits constructed from GaAs quantum dots have limited usefulness, because quantum information stored in GaAs devices can be lost due to spin-decoherence. Sources of spin-decoherence in GaAs include the spin-

orbit, hyperfine, and electron-phonon interactions. Graphene, [38] a 2-dimensional lattice structure formed by carbon, is a promising material for avoiding spin-decoherence. [13] Graphene has not only weak spin-orbit coupling, but also a negligible hyperfine interaction, since carbon-12 has zero nuclear spin. These advantages of graphene have driven researchers towards developing a graphene-based qubit. One proposed model for the graphene qubit is the graphene nanoribbon quantum dot, [13, 39] which has been experimentally realized by several groups. [40–44]

Previous theoretical efforts to model graphene nanoribbon quantum dots [13] offer only estimates of the electron-electron interaction and many-particle effects in graphene. Consequently, it is not clear if the predicted long-range Heisenberg exchange coupling between the dots—which is necessary for qubit operations in universal quantum computing—can be achieved in practice. Nor are the effects of gate voltage changes on the electronic structure and the exchange coupling in the multi-electron regime well understood. Realistic models of graphene qubit operation require a better understanding of these effects. [37] To understand how the graphene nanoribbon quantum dot qubit functions in real applications, we study a more complete model of the graphene qubit using a numerical approach. An unrestricted Hartree-Fock method that employs a generalized-valence-bond wave function to calculate the electronic configuration of a quantum dot qubit was previously proposed. [45] In this work, we employ this numerical scheme and the Dirac equation to provide a realistic simulation of a graphene nanoribbon quantum dot qubit.

Chapter 2

Charge and energy transport through quantum dot molecules

2.1 Green's function for single impurity Anderson model

A single-level model Hamiltonian for a single isolated quantum dot[46] is

$$H_{QD} = \sum_{\sigma=\uparrow,\downarrow} E_\sigma n_\sigma + U n_\uparrow n_\downarrow \tag{2.1}$$

where $\sigma = \uparrow, \downarrow$ denotes the electron spin degree of freedom, E_σ denotes the on-site energy, $d_\sigma^\dagger$ and d_σ are the creation and annihilation operators for electrons in spin σ state, U denotes the on-site Coulomb integral, $n_\sigma = d_\sigma^\dagger d_\sigma$. For this Hamiltonian, the one-site one-particle retarded Green's function in the frequency domain can be defined and analytically solved to be

$$G_{\sigma\sigma}^{r(1)}(\epsilon) \equiv -i \int dt e^{i\epsilon t} \theta(t) \langle \{ d_\sigma(t), d_\sigma^\dagger \} \rangle \tag{2.2}$$

$$= \frac{1 - \langle n_{-\sigma} \rangle}{\epsilon - E_\sigma + i\delta} + \frac{\langle n_{-\sigma} \rangle}{\epsilon - E_\sigma - U + i\delta}, \tag{2.3}$$

where θ is the step function, δ is an infinitesimal regulator. For a quantum dot coupled to two metallic electrodes, the model Hamiltonian is the single impurity Anderson model[47]

$$H = H_{QD} + H_T + H_{electrode} \tag{2.4}$$

$$H_{QD} = \sum_{\sigma=\uparrow,\downarrow} E_\sigma n_\sigma + U n_\uparrow n_\downarrow \tag{2.5}$$

$$H_T = \sum_{\substack{\alpha=L,R,\sigma=\uparrow,\downarrow \\ k\in(-\infty,\infty)}} V_{\alpha,k} d_\sigma^\dagger c_{\alpha,k,\sigma} + h.c. \tag{2.6}$$

$$H_{electrode} = \sum_{\substack{\alpha=L,R,\sigma=\uparrow,\downarrow \\ k\in(-\infty,\infty)}} \epsilon_k c_{\alpha,k,\sigma}^\dagger c_{\alpha,k,\sigma}, \tag{2.7}$$

where $c^{\dagger}_{\alpha,k,\sigma}$ and $c_{\alpha,k,\sigma}$ are the creation and annihilation operators for electrons in electrodes α with momentum k and spin σ.

This model is not exactly solvable. The question we are trying to ask is: What is the Green's function in the Coulomb blockade regime? Three different tunneling physics occur in different orders of perturbation theory:

- Sequential tunneling (2nd order).
- Cotunneling (4th order).
- Kondo physics (up to infinite order, needs renormalization group[48–51] treatment).

We are looking for a solution only including the lowest order sequential tunneling. Three solutions are summarized in Pals and MacKinnon [52]:

	$G^{r(1)}_{\sigma\sigma}(\epsilon) =$
Equilibrium	$\frac{1-\langle n_{-\sigma}\rangle}{\epsilon-E_\sigma+i\delta}+\frac{\langle n_{-\sigma}\rangle}{\epsilon-E_\sigma-U+i\delta}$
Scheme 1 Hartree approximation(Lacroix, 1981[53])	$\frac{\epsilon-E_\sigma-U(1-\langle n_{-\sigma}\rangle)}{(\epsilon-E_\sigma)(\epsilon-E_\sigma-U)-\Sigma^r_{0\sigma}(\epsilon-E_\sigma-U(1-\langle n_{-\sigma}\rangle))}$
Scheme 2 (Pals MacKinnon, 1996[52])	$\frac{1-\langle n_{-\sigma}\rangle}{\epsilon-E_\sigma-\Sigma^r_{0\sigma}}+\frac{\langle n_{-\sigma}\rangle}{\epsilon-E_\sigma-U-\Sigma^r_{0\sigma}}$
Scheme 3 (Meir Wingreen Lee, 1991[54])	$\frac{1-\langle n_{-\sigma}\rangle}{\epsilon-E_\sigma-\Sigma^r_{0\sigma}+\frac{U\Sigma^r_{1\sigma}}{\epsilon-E_\sigma-U-\Sigma^r_{0\sigma}-\Sigma^r_{3\sigma}}}+\frac{\langle n_{-\sigma}\rangle}{\epsilon-E_\sigma-U-\Sigma^r_{0\sigma}-\frac{U\Sigma^r_{2\sigma}}{\epsilon-E_\sigma-\Sigma^r_{0\sigma}-\Sigma^r_{3\sigma}}}$

According to the comparative study of Pals and MacKinnon [52], scheme 1 gives unphysical result for Zeeman-splitted single QD. Scheme 2 and 3 produces similar results, but scheme 3 is numerically harder to handle. However, it is known that scheme 3 produces Kondo peaks qualitatively, while scheme 2 has no Kondo physics at all. There are many different EOM approaches which describe the tunneling physics to different extend.[53–59] For example, the approaches in Lacroix [53], Meir *et al.* [55], Shiau *et al.* [57], Xin and Zhou [59] all give qualitative Kondo physics. A discussion of the validity of EOM and how EOM fails in the Kondo regime can be found in Kashcheyevs *et al.* [56]. Also notice that the non-crossing approximation[60] can also describe Kondo physics.

In this work, we are interested in the case where the electrons are strongly correlated within QD but weakly coupled to the electrode. The symmetries in QD system can be broken by gate voltage in general. We look for multiple QD extension of Pals and MacKinnon [52] scheme 2 solution. While the tunneling physics is treated by Pals and MacKinnon [52] scheme 2, the correlation within QDMs degrees of freedom is treated exactly. The two QD extension of Pals and MacKinnon [52] scheme 2 is the Bułka-Kostyrko ansatz[30]. It has been applied to multiple level Anderson model without hopping (Kuo and Chang [29]), double QD with hopping (Bułka and Kostyrko [30], Kuo *et al.* [31]), and triple QD with hopping (Chen *et al.* [11, 12]).

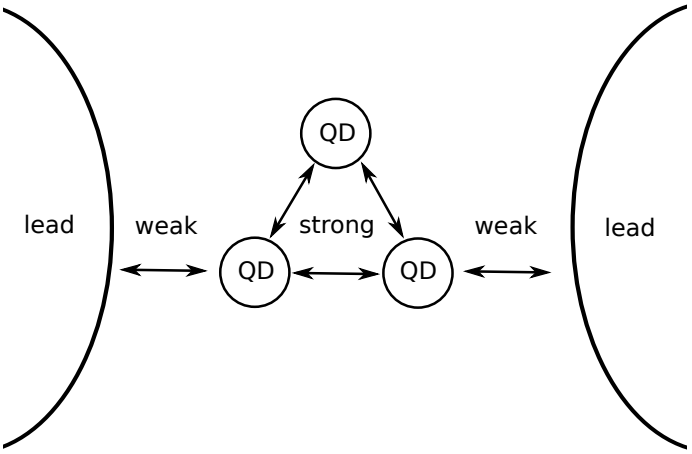

Figure 2.1: Illustration of the QDMs junction of interest. The electrons within the QDs are strongly correlated, while the interaction between QDs and electrodes is weak. The symmeties of QD Hamiltonian can be broken by detuning in general.

2.2 Equation of motion for couple quantum dots

In this section, we describe the equation of motion (EOM) method for the non-equilibrium Green's function[46]. The formalism provides a tool to calculate the transport properties of strongly-correlated multiple quantum dots (MQD) system in the Coulomb blockade regime. [29–31, 52, 58, 61] The electron degrees of freedom within the MQD is treated exactly by the full many-body EOM, while the tunnelling effect to the metallic electrodes is included as the electron self-energy.

2.2.1 Equation of motion

We consider an N quantum dot (QD) system (one level for each QD) with electron hopping and Coulomb interactions. This MQD system is weakly coupled to some metallic electrodes. The model Hamiltonian is

$$H = H_{QD} + H_T + H_{electrodes} \tag{2.8}$$

$$H_{QD} = \sum_{ij=1}^{N} t_{ij} d_i^\dagger d_j + \sum_{i<j=1}^{N} U_{ij} n_i n_j \tag{2.9}$$

$$H_T = \sum_{ik} (V_{ki} c_k^\dagger d_i + h.c.) \tag{2.10}$$

$$H_{electrodes} = \sum_{k} \epsilon_k c_k^\dagger c_k \ , \tag{2.11}$$

where t_{ij} denotes the electron hopping, and U_{ij} denotes the electron Coulomb interaction (which is real symmetric with zero diagonal elements), $d_j^\dagger$ and d_j are the creation and the annihilation operators for the electron at QD j, and

$n_j = d_j^\dagger d_j$. The indices i, j labels all the discrete quantum numbers for the electrons in the MQD, including the spin. $c_k^\dagger$ and c_k are the creation and the annihilation operators for the electrons in the electrodes. The variable k labels all the quantum numbers for the electrons in the reservoirs including the momentum, the spin and the label for the reservoirs. We can derive the equation of motion which describes the full many-body degrees of freedom of electrons within the quantum dots. The reservoirs are taken into account by including the self-energy term. This approach is valid above the Kondo temperature.[29–31, 52, 58, 61] For the contour-ordered double-time n-particle Green's function[46, 62]

$$G^{(n)}_{i_1 i_2 \ldots i_{2n}}(t,t') = -i\langle T[d^\dagger_{i_1}(t)\ldots d^\dagger_{i_{n-1}}(t) d_{i_n}(t)\ldots d_{i_{2n-1}}(t) d^\dagger_{i_{2n}}(t')]\rangle, \tag{2.12}$$

the EOM is

$$\begin{aligned} i\partial_t G^{(n)}_{i_1\ldots i_{2n}}(t,t') = \quad & \delta(t-t')\sum_{\mu=n}^{2n-1}(-1)^{(\mu+1)}\delta_{i_\mu,i_{2n}}\langle d^\dagger_{i_1}\ldots d^\dagger_{i_{n-1}} d_{i_n}\ldots d_{i_{\mu-1}} d_{i_{\mu+1}}\ldots d_{i_{2n-1}}\rangle \\ & +(-\sum_{\mu=1}^{n-1}\sum_j \bar{t}_{i_\mu j} + \sum_{\mu=n}^{2n-1}\sum_j t_{i_\mu j}) G^{(n)}_{i_1\ldots i_{\mu-1} j i_{\mu+1}\ldots i_{2n-1} i_{2n}}(t,t') \\ & +(-\sum_{\mu=1}^{n-1}\sum_{\nu=\mu+1}^{n-1} U_{i_\mu i_\nu} + \sum_{\mu=n}^{2n-1}\sum_{\nu=n}^{\mu-1} U_{i_\mu i_\nu}) G^{(n)}_{i_1\ldots i_{2n}}(t,t') \\ & +(-\sum_{\mu=1}^{n-1} + \sum_{\mu=n}^{2n-1})\sum_j U_{i_\mu j} G^{(n+1)}_{i_1\ldots i_{n-1} j j i_n\ldots i_{2n-1} i_{2n}}(t,t') \\ & +\int d\tau[-\sum_{\substack{\mu=1\\ i_\mu\in I'}}^{n-1}\bar{\Sigma}_{i_\mu i_\mu}(t,\tau) + \sum_{\substack{\mu=n\\ i_\mu\in I}}^{2n-1}\Sigma_{i_\mu i_\mu}(t,\tau)] G^{(n)}_{i_1\ldots i_{2n}}(\tau,t'), \end{aligned} \tag{2.13}$$

where the symbol "$\bar{A}$" denotes "taking the complex conjugate" of A. For $n = 1$ the contact term should be defined as $\delta_{i_1 i_2}\delta(t-t')$. I and I' are some extra selection rules we may impose according to the phenomenology. The detail of these selection rules is discussed in the last section. The hierarchy of equations terminates at $n = N$ since $G^{(N+1)} = 0$. Taking the Fourier transform and analytic continuation[46] leads to a set of linear equations for the

retarded and the lessor Green's functions $G^{r(n)}_{i_1 i_2 \ldots i_{2n}}$ and $G^{<(n)}_{i_1 i_2 \ldots i_{2n}}$ in the frequency domain:

$$\begin{aligned}
\epsilon G^{r(n)}_{i_1 \ldots i_{2n}}(\epsilon) &= \sum_{\mu=n}^{2n-1} (-1)^{(\mu+1)} \delta_{i_\mu, i_{2n}} \langle d^\dagger_{i_1} \ldots d^\dagger_{i_{n-1}} d_{i_n} \ldots d_{i_{\mu-1}} d_{i_{\mu+1}} \ldots d_{i_{2n-1}} \rangle \\
&+ (- \sum_{\mu=1}^{n-1} \sum_j \bar{t}_{i_\mu j} + \sum_{\mu=n}^{2n-1} \sum_j t_{i_\mu j}) G^{r(n)}_{i_1 \ldots i_{\mu-1} j i_{\mu+1} \ldots i_{2n-1} i_{2n}}(\epsilon) \\
&+ (- \sum_{\mu=1}^{n-1} \sum_{\nu=\mu+1}^{n-1} U_{i_\mu i_\nu} + \sum_{\mu=n}^{2n-1} \sum_{\nu=n}^{\mu-1} U_{i_\mu i_\nu}) G^{r(n)}_{i_1 \ldots i_{2n}}(\epsilon) \\
&+ (- \sum_{\mu=1}^{n-1} + \sum_{\mu=n}^{2n-1}) \sum_j U_{i_\mu j} G^{r(n+1)}_{i_1 \ldots i_{n-1} j j i_n \ldots i_{2n-1} i_{2n}}(\epsilon) \\
&+ [- \sum_{\substack{\mu=1 \\ i_\mu \in I'}}^{n-1} \bar{\Sigma}^r_{i_\mu i_\mu}(\epsilon) + \sum_{\substack{\mu=n \\ i_\mu \in I}}^{2n-1} \Sigma^r_{i_\mu i_\mu}(\epsilon)] G^{r(n)}_{i_1 \ldots i_{2n}}(\epsilon),
\end{aligned}$$

$$\begin{aligned}
\epsilon G^{<(n)}_{i_1 \ldots i_{2n}}(\epsilon) &= (- \sum_{\mu=1}^{n-1} \sum_j \bar{t}_{i_\mu j} + \sum_{\mu=n}^{2n-1} \sum_j t_{i_\mu j}) G^{<(n)}_{i_1 \ldots i_{\mu-1} j i_{\mu+1} \ldots i_{2n-1} i_{2n}}(\epsilon) \\
&+ (- \sum_{\mu=1}^{n-1} \sum_{\nu=\mu+1}^{n-1} U_{i_\mu i_\nu} + \sum_{\mu=n}^{2n-1} \sum_{\nu=n}^{\mu-1} U_{i_\mu i_\nu}) G^{<(n)}_{i_1 \ldots i_{2n}}(\epsilon) \\
&+ (- \sum_{\mu=1}^{n-1} + \sum_{\mu=n}^{2n-1}) \sum_j U_{i_\mu j} G^{<(n+1)}_{i_1 \ldots i_{n-1} j j i_n \ldots i_{2n-1} i_{2n}}(\epsilon) \\
&+ (- \sum_{\substack{\mu=1 \\ i_\mu \in I'}}^{n-1} \bar{\Sigma}^r_{i_\mu i_\mu}(\epsilon) + \sum_{\substack{\mu=n \\ i_\mu \in I}}^{2n-1} \Sigma^r_{i_\mu i_\mu}(\epsilon)) G^{<(n)}_{i_1 \ldots i_{2n}}(\epsilon) \\
&+ [- \sum_{\substack{\mu=1 \\ i_\mu \in I'}}^{n-1} \bar{\Sigma}^<_{i_\mu i_\mu}(\epsilon) + \sum_{\substack{\mu=n \\ i_\mu \in I}}^{2n-1} \Sigma^<_{i_\mu i_\mu}(\epsilon)] G^{(n)a}_{i_1 \ldots i_{2n}}(\epsilon).
\end{aligned}$$

These equations can be viewed as a generalization of the Dyson equation and the Keldysh equation[46] to the n-particle Green's function. They can be solved by any standard linear solver. In equilibrium, it can be shown that the equation for the lessor Green's function reduces to the fluctuation-dissipation theorem

$$G^{<(n)}_{i_1 \ldots i_{2n}}(\epsilon) = -2if(\epsilon) \Im[G^{r(n)}_{i_1 \ldots i_{2n}}(\epsilon)] \,, \tag{2.14}$$

where $\Im$ stands for taking the imaginary part. The self-consistent calculation is closed by the integral relation

$$\langle d^\dagger_{i_1} \ldots d^\dagger_{i_n} d_{i_{n+1}} \ldots d_{i_{2n}} \rangle = \int \frac{d\epsilon}{2\pi i} G^{<(n)}_{i_2 \ldots i_{2n} i_1}(\epsilon) \,. \tag{2.15}$$

We are interested in the solution at the wide-band limit,[63]

$$\Sigma^r_{jj}(\epsilon) = -i\sum_\alpha \frac{\Gamma^\alpha_j}{2} \tag{2.16}$$

$$\Sigma^<_{jj}(\epsilon) = i\sum_\alpha \Gamma^\alpha_j f_\alpha(\epsilon)\ , \tag{2.17}$$

where α is the label for the reservoirs, Γ^α_j is the tunnelling rate between the reservoir α and the level j, and f_α is the Fermi function for the reservoir α. After solving for the Green's function, we can obtain the non-equilibrium steady-state current flowing from the reservoir α into the QD system by the Meir-Wingreen formula [28]

$$J_\alpha = \frac{ie}{h}\int d\epsilon \sum_j \Gamma^\alpha_j [G^{<(1)}_{jj}(\epsilon) + f_\alpha(\epsilon)(G^{r(1)}_{jj}(\epsilon) - G^{(1)a}_{jj}(\epsilon))]. \tag{2.18}$$

2.2.2 Self-energy term

The non-equilibrium tunnelling is treated by the Bułka-Kostyrko ansatz.[30] The recipe provides a good lowest order approximation to the transport physics in the Coulomb blockade regime. [29–31, 52, 58, 61] In this section, we give a derivation[64–66] which makes the Bułka-Kostyrko ansatz plausible. The higher order effect may be included by employing more complicated self-energy term. [53, 54, 56]

For the Hamiltonian of Eq. (2.8), the EOM is $i\partial_t G^{(n)}_{i_1\ldots i_{2n}}$ =(equilibrium term) + (self-energy term), where the equilibrium term is generated by H_{QD} and the self-energy term is generated by $H_T + H_{electrodes}$. The equilibrium term can be derived straight forwardly (see Appendix A for detail), so we focus on the self-energy term here. The derivatives of the operators of the electrons in the reservoirs are

$$i\partial_t c_k(t) = \epsilon_k c_k(t) + \sum_j V_{kj} d_j(t) \tag{2.19}$$

$$i\partial_t c^\dagger_k(t) = -\epsilon_k c^\dagger_k(t) + \sum_j -\bar{V}_{kj} d^\dagger_j(t)\ . \tag{2.20}$$

Integrate these equations to get

$$c_k(t) = \sum_j V_{kj}\int d\tau g_k(t,\tau) d_j(\tau) \tag{2.21}$$

$$c^\dagger_k(t) = \sum_j \bar{V}_{kj}\int d\tau \bar{g}_k(t,\tau) d^\dagger_j(\tau)\ , \tag{2.22}$$

where $g_k(t,t') = (i\partial_t - \epsilon_k)^{-1}$ and $\bar{g}_k(t,t') = (-i\partial_t - \epsilon_k)^{-1}$.

Consider the derivatives of the operators of the electrons in the QDs, the contribution of $H_T + H_{electrodes}$ is

$$i\partial_t d_j(t) = \sum_k \bar{V}_{kj} c_k(t) \tag{2.23}$$

$$i\partial_t d_j^\dagger(t) = \sum_k -V_{kj} c_k^\dagger(t) \; . \tag{2.24}$$

Now we can eliminate the electrodes degrees of freedom,

$$i\partial_t d_j(t) = \int d\tau \sum_{kl} \bar{V}_{kj} V_{kl} g_k(t,\tau) d_l(\tau) \tag{2.25}$$

$$= \int d\tau \sum_l \Sigma_{jl}(t,\tau) d_l(\tau) \tag{2.26}$$

$$i\partial_t d_j^\dagger(t) = -\int d\tau \sum_{kj} V_{kj} \bar{V}_{kl} \bar{g}_k(t,\tau) d_l^\dagger(\tau) \tag{2.27}$$

$$= -\int d\tau \sum_l \bar{\Sigma}_{jl}(t,\tau) d_l^\dagger(\tau) \; . \tag{2.28}$$

If we take the Markov approximation[66] and consider only the diagonal tunnelling matrix elements, then we have

$$i\partial_t (d_{i_1}^\dagger ... d_{i_{n-1}}^\dagger d_{i_n} ... d_{i_{2n-1}}(t)) = \int d\tau \{ [-\sum_{\mu=1}^{n-1} \bar{\Sigma}_{i_\mu i_\mu}(t,\tau) + \sum_{\mu=n}^{2n-1} \Sigma_{i_\mu i_\mu}(t,\tau)] [d_{i_1}^\dagger ... d_{i_{n-1}}^\dagger d_{i_n} ... d_{i_{2n-1}}(\tau)] \}, \tag{2.29}$$

and hence we get the final result,

$$\text{self-energy term} = \int d\tau [-\sum_{\mu=1}^{n-1} \bar{\Sigma}_{i_\mu i_\mu}(t,\tau) + \sum_{\mu=n}^{2n-1} \Sigma_{i_\mu i_\mu}(t,\tau)] G^{(n)}_{i_1 ... i_{2n}}(\tau, t'). \tag{2.30}$$

The self-energy term is quiet general, but it contains many extra terms comparing to the previous works. [29–31, 52, 58, 61] Numerical experiments also show that these terms break the particle-hole symmetry. This is due to the larger broadening appears in the higher particle Green's functions, which comes from the extra terms. This fact is easy to see from the expression.

The remedy is to employ some phenomenological arguments to drop certain self-energy terms. The selection rules are:

1. If one creation operator $d_i^\dagger(t)$ and one annihilation operator $d_i(t)$ of the same level i appear simultaneously, this pair is assumed to be stationary and the associated self-energy is dropped.

2. If the annihilation operator $d_i(t)$ is of the opposite spin with respect to the creation operator $d_j^\dagger(t')$, then the associated self-energy is dropped.

3. The remaining self-energy associated with the creation operator $d_i^\dagger(t)$ is dropped.

With these restrictions, the self-energy term above becomes the Bułka-Kostyrko ansatz:

$$\text{self-energy term} = \int d\tau \sum_{i_\mu \in I_{BK}} \Sigma_{i_\mu i_\mu}(t,\tau) G^{(n)}_{i_1 \ldots i_{2n}}(\tau, t'), \tag{2.31}$$

where

$$I_{BK} = \{i_\mu | n \leq \mu \leq 2n-1, \text{spin}(i_\mu) \neq \text{spin}(i_{2n})\} \setminus \{i_\mu | 1 \leq \mu \leq n-1\}. \tag{2.32}$$

This is the formula used in practical simulations.

In summary, we have made three approximations to treat the tunneling physics: (1) Markov approximation[66], (2) Wide-band limit[63], and (3) Bułka-Kostyrko ansatz[30]. These approximations allow us to close the infinite hierarchy of the tunneling hybridization, and include the tunneling physics as self-energy terms in a simple form. The details of the limitation for each approximation could be found in the corresponding references.

2.3 Exterior algebraic formulae for equation of motion

To calculate the transport properties of the strongly-correlated nano-scale structures, the equation of motion method for the non-equilibrium Green's function is a powerful tool. [46] One resorts to the Heisenberg commutators to derive the many-body equation of motion to solve for the contour-ordered Green's function. The derivation is generally too complicated to do for large systems with complicated interactions, and people generally employ different mean-field approximation to decouple the equations. [46, 52]

In this section, we try to develop a method to generate the exact many-body equation of motion by a computer program automatically. It is known that the classical Hamilton equation and Maxwell's equations could be reformulated in the language of differential form. [67, 68] Since the Fermionic path integral is also formulated in Grassmann algebra, [69, 70] it is natural to construct the many-body equation of motion in terms of the differential forms. A correspondence between the Fermionic zero-temperature equal-time correlators and the differential forms was employed in the proof of Morse theory. [67, 68] We construct a different structure, which is convenient to work with general finite temperature and non-equilibrium Green's functions. The details could be found in Appendix A.

2.3.1 Equilibrium EOM

From the algebraic structure (the coordinate transform and anti-symmetry of the indices), the n-particle Green's functions can be viewed as a tensor in the space $\Omega^{(n-1),n}(\mathbb{C}^N) \otimes \Omega^{1,0}(\mathbb{C}^N) \equiv \Theta^n$, where $\Omega^{m,n}(\mathbb{C}^N)$ is the space

of the complex form on the complex manifold $\mathbb{C}^N$. In the coordinate basis which satisfies the transformation rule $z^i = \sum_j u_{ij} z^j$ corresponds to a unitary transformation of the Fermionic basis $d_i = \sum_j u_{ij} d_j$, it is

$$\hat{G}^{r(n)}(\tau,\tau') \in \Theta^n \tag{2.33}$$

$$\hat{G}^{r(n)}(\tau,\tau') = \frac{1}{(n-1)!n!} \sum_{i_1,\ldots,i_{2n}} G^{r(n)}_{i_1 i_2 \ldots i_{2n}}(\tau,\tau') dz^{i_1} \wedge \ldots \wedge dz^{i_{n-1}} \wedge d\bar{z}^{i_n} \wedge \ldots d\bar{z}^{i_{2n-1}} \otimes dz^{i_{2n}}, \tag{2.34}$$

This definition is well-defined since in the definition for the Green's function, the operators at time t are always kept in normal-order. Similarly, the correlation functions are tensors on $\Omega^{n,n}(\mathbb{C}^N)$

$$\hat{C}^{(n)} \in \Omega^{n,n}(\mathbb{C}^N) \tag{2.35}$$

$$\hat{C}^{(n)} = \frac{1}{n!n!} \sum_{i_1,\ldots,i_{2n}} \langle d^\dagger_{i_1} \ldots d^\dagger_{i_n} d_{i_{n+1}} \ldots d_{i_{2n}} \rangle dz^{i_1} \wedge \ldots \wedge dz^{i_n} \wedge d\bar{z}^{i_{n+1}} \wedge \ldots \wedge d\bar{z}^{i_{2n}}. \tag{2.36}$$

For an $N \times N$ Hermitian matrix h, consider the unitary group element $e^{ih\tau} \in U(N)$ acting on the manifold $\mathbb{C}^N$. The induced vector field is

$$X[h] = \sum_{j,k=1}^{N} i h_{kj} z^j \partial_k - i \bar{h}_{kj} \bar{z}^j \partial_{\bar{k}}, \tag{2.37}$$

and we define the following linear operators

$$\hat{\nabla}^1_t : \Theta^n \mapsto \Theta^n \tag{2.38}$$

$$\hat{\nabla}^2_U : \Theta^n \mapsto \Theta^n \tag{2.39}$$

$$\hat{\nabla}^-_U : \Theta^{(n+1)} \mapsto \Theta^n \tag{2.40}$$

$$\hat{\nabla}^+ : \Omega^{(n-1),(n-1)}(\mathbb{C}^N) \mapsto \Theta^n \tag{2.41}$$

by the expressions

$$\hat{\nabla}^1_t = i\mathcal{L}_{X[\bar{t}]} \otimes \mathbb{1} \tag{2.42}$$

$$\hat{\nabla}^2_U = \frac{-i}{2} \sum_{jk} U_{jk} \mathcal{L}_{X[\eta_j]} \mathcal{L}_{JX[\eta_k]} \otimes \mathbb{1} \tag{2.43}$$

$$\hat{\nabla}^-_U = -i \sum_{jk} U_{jk} \mathcal{L}_{X[\eta_j]} \hat{i}_{\partial_k} \hat{i}_{\partial_{\bar{k}}} \otimes \mathbb{1} \tag{2.44}$$

$$\hat{\nabla}^+ = \sum_j d\bar{z}^j \wedge (\cdot) \otimes dz^j, \tag{2.45}$$

where $\mathcal{L}$ is the Lie derivatives, $\mathbb{1}$ is the identity map on $\Omega^{1,0}(\mathbb{C}^N)$, $J = \sum_l idz^j \otimes \partial_j - id\bar{z}^j \otimes \partial_{\bar{j}}$ is the almost complex structure, $\hat{i}$ is the interior product, η_j is the matrix which has only one non-zero element $(\eta_j)_{j,j} = 1$. It can be checked that these maps are invariant under a unitary transformation of the fermionic basis. Now the EOM can be written as

$$(i\partial_\tau - \hat{\nabla}_t^1 - \hat{\nabla}_U^2)\hat{G}^{r(n)}(\tau,\tau') = \delta(\tau-\tau')\hat{\nabla}^+\hat{C}^{(n-1)} + \hat{\nabla}_U^-\hat{G}^{r(n+1)}(\tau,\tau'). \tag{2.46}$$

The Fourier transform leads to the equations on the frequency domain

$$(\epsilon - \hat{\nabla}_t^1 - \hat{\nabla}_U^2)\hat{G}^{r(n)}(\epsilon) = \hat{\nabla}^+\hat{C}^{(n-1)} + \hat{\nabla}_U^-\hat{G}^{r(n+1)}(\epsilon). \tag{2.47}$$

The EOM is closed by the fluctuation-dissipation theorem

$$\hat{C}^{(n)} = \frac{-1}{\pi}\hat{\nabla}^< \int d\epsilon f(\epsilon)\Im[\hat{G}^{r(n)}(\epsilon)] \tag{2.48}$$

$$\hat{\nabla}^{<(n)} : \Theta^n \mapsto \Omega^{n,n}(\mathbb{C}^N) \tag{2.49}$$

$$\hat{\nabla}^{<(n)} = \frac{1}{n}\sum_j dz^j \wedge (\cdot) \otimes \hat{i}_{\partial_j}. \tag{2.50}$$

In practice, we put these equations in matrix form to solve them numerically. Taking the matrix elements in each n-particle subspace, we obtain $G^{r(n)} = \langle\beta(\Theta^n)|\hat{G}^{(n)}\rangle$, $\nabla_t^{1(n)} = \langle\beta(\Theta^n)|\hat{\nabla}_t^1|\beta(\Theta^n)\rangle$, $C^{(n)} = \langle\beta(\Omega^{n,n}(\mathbb{C}^N))|\hat{C}^{(n)}\rangle$, $\nabla_U^{2(n)} = \langle\beta(\Theta^n)|\hat{\nabla}_U^2|\beta(\Theta^n)\rangle$, $\nabla_U^{-(n+1)} = \langle\beta(\Theta^n)|\hat{\nabla}_U^-|\beta(\Theta^{(n+1)})\rangle$, $\nabla^{+(n-1)} = \langle\beta(\Theta^n)|\hat{\nabla}^+|\beta(\Omega^{(n-1),(n-1)}(\mathbb{C}^N))\rangle$, $\nabla^{<(n)} = \langle\beta(\Omega^{n,n}(\mathbb{C}^N))|\hat{\nabla}^{<(n)}|\beta(\Theta^n)\rangle$. Then we get

$$(\epsilon - \nabla_t^{1(n)} - \nabla_U^{2(n)})G^{r(n)}(\epsilon) = \nabla^{+(n-1)}C^{(n-1)} + \nabla_U^{-(n+1)}G^{r(n+1)}(\epsilon) \tag{2.51}$$

$$C^{(n)} = \frac{-1}{\pi}\nabla^{<(n)}\int d\epsilon f(\epsilon)\Im[G^{r(n)}(\epsilon)]. \tag{2.52}$$

In each iteration, it can be solved efficiently by the backward substitution from N-particle to 1-particle Green's function,

$$G^{r(n)}(\epsilon) = \mathcal{G}^{(n)}(\epsilon)(\nabla^{+(n-1)}C^{(n-1)} + \nabla_U^{-(n+1)}G^{r(n+1)}(\epsilon)), \tag{2.53}$$

where $\mathcal{G}^{(n)}(\epsilon) = (\epsilon - \nabla_t^{1(n)} - \nabla_U^{2(n)})^{-1}$.

2.3.2 Nonequilibrium EOM

We can now apply the method to the nonequilibrium Green's function[46]. With the same definition from the previous section, the self-consistent matrix EOM under Markov approximation can be written as

$$(\epsilon - \nabla_t^{1(n)} - \nabla_U^{2(n)} - \nabla_{\Sigma^r}^{s(n)}) G^{r(n)}(\epsilon) = \nabla^{+(n-1)} C^{(n-1)} + \nabla_U^{-(n+1)} G^{r(n+1)}(\epsilon) \quad (2.54)$$

$$(\epsilon - \nabla_t^{1(n)} - \nabla_U^{2(n)} - \nabla_{\Sigma^r}^{s(n)}) G^{<(n)}(\epsilon) = \nabla_{\Sigma^<}^{s(n)} G^{a(n)}(\epsilon) + \nabla_U^{-(n+1)} G^{r(n+1)}(\epsilon) \quad (2.55)$$

$$C^{(n)} = \frac{1}{2\pi i} \nabla^{<(n)} \int d\epsilon G^{<(n)}(\epsilon). \quad (2.56)$$

$\nabla^s = \nabla^1$ in general, and it may be modified according to the selection rule imposed. These equations are the n-particle generalization of the Dyson equation and the Keldysh equation. For $U = 0$, they reduce to the simple Dyson and Keldysh equation.

2.4 Computational implementation

2.4.1 Computational cost

We compare the computational effort of our Green's function approach to the rate equation approach. In the rate equation, the quantity to be solved is the density matrix of the size $2^N \times 2^N = 4^N$, which grows exponentially. In our Green's function approach, the number of correlators to be solved is $\sum_{n=1}^{N} \binom{N}{n}\binom{N}{n} = \binom{2N}{N} - 1 \to \frac{4^N}{\sqrt{\pi N}}$, which grows sub-exponentially. However, to get these correlators, the number of Green's functions to be solved is $\sum_{n=1}^{N} \binom{N}{n-1}\binom{N}{n} N$, which grows super-exponentially.

For the triple QD system ($N = 6$), we need to solve for 4752 Green's functions to get 923 correlators, while the number of the density matrix elements is 4096.

2.4.2 Numerical comparison

In this section, we compare the results of GFEOM code (see Appendix A for details) with some other calculations, including single QD (Pals and MacKinnon [52]), double QD (Bułka and Kostyrko [30]), and triple QD (Chang and Kuo [61]). The tests shown here are calculated with GFEOM version 1.5.8. compiled by Intel Fortran Composer XE 2013 SP1 for Linux on Intel CPUs. Notice that earlier versions of Intel Fortran compiler has a bug in pointer bound remapping, and should not be used to compile GFEOM code. The bug was reported by the author and fixed by Intel in 2012. [71, 72]

Figure 2.2 shows nonequilibrium current and differential conductance for a single dot compared with Pals and

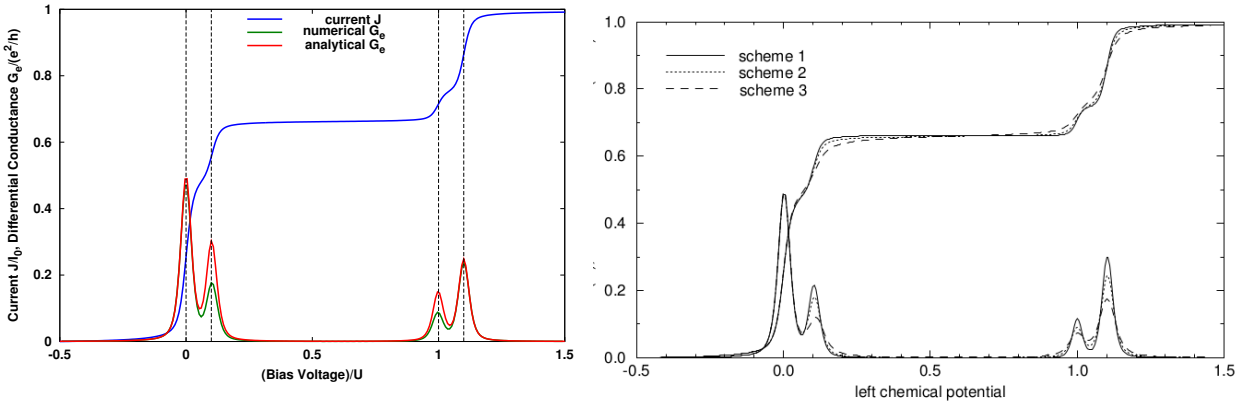

Figure 2.2: Nonequilibrium current and differential conductance for a single dot compared with Pals and MacKinnon [52] calculation. The left figure is produced by GFEOM code, and the right figure is taken from Pals and MacKinnon [52].

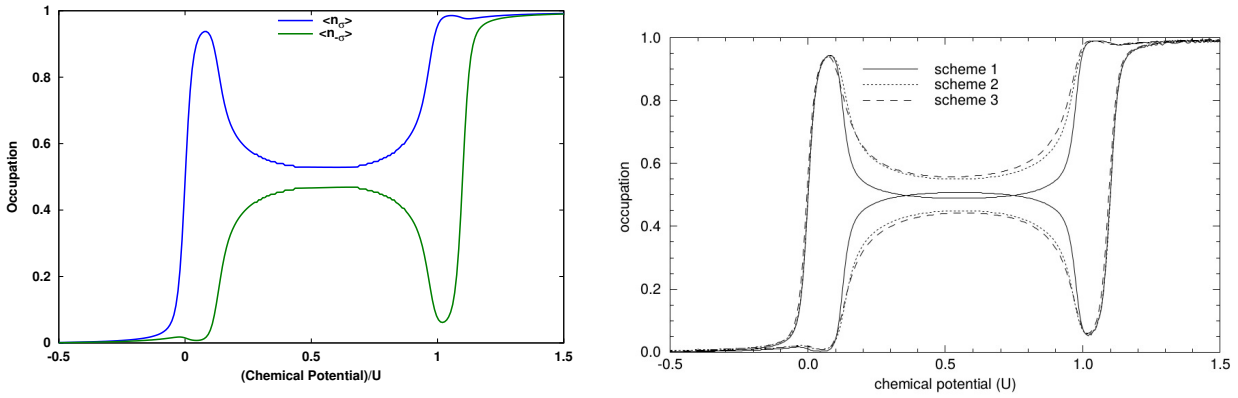

Figure 2.3: Occupation for a single dot compared with Pals and MacKinnon [52] calculation. The left figure is produced by GFEOM code, and the right figure is taken from Pals and MacKinnon [52].

MacKinnon [52] calculation. Our data is to be compared with the scheme 2. Parameters are $\mu_R = -0.5U$, $T = \Gamma_L = \Gamma_R = 0.01U$, $E_\sigma = 0$, $E_{\bar{\sigma}} = 0.1U$. The black vertical dashed lines label the theoretically predicted peak positions (from left to right): $p_1 = E_\sigma$, $p_2 = E_{\bar{\sigma}}$, $p_3 = E_\sigma + U$, $p_4 = E_{\bar{\sigma}} - U$.

Figure 2.3 occupation for a single dot compared with Pals and MacKinnon [52] calculation. Our data is to be compared with the scheme 2. Parameters are $T = \Gamma_L = \Gamma_R = 0.01U$, $E_\sigma = 0$, $E_{\bar{\sigma}} = 0.1U$. The black vertical dashed lines label the theoretically predicted peak positions (from left to right): $p_1 = E_\sigma$, $p_2 = E_{\bar{\sigma}}$, $p_3 = E_\sigma + U$, $p_4 = E_{\bar{\sigma}} - U$.

Figure 2.4 shows linear response differential conductance and correlation functions for a double dot compared with Bułka and Kostyrko [30] calculation. Parameters are $t_{12} = 1$, $U_i = 6$, $U_{ij} = 1.6$, $\Gamma_L = \Gamma_R = 0.2$, $\epsilon_1 = \epsilon_2$, $T = 0$. Notice that their definition of Γ is different from our definition by a factor of 2. The black vertical dashed lines

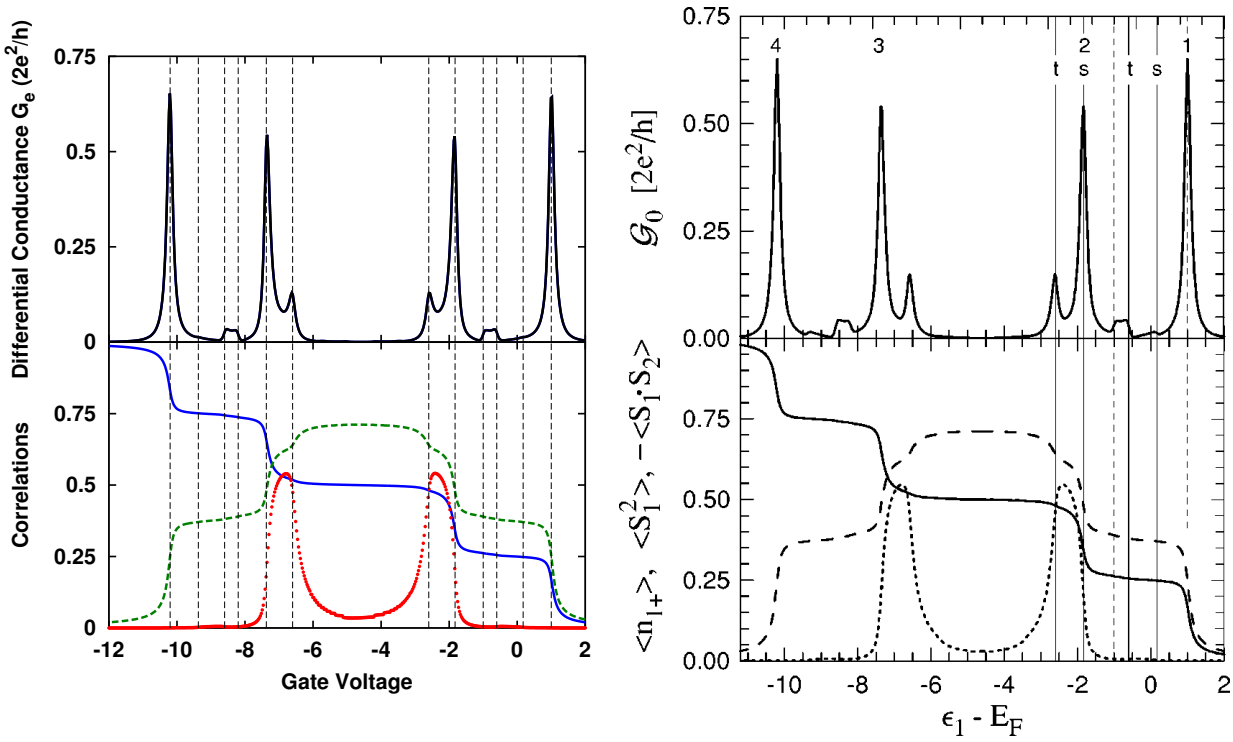

Figure 2.4: Linear response differential conductance and correlation functions for a double dot compared with Bułka and Kostyrko [30] calculation. The left figure is produced by GFEOM code, and the right figure is taken from Bułka and Kostyrko [30].

label the theoretically predicted peak positions (from left to right): $p_1 = -\epsilon_1 - t_{12} - U_0 - 2U_1$, $p_2 = -\epsilon_1 - t_{12} - (U_0 + 3U_1 + \Delta)/2$, $p_3 = -\epsilon_1 - t_{12} - U_0 - U_1$, $p_4 = -\epsilon_1 + t_{12} - U_0 - 2U_1$, $p_5 = -\epsilon_1 + t_{12} - (U_0 + 3U_1 + \Delta)/2$, $p_6 = -\epsilon_1 + t_{12} - U_0 - U_1$, $p_7 = -\epsilon_1 - t_{12} - U_1$, $p_8 = -\epsilon_1 - t_{12} - (U_0 + U_1 - \Delta)/2$, $p_9 = -\epsilon_1 - t_{12}$, $p_{10} = -\epsilon_1 + t_{12} - U_1$, $p_{11} = -\epsilon_1 + t_{12} - (U_0 + U_1 - \Delta)/2$, $p_{12} = -\epsilon_1 + t_{12}$, where $\Delta = \sqrt{16t_{12}^2 + (U_0 - U_1)^2}$.

Figure 2.5 shows nonequilibrium differential conductance and correlation functions for a double dot compared with Bułka and Kostyrko [30] calculation. Parameters are $t_{12} = 1$, $U_i = 6$, $U_{ij} = 1.6$, $\Gamma_L = \Gamma_R = 0.2$, $\epsilon_1 = \epsilon_2 = 2$, $T = 0$. Notice that their definition of Γ is different from our definition by a factor of 2. The black vertical dashed lines label the theoretically predicted peak positions (from left to right): $p_1 = \epsilon_1 - t_{12}$, $p_2 = \epsilon_1 - t_{12} + U_1$, $p_3 = \epsilon_1 + t_{12}$, $p_4 = \epsilon_1 + t_{12} + (U_0 + U_1 - \Delta)/2$, $p_5 = \epsilon_1 + U_1 + t_{12}$, where $\Delta = \sqrt{16t_{12}^2 + (U_0 - U_1)^2}$.

Figure 2.6 shows nonequilibrium current and differential conductance for a triple dot compared with Chang and Kuo [61] calculation. Notice that the correlations are factorized in Chang and Kuo [61], so only the peak positions are exact. Parameters are $\Gamma_L = \Gamma_R = 0.001$, $E_1 = 0.78$, $E_2 = E_1 + 0.236 = 1.016$, $E_3 = E_1 + 0.456 = 1.236$, $U_1 = 0.137$, $U_2 = 0.07$, $U_3 = 0.06$, $U_{12} = 0.122$, $U_{13} = 0.1$, $U_{23} = 0.04$, $T = 0$, and $E_i = E_i - 0.61V_g$. The black vertical dashed lines label the theoretically predicted peak positions (from left to right): $p_1 = E_1/0.61$, $p_2 = (E_1 + U_1)/0.61$, $p_3 = E_2/0.61$, $p_4 = (E_1 + U_1 + U_{12})/0.61$, $p_5 = (E_2 + U_2)/0.61$, $p_6 = (E_2 + U_{12})/0.61$,

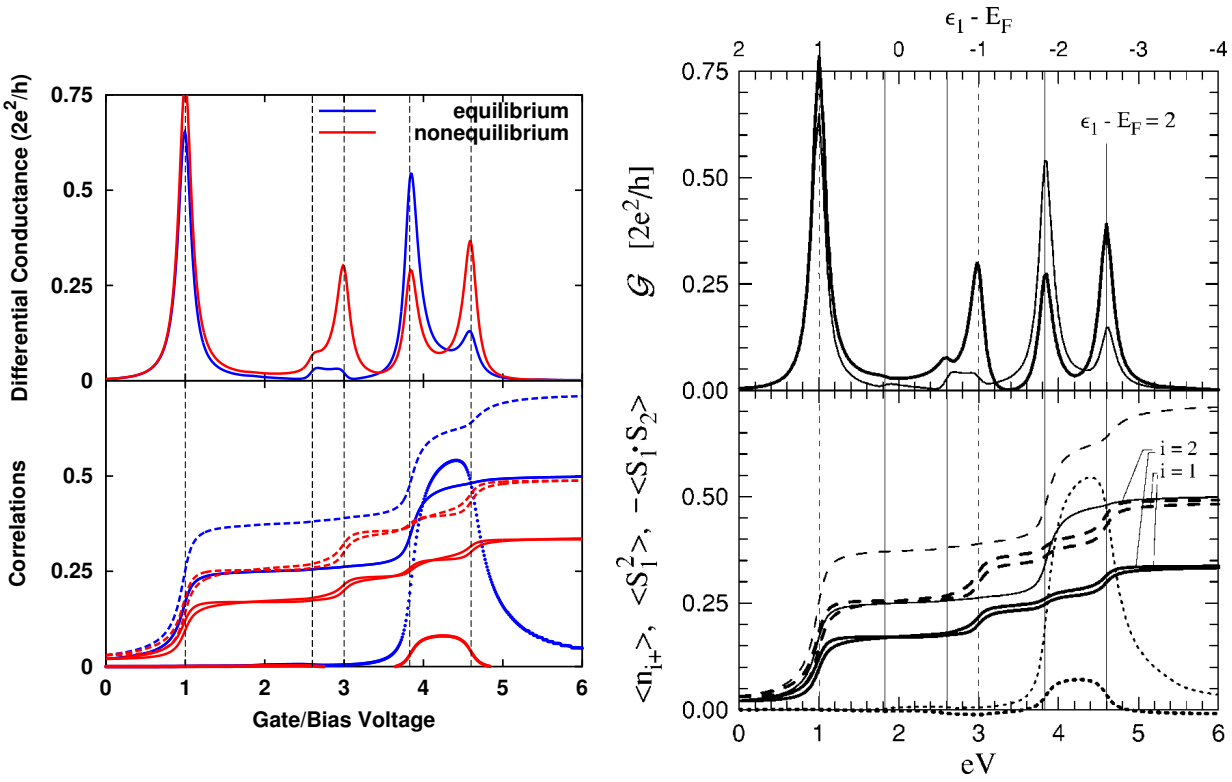

Figure 2.5: Nonequilibrium differential conductance and correlation functions for a double dot compared with Bułka and Kostyrko [30] calculation. The left figure is produced by GFEOM code, and the right figure is taken from Bułka and Kostyrko [30].

$p_7 = (E_1 + U_1 + 2U_{12})/0.61, p_8 = (E_2 + U_2 + U_{12})/0.61.$

2.5 Application: Quantum interference and electron correlation in charge transport through triangular quantum dot molecules

2.5.1 Model

We consider an artificial molecule made of nanoscale QDs, in which the energy level separations are much larger than the on-site Coulomb interactions and thermal energies. [11] Thus, only one energy level for each quantum dot is included. The extended Hubbard-Anderson model is employed to simulate the TQDM junction with Hamiltonian given by $H = H_0 + H_T + H_{QDs}$, where $H_0 = \sum_{\mathbf{k},\sigma,\alpha} \epsilon_{\mathbf{k}} c^\dagger_{\mathbf{k},\sigma,\alpha} c_{\mathbf{k},\sigma,\alpha}$ is the Hamiltonian for free electrons in the electrodes. $c^\dagger_{k,\sigma,\alpha}(c_{\mathbf{k},\sigma,\alpha})$ creates (destroys) an electron of momentum $\mathbf{k}$ and spin σ with energy ϵ_k in the α electrode. $H_T = \sum_{\mathbf{k},\ell,\alpha}(V_{k,\alpha,\ell} c^\dagger_{\mathbf{k},\sigma,\alpha} d_{\ell,\sigma} + V^*_{\mathbf{k},\alpha,\ell} d^\dagger_{\ell,\sigma} c_{\mathbf{k},\sigma,\alpha})$. $V_{\mathbf{k},\alpha,\ell}$ describes the coupling between the α electrode and the ℓ-th QD. $d^\dagger_{\ell,\sigma}$ $(d_{\ell,\sigma})$ creates (destroys) an electron in the ℓ-th dot. H_{QDs} is the extended Hubbard Hamiltonian for

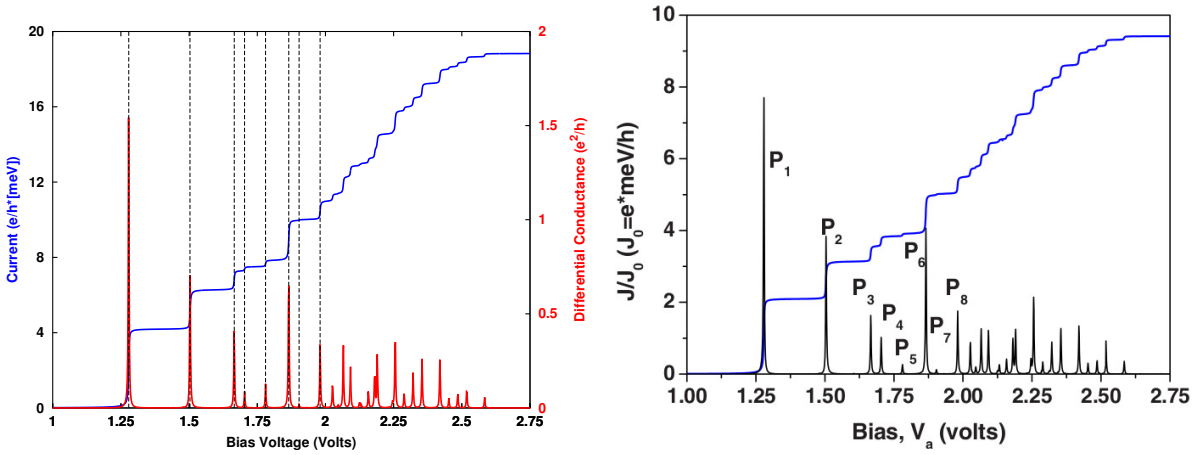

Figure 2.6: Nonequilibrium current and differential conductance for a triple dot compared with Chang and Kuo [61] calculation. The left figure is produced by GFEOM code, and the right figure is borrowed from Chang and Kuo [61].

multiple QDs.

$$H_{QDs} = \sum_{\ell,\sigma} E_\ell n_{\ell,\sigma} + \sum_{\ell} U_\ell n_{\ell,\sigma} n_{\ell,\bar{\sigma}} + \sum_{\ell<j,\sigma,\sigma'} U_{\ell j} n_{\ell,\sigma} n_{j,\sigma'} + \sum_{\ell\neq j,\sigma} t_{\ell j} d^\dagger_{\ell,\sigma} d_{j,\sigma}, \tag{2.57}$$

where E_ℓ is the spin-independent QD energy level, $n_{\ell,\sigma} = d^\dagger_{\ell,\sigma} d_{\ell,\sigma}$, U_ℓ and $U_{\ell j}$ $(\ell < j)$ denote the intradot and interdot Coulomb interactions, respectively and $t_{\ell j}$ describes the electron interdot coupling. The interdot Coulomb interactions as well as intradot Coulomb interactions are important for nanoscale semiconductor QDs and molecules. Therefore, $U_{\ell,j}$ cannot be ignored.

Using the Keldysh-Green's function technique[28, 46], the electrical current from reservoir α to the TQDM junction is calculated according to the Meir-Wingreen formula

$$J_\alpha = \frac{ie}{h} \int d\epsilon \sum_{j\sigma} \Gamma^\alpha_j [G^<_{j\sigma}(\epsilon) + f_\alpha(\epsilon)(G^r_{j\sigma}(\epsilon) - G^a_{j\sigma}(\epsilon))], \tag{2.58}$$

where $\Gamma^\alpha_j(\epsilon) = \sum_{\mathbf{k}} |V_{\mathbf{k},\alpha,j}|^2 \delta(\epsilon - \epsilon_{\mathbf{k}})$ is the tunneling rate between the α-th reservoir and the j-th QD. Throughout the paper, for two-terminal devices we assume that the left (right) lead is only coupled to the left (right) QD with tunneling rate Γ_L (Γ_R), while there is no coupling between the center QD and the two leads. For three-terminal devices, the coupling between the center QD and a third gate is described by the tunneling rate Γ_C. $f_\alpha(\epsilon) = 1/\{\exp[(\epsilon - \mu_\alpha)/k_B T] + 1\}$ denotes the Fermi distribution function for the α-th electrode, where μ_α is the chemical potential and T is the temperature of the system. e, h, and k_B denote the electron charge, the Planck's constant, and the Boltzmann constant,

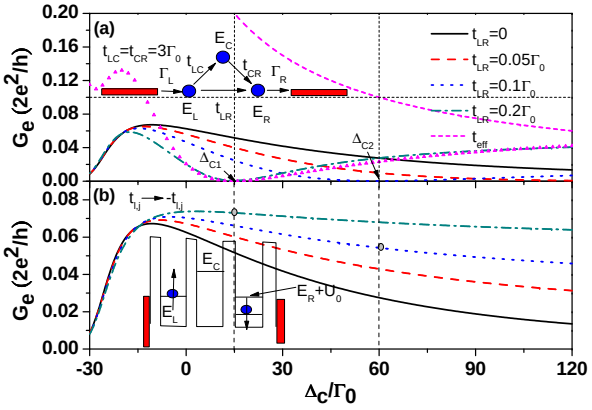

Figure 2.7: Electrical conductance (G_e) of TQDM as a function of central QD energy for different t_{LR} strengths in the Pauli spin blockade configuration with $E_L = E_F$ and $E_R = E_F - U_R$. (a) $t_{LC} = t_{CR} = 3\Gamma_0$, and (b) $t_{\ell,j}$ replaced by $-t_{\ell,j}$. Other physical parameters are $k_BT = 1\Gamma_0$, $\Gamma = 0.3\Gamma_0$, $U_{LC} = U_{CR} = 30\Gamma_0$, and $U_{LR} = 0$. Figure borrowed from Chen *et al.* [11].

respectively. $G^<_{j\sigma}(\epsilon)$, $G^r_{j\sigma}(\epsilon)$, and $G^a_{j\sigma}(\epsilon)$ are the frequency domain representations of the one-particle lessor, retarded, and advanced Green's functions $G^<_{j\sigma}(t,t') = i\langle d^\dagger_{j,\sigma}(t')d_{j,\sigma}(t)\rangle$, $G^r_{j\sigma}(t,t') = -i\theta(t-t')\langle\{d_{j,\sigma}(t), d^\dagger_{j,\sigma}(t')\}\rangle$, and $G^a_{j\sigma}(t,t') = i\theta(t'-t)\langle\{d_{j,\sigma}(t), d^\dagger_{j,\sigma}(t')\}\rangle$, respectively. These one-particle Green's functions are related recursively to other Green's functions and correlators via the many-body equation of motion,[29–31] which we solve via an iterative numerical procedure to obtain all n-particle Green's functions ($n = 1, \cdots, 6$) and correlators for the TQDM. (See supplemental materials.) Our procedure is valid in the Coulomb blockade regime, but not the Kondo regime.[73, 74] Throughout this paper, we assume the on-site Coulomb interaction $U_\ell = U_0 = 100\Gamma_0$ for all three QDs and the same tunneling rates at all leads, $\Gamma^\alpha_j = \Gamma$ with j labeling the QD directly connected to lead α.

2.5.2 Results and discussion

Although the QI of TQDM was theoretically investigated previously[75, 76], the effect of intradot and interdot Coulomb interactions was not considered. Here, we utilize the LDCT effect to tune the effective hopping strength between outer QDs to achieve the destructive and constructive QIs in the presence of electron Coulomb interaction. We consider a TQDM junction in the Pauli spin blockade (PSB) configuration[4, 31] with $E_L = E_F$, $E_R = E_F - U_0$, $t_{LC} = t_{CR} = 3\Gamma_0$, $\Gamma_L = \Gamma_R = 0.3\Gamma_0$, $U_{LC} = U_{CR} = 30\Gamma_0$, and $U_{LR} = 0$. Fig.2.7(a) shows the electrical conductance (G_e) as a function of central QD energy level ($\Delta_C = E_C - E_F$) for t_{LR} varying from 0 to $0.2\Gamma_0$ at $k_BT = 1\Gamma_0$ (in weak interdot coupling regime). For Δ_C less than $-15\Gamma_0$, G_e is not sensitive to the variation of t_{LR}, indicating that the transport is mainly through the upper path involving the center QD as shown in the inset of Fig.2.7(a). In the case of $t_{LR} = 0$, G_e can be well explained by the LDCT effect when E_C is far away from

E_F.[77] The central QD provides an intermediated state for electrons in the outer QDs. Through the upper path, TQDM behaves like a double QD with an effective hopping $t_{eff} = -t_{LC}t_{CR}/(U_{CR} + \Delta_C)$, which can also be understood by the second order perturbation theory.[77] Once $t_{LR} \neq 0$ (the lower path turns on), electron transport through the two paths with t_{eff} and t_{LR} lead to a destructive QI. Note that G_e for the case of $t_{LR} \neq 0$ is reduced compared to the case of $t_{LR} = 0$. In particular, G_e is vanishingly small at the value of Δ_C where $|t_{eff}|$ crosses t_{LR} as indicated by dashed lines in Fig.2.7(a). For illustration, the curve for $|t_{eff}| = |t_{LC}t_{CR}|/(U_{CR} + \Delta_C)$ is also shown in Fig.2.7(a). (See short-dashed curve) The vanishing G_e occurs at lower Δ_C with increasing $|t_{LR}|$ (Compare dash-dotted with dashed curves). Due to topological effect, the electron-hole symmetry does not hold for the energy spectrum of TQDM.[26] When TQDM has identical QD energy levels ($E_\ell = E_0$) and homogenous electron hopping strengths $t_{\ell,j} = t$, we have one level $\epsilon = E_0 + 2t$ and one doubly degenerate level with $\epsilon = E_0 - t$ for the case of $U_\ell = U_{\ell,j} = 0$. Unlike the cases of DQDs and SCTQDs, the lowest energy level depends on the sign of $t_{\ell,j}$. This is a manifesting result of electron-hole asymmetrical behavior of TQDM. Therefore, it will be interesting to examine the sign effect of $t_{\ell,j}$ on the QI behavior. Physically, the sign of $t_{\ell,j}$ depends on the symmetry properties of orbitals, which can change in different configurations. We can replace $t_{\ell,j}$ by $-t_{\ell,j}$ to examine the QI effect with respect to the electron-hole symmetry. The results are shown in Fig.2.7(b). We find that G_e is enhanced with increasing t_{LR}, which is attributed to the constructive QI effect, in contrast to the destructive QI effect shown in Fig.2.7(a).

To gain deeper understanding of the destructive and constructive QI shown in Fig.2.7, we compare our full calculation with the weak interdot-coupling theory,[31, 77] which allows simple closed-form expression for the electrical conductance of TQDM. We obtain $G_e = 2e^2/h \int d\epsilon \mathcal{T}(\epsilon)[\partial f(\epsilon)/\partial E_F] \approx (2e^2/h)\mathcal{T}(E_F)$ at low-temperature limit, where the transmission coefficient $\mathcal{T}(\epsilon)$ with 64 configurations is approximately given by

$$\mathcal{T}_{PSB}(\epsilon) = \frac{4\Gamma_L\Gamma_R P_{PSB} F_{QI}}{|\mu_1\mu_2\mu_3 - t_{CR}^2\mu_1 - t_{LC}^2\mu_3 - t_{LR}^2\mu_2 - 2t_{LR}t_{LC}t_{CR}|^2}, \tag{2.59}$$

where $F_{QI} = \mu_2^2(t_{LC}t_{CR}/\mu_2 + t_{LR})^2$ is a factor related to QI. $\mu_1 = \epsilon - E_L + i\Gamma_L$, $\mu_2 = \epsilon - E_C - U_{RC}$ and $\mu_3 = \epsilon - E_R - U_R + i\Gamma_R$. P_{PSB} denotes the probability weight in the PSB configuration.[31] From Eq. 2.59, we have

$$G_e = \frac{2e^2}{h} \frac{P_{PSB} 4\Gamma^2 (t_{eff} + t_{LR})^2}{(\Gamma^2 + 2t_{eff}t_{LR} + t_{LR}^2)^2 + \Gamma^2 (t_{h1} + t_{h2})^2}, \tag{2.60}$$

where $t_{eff} = -t_{LC}t_{CR}/(U_{CR} + \Delta_C)$, $t_{h1} = -t_{LC}^2/(U_{CR} + \Delta_C)$, and $t_{h2} = -t_{CR}^2/(U_{CR} + \Delta_C)$ with $\Gamma_L = \Gamma_R \equiv \Gamma$. For $t_{LC} = t_{CR} = t_c = 0$, Eq. 2.60 reduces to the conductance of DQD,[17] while for $t_{LR} = 0$, it reduces to the G_e of SCTQD.[77] At $\Delta_C = 15\Gamma_0$ and $60\Gamma_0$, which satisfy the condition of $t_{eff} + t_{LR} = 0$ for

$t_{LR} = 0.2\Gamma_0$ and $t_{LR} = 0.1\Gamma_0$, respectively, and we see G_e vanishes there. This well illustrates the destructive QI seen in Fig.2.7(a). Once we make the substitution $t_{\ell,j} \rightarrow -t_{\ell,j}$ in Eq. 2.60, we can reveal the constructive QI in G_e as shown in Fig.2.7(b). Note that in the weak coupling regime ($t_{eff}/\Gamma \ll 1$), the probability weight P_{PSB} of Eq. 2.60 calculated according to the procedures in Ref. 31, where the interdot two-particle correlation functions are factorized as the product of single occupation numbers, is consistent with the full calculation, but not for $t_{eff}/\Gamma \gg 1$. Away from the weak coupling regime, the interdot electron correlations become important. To explicitly reveal the importance of electron correlation effects, we plot the curve of $t_{LR} = 0.2\Gamma_0$ (with triangle marks) calculated by the procedure of Ref. 31 (including 64 configurations) in Fig.2.7(a). Comparison between the full solution and the approximation considered in Ref. 18, we find that the electron correlation effects become very crucial when $t_{eff}/\Gamma \gg 1$. Once electron transport involves more electrons, the high-order (beyond two-particle) Green functions and correlation functions should be included (see the results of Fig.2.8). The difference between the conventional mean-field theory of Ref. 17 with the full solution is even larger. The comparison between mean-field theory and the procedure of Ref. 31 has been discussed in the appendix of Ref. 31.

According to Eq. 2.60, constructive and destructive QI effects depend on the sign of $t_{\ell,j}$. Therefore, if the wavefunction of the center dot has opposite parity (say, an x-like state) with respect to the wavefunctions in two outer dots (assumed to be s-like), then t_{LC} will have opposite sign compared with t_{CR} and t_{LR}, and the sign of t_{eff} will be flipped. Consequently, the destructive QI shown in Fig.2.7(a) will become constructive QI. Thus, for a center QD with an s-like ground state and an excited p-like state, it is possible to see the change of QI between destructive and constructive by tuning the gate voltage, which sweeps through different resonance energies of the center QD in addition to the change of sign of t_{eff} when the Fermi level goes from below the resonance level to above the resonance level. From the results of Fig.2.7, QI effect can be electrically controlled by the energy level E_c. This advantage of TQDM may be useful for improving the spin filtering of DQDs [4].

In addition to QI effects, spin frustration and topological effects (due to electron-hole asymmetry) on the measured quantities (electrical conductance or current) are also interesting issues.[24] Fig.2.8(a) shows G_e as a function of gate voltage, Δ_g for $E_\ell = E_F + 10\Gamma_0 - \Delta_g$; $\ell = L, C, R$ at two different temperatures, $k_BT = 0$ and $1\Gamma_0$. Here, we consider the homogenous configuration with $U_{LR} = U_{LC} = U_{CR} = 30\Gamma_0$ and $t_{\ell,j} = t_c = 3\Gamma_0$. At low temperature, there are six main peaks in the G_e spectrum, labeled by ϵ_n, $n = 1, \cdots, 6$ and some secondary peaks. At higher temperature, the six main peaks are suppressed and broadened as shown by the dashed curve, and the secondary peaks are washed out. We also plot the total occupation number, $N = \sum_\sigma (N_{L,\sigma} + N_{R,\sigma} + N_{C,\sigma})$ as the black solid curve, which shows a stair-case behavior with plateaus at $N = 1, \cdots, 6$, corresponding to the filling of TQDM with 1 to 6 electrons. It can be seen that the six main peaks occur at Δ_g where N is increased by 1. Thus, the peak positions ϵ_n correspond to the chemical potential of electrons in TQDM, i.e. the energy needed to

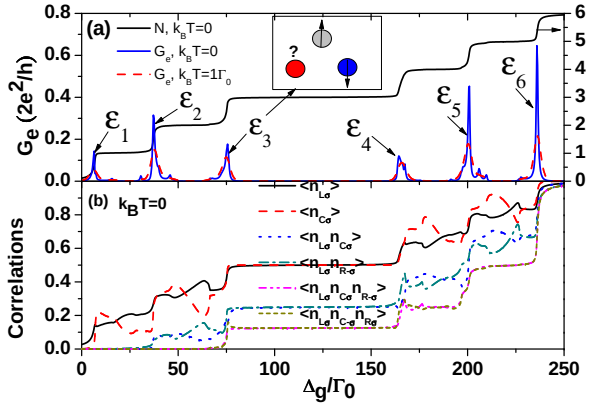

Figure 2.8: (a) Electrical conductance of TQDMs as a function of gate voltage Δ_g with $E_L = E_R = E_C = E_F + 10\Gamma_0 - \Delta_g$ and $\Gamma = 1.6\Gamma_0$.(b) Correlation functions for $k_BT = 0\Gamma_0$. Other physical parameters are $t_{\ell,j} = 3\Gamma_0$ and $U_{LR} = U_{LC} = U_{CR} = 30\Gamma_0$. Figure borrowed from Chen *et al.* [11].

add an electron to the system. The main peak positions can be approximately obtained by the calculation of chemical potential of TQDM without considering the coupling with leads as done in Ref. 26. For example, $\epsilon_1 = E_L - 2|t_c|$, $\epsilon_2 = E_L + U_{LC} - 8t^2/(U_0 - U_{LC})$ and $\epsilon_3 = E_L + 2U_{\ell,j} - 3J_{ex}/2 + 2|t_c| + 16t_c^2/(U_0 - U_{LC})$ under the condition $U_0 > U_{LC} \gg t_c$, where $J_{ex} \equiv E_0(S = 3/2) - E_0(S = 1/2)$ is the difference in energy between the spin-3/2 and spin-1/2 configuration.[26] However, the relative strengths of peaks in the conductance spectrum can only be obtained by solving the full Anderson-Hubbard model self-consistently.

Unlike the G_e spectrum of DQDs,[30] the G_e spectrum of TQDM does not show the electron-hole symmetry due to topological effect. Note that $N = 4$ and $N = 5$ correspond to two-hole and one-hole configurations, respectively. A large Coulomb blockade separation between ϵ_3 and ϵ_4 is given by $\Delta_{34} = U_0 + 3J_{ex} - 4t_c - 8t_c^2/(U_0 - U_{LC})$. Here, ϵ_4 corresponds to the two hole ground state with spin triplet instead of singlet. The magnitude of G_e is smaller than the quantum conductance $2e^2/h$ for $t_{LR}/\Gamma \gg 1$ as a result of electron Coulomb interactions.[30] The mechanism for understanding the unusual G_e behavior in nanostructure junction systems is a subject of high interest.[78] Due to electron Coulomb interactions, the magnitudes of peaks are related to the probability weights of quantum paths, which are related to single-particle occupation numbers and many-particle correlation functions.[31]

To reveal the configurations for each main peak, the one-particle occupation number $N_{\ell,\sigma} \equiv \langle n_{\ell,\sigma} \rangle$, inter-dot two particle correlation functions $\langle n_{\ell,\sigma} n_{j,\bar{\sigma}} \rangle$, and three particle correlation functions ($\langle n_{L,\sigma} n_{C,-\sigma} n_{R,\sigma} \rangle$, and $\langle n_{L,\sigma} n_{C,-\sigma} n_{R,\sigma} \rangle$) are plotted in Fig.2.8(b). We always have the relation $N_{L,\sigma} = N_{R,\sigma} \neq N_{C,\sigma}$, because the outer QDs are directly coupled to electrodes, but not the central QD. Such a relation also holds for two-particle and three-particle correlation functions. The six main peaks in Fig.2.8(a) indicate the filling of TQDM up to the n-electron ground state for $n = 1, \cdots, 6$. For example, ϵ_2 indicates the formation of two-electron state with spin

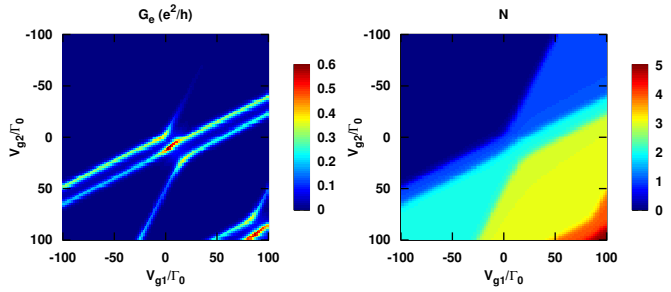

Figure 2.9: Charge stability diagram of TQDM. $\Gamma_\ell = \Gamma_0$, $k_BT = 1.5\Gamma_0$, $U_{LC} = U_{CR} = U_{LR} = 12\Gamma_0$, $t_{\ell,j} = 3\Gamma_0$. The energy levels are shifted according to $E_\ell = E_F - U_{LR} - \sum_{m=1}^{2} \beta_{\ell,m} e V_{gm}$, where the gate coupling constants are $\beta_{L,1} = 0.5$, $\beta_{C,1} = 1$, $\beta_{R,1} = 0.5$, $\beta_{L,2} = 1$, $\beta_{C,2} = 0.5$, and $\beta_{R,2} = 1$. Figure borrowed from Chen *et al.* [11].

singlet, while ϵ_3 indicates the formation of three-particle state with total spin $S = 1/2$, which can be described as the spin-frustration state[24, 26, 79]. Because the on-site Coulomb interaction favors homogeneous distribution of three electrons in TQDM, whereas the interdot Coulomb repulsion favors the charge fluctuation. As seen in Fig.2.8(b), for $\Delta_g \leq \epsilon_3$ ($78\Gamma_0$) N_ℓ in each dot clearly displays the charge fluctuation behavior. When TQDM goes into a three-particle state ($\Delta_g > \epsilon_3$), the charge fluctuation is suppressed, and each QD is filled with one particle (with $N_{L,\sigma} = N_{R,\sigma} = N_{C,\sigma} = 0.5$), while $\langle n_{L,\sigma} n_{C,\sigma} n_{R,-\sigma}\rangle$=$\langle n_{L,\sigma} n_{C,-\sigma} n_{R,\sigma}\rangle = \langle n_{L,-\sigma} n_{C,\sigma} n_{R,-\sigma}\rangle$. This also demonstrates the spin frustration condition as depicted in the inset of Fig.2.8(a).

Figure2.9 shows the charge stability diagram for zero-bias electrical conductance (G_e) and total occupation number (N) as functions of gate voltages exerted on any two QDs (labeled by V_{g1} and V_{g2}) for a TQDM connected to three terminals. The magnitudes of G_e and N are indicated by different colors. It is noticed that G_e is enhanced on the borders that separate domains of different values of occupation number (N) with larger G_e occurring at $V_{g1} = V_{g2}$. This is a result of higher degeneracy and charge-fluctuation in the state. The largest G_e for $N \leq 3$ occurs at the junction between $N = 1$ and $N = 2$ domains when $V_{g1} = V_{g2}$. This feature corresponds to the ϵ_2 peak of Fig.2.9(a). The diagram Fig.2.9(a) is simply a collection of curves displayed in Fig.2.8(a) at different values of V_{g2} that shifts the QD energy levels. We note that in the domains of $N = 1$ and $N = 2$, the areas with stripes are not symmetrical with respect to gate voltage. In Ref. 24, a capacitive interaction model was employed to plot the diagram of N. In their model, the electron hopping strength $t_{\ell,j}$ was ignored. Consequently, the charge stability diagram of G_e cannot be obtained. The charge stability diagram of G_e obtained by our full calculation [as shown in Fig.2.9(a)] bears close resemblance to the experimental results as shown in Fig. 2 of Ref. 24.

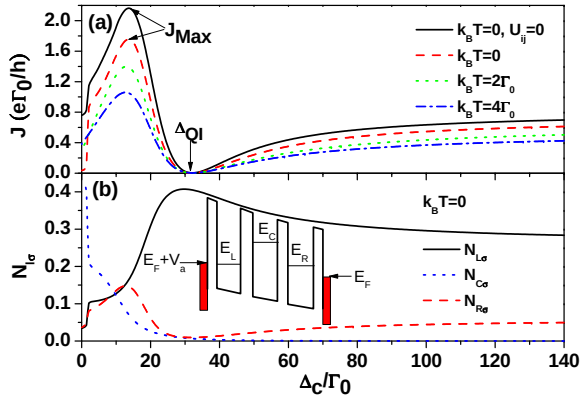

Figure 2.10: (a) Tunneling current as a function of $\Delta_C = E_C - E_F$ at finite bias $V_a = 10\Gamma_0$ for various temperatures. (b) Occupation numbers as a function of Δ_C at $k_BT = 0$. The other physical parameters used are $E_L = E_R = E_F + 10\Gamma_0$, $U_{LC} = U_{CR} = 30\Gamma_0$, $U_{LR} = 10\Gamma_0$, $t_{LC} = t_{CR} = 3\Gamma_0$, $t_{LR} = 0.4\Gamma_0$, and $\Gamma = \Gamma_0$. Figure borrowed from Chen *et al.* [11].

So far, the results shown in Figs.2.7-2.9 are all related to the linear response. To further clarify the QI effect at finite bias ($V_a = 10\Gamma_0$) for different temperatures, we plot in Fig.2.10(a) the tunneling current as a function of center QD energy, $E_C = E_F + \Delta_c$ for the configuration shown in the inset of Fig.2.10(b). For $\Delta_C \geq 2\Gamma_0$, the tunneling current is suppressed as temperature increases. This is attributed to a reduction of electron population in the electrodes for electrons with energy near $E_F + 10\Gamma_0$. For $\Delta_C \leq 2\Gamma_0$, we notice that $N_{c,\sigma}$ quickly jumps to 0.4, indicating that the central QD is filled with charge, which causes an interdot Coulomb blockade for electrons entering the left QD. (See the reduction of $N_{L,\sigma}$ in Fig.2.10(b)). This explains the sharp dip of G_e for $\Delta_C \leq 2\Gamma_0$ in Fig.2.10(a). As temperature increases, such a dip in tunneling current is smeared out. At $\Delta_C = 10\Gamma_0 + t_{LC}t_{CR}/t_{LR} \equiv \Delta_{QI}$, the tunneling current vanishes for all temperatures considered due to the QI effect. Such a robust destructive QI effect with respect to temperature provides a remarkable advantage for the realization of single electron QI transistors at room temperature.[25] To understand the interdot correlation effect, we also plot the case without interdot Coulomb interaction ($U_{\ell,j} = 0$) for $k_BT = 0$ in Fig.2.10(a). (See solid curve) We notice that the QI effect remains qualitatively the same, except that the tunneling current is slightly enhanced with interdot Coulomb interaction turned off. As the QI effect suppresses the current flow, the charge will accumulate in the left dot. Thus, $N_{L,\sigma}$ reaches the maximum at $\Delta_C = \Delta_{QI}$ while N_R reaches the minimum as seen in Fig.2.10(b). This implies that the QI effect can be utilized to control charge storage in TQDM.

2.6 Application: Quantum interference and structure-dependent orbital-filling effects on the thermoelectric properties of quantum dot molecules

The quantum interference and orbital filling effects on the thermoelectric (TE) properties of quantum dot molecules with high figure of merit are illustrated via the full solution to the Hubbard-Anderson model in the Coulomb blockade regime.[12] It is found that under certain condition in the triangular QD molecule (TQDM), destructive quantum interference (QI) can occur, which leads to vanishing small electrical conductance, while the Seebeck coefficient is modified dramatically. When TQDM is in the charge localization state due to QI, the Seebeck coefficient is seriously suppressed at low temperature, but highly enhanced at high temperature. Meanwhile, the behavior of Lorenz number reveals that it is easier to block charge transport via destructive QI than the electron heat transport at high temperatures. The maximum power factor (PF) in TQDM occurs at full-filling condition. Nevertheless, low-filling condition is preferred for getting maximum PF in serially coupled triple QDs in general. In double QDs, the maximum PF can be achieved either with orbital-depletion or orbital-filling as a result of electron-hole symmetry. Our theoretical work provides a useful guideline for advancing the nanoscale TE technology.

Chapter 3

Graphene nanoribbon quantum dot qubits

3.1 Method

3.1.1 One-particle problem

Consider a graphene nanoribbon (GNB) with width W and length L and armchair boundary conditions. Let the x-axis be the direction across the width of the nanoribbon and the y-axis be the direction parallel to the length of the ribbon. The low-energy behavior of an electron in this system can be described by the Dirac equation [13, 38, 39]

$$H_1|\psi\rangle = \frac{\epsilon}{\hbar v q_0}|\psi\rangle \tag{3.1}$$
$$H_1 = \frac{-i}{q_0}\begin{pmatrix} \sigma_x\partial_x + \sigma_y\partial_y & 0 \\ 0 & -\sigma_x\partial_x + \sigma_y\partial_y \end{pmatrix} + \frac{V(y)}{\hbar v q_0},$$

where $\hbar$ is Planck's constant, v is the Fermi velocity of graphene, $q_0 = \frac{\pi}{3W}$ is a characteristic momentum that will be explained below, σ_x, σ_y are Pauli matrices, ∂_x, ∂_y are partial derivatives, and $V(y)$ is the electrical confining potential along the y-axis. In this work, $1/q_0$ is the characteristic length scale and $\hbar v q_0$ is a characteristic energy scale. $|\psi\rangle$ is a 4-component spinor in the form

$$|\psi\rangle = \begin{pmatrix} \psi(K, A) \\ \psi(K, B) \\ -\psi(K', A) \\ -\psi(K', B) \end{pmatrix}, \tag{3.2}$$

where K, K' label the two valleys in the Brillouin zone of graphene, A, B label the two sublattices of graphene, and ψ is the envelope function.

We use the basis expansion of the electron envelope function

$$|\psi\rangle = \sum_{m,s,n} \phi_s^{m,n} |\psi_s^{m,n}\rangle \tag{3.3}$$

$$\langle x, y|\psi_s^{m,n}\rangle = \frac{1}{\sqrt{2WL}} \begin{pmatrix} \chi_s e^{iq_n x} \\ \chi_s e^{-iq_n x} \end{pmatrix} f_m(y), \tag{3.4}$$

where $\{f_m(y)\}$ is a set of basis functions of variable y, $s = A, B$ denotes the two sublattices, and the constant two-component spinors are

$$\chi_A = \begin{pmatrix} 1 \\ 0 \end{pmatrix} \tag{3.5}$$

$$\chi_B = \begin{pmatrix} 0 \\ 1 \end{pmatrix}. \tag{3.6}$$

The boundary conditions are

$$\langle x, y|\psi\rangle|_{x=0} = \begin{pmatrix} 0 & 1 \\ 1 & 0 \end{pmatrix} \langle x, y|\psi\rangle|_{x=0} \tag{3.7}$$

$$\langle x, y|\psi\rangle|_{x=W} = \begin{pmatrix} 0 & e^{+i\frac{2\pi\mu}{3}} \\ e^{-i\frac{2\pi\mu}{3}} & 0 \end{pmatrix} \langle x, y|\psi\rangle|_{x=W}, \tag{3.8}$$

where $\mu = \pm 1, 0$ is a constant determined by the width of the ribbon. $\mu = \pm 1$ defines the semiconducting boundary condition. In Eqs. (3.7) and (3.8), each number in the matrices should be understood as the number times a 2×2 identity matrix. Imposing the semiconducting boundary conditions on the basis functions leads to quantization of the electronic states in the x-direction

$$q_n = \frac{\pi}{W}(n + \frac{\mu}{3}), n \in \mathbb{Z} \tag{3.9}$$

$$= (3n + \mu)q_0, \tag{3.10}$$

where the momentum scale $q_0 = \frac{\pi}{3W}$ is defined. We consider only the condition $n = 0$ and $\mu = +1$ throughout this paper.

The basis functions $f_m(y)$ are chosen to be sinusoidal functions confined within the interval $[0, L]$,

$$f_m(y) \quad = \quad \sqrt{2}\sin(\frac{\pi m y}{L}). \tag{3.11}$$

The matrix elements of the one-particle Hamiltonian and the overlap matrix can then be written down analytically. The equation of motion then becomes a generalized eigenvalue problem

$$\sum_{ms}\langle\psi_{s'}^{m'n}|H_1|\psi_s^{m,n}\rangle\phi_s^{m,n} = \frac{\epsilon}{\hbar v q_0}\sum_{ms}\langle\psi_{s'}^{m'n}|\psi_s^{m,n}\rangle\phi_s^{m,n}, \tag{3.12}$$

which is solved using a numerical solver.

3.1.2 Two-particle problem

To evaluate the exchange coupling between two qubits, we need to consider the mutual Coulomb interaction and exchange term between two electrons localized in neighboring GNB quantum dots. The Coulomb interaction in two-dimension is

$$v_{ee} = \frac{e^2}{4\pi\epsilon\hbar v}\frac{1}{q_0}\frac{1}{\sqrt{(x_1-x_2)^2+(y_1-y_2)^2}},$$

where $\frac{e^2}{4\pi\epsilon\hbar v}$ is the dimensionless Coulomb parameter, i.e., the fine-structure constant of graphene. One expects $\frac{e^2}{4\pi\epsilon\hbar v} = 2.2$ or smaller values for a suspended graphene.[80–82] In this work we use $\frac{e^2}{4\pi\epsilon\hbar v} = 1.43$ for graphene on quartz substrate. [80]

We apply the unrestricted Hartree-Fock method for the generalized-valence-bond wave function [45] to solve the two-particle problem. The spatial part of the singlet($+$) and triplet($-$) wave functions are

$$|\psi_\pm\rangle = \frac{1}{\sqrt{2(1\pm S^2)}}(|\phi_L,\phi_R\rangle \pm |\phi_R,\phi_L\rangle), \tag{3.13}$$

where $S = |\langle\phi_L|\phi_R\rangle|$. The Hamiltonian is

$$H = H_1\otimes 1 + 1\otimes H_1 + v_{ee}. \tag{3.14}$$

The Schrodinger equation is

$$H|\psi_\pm\rangle \quad = E|\psi_\pm\rangle. \tag{3.15}$$

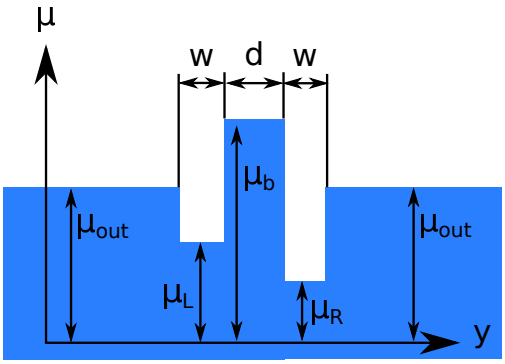

Figure 3.1: Double well potential profile along the graphene ribbon length. The size of each well is lowercase w, the well-to-well separation distance is d, the barrier outside both wells is μ_{out}, the barrier potential height is μ_b, and the potential heights of the left well and right well are μ_{wL} and μ_{wR}, respectively. Figure borrowed from Chen and Chang [14].

In each iteration, given ϕ_R, we solve for

$$\langle n', \phi_R|H|\psi_\pm\rangle \quad = E\langle n', \phi_R|\psi_\pm\rangle. \tag{3.16}$$

Given the expansion of $|\phi_L\rangle$ within an non-orthonormal basis set $\{|n\rangle\}$ and choosing normalized $|\phi_R\rangle$, the generalized eigenvalue problem to be solved is

$$\langle n'|H_{GVB}|n\rangle\langle n|\phi_L\rangle = E\langle n'|S_{GVB}|n\rangle\langle n|\phi_L\rangle, \tag{3.17}$$

where the Hamiltonian and overlap matrices elements are

$$\begin{aligned}
\langle n'|H_{GVB}|n\rangle &= \langle n'|H_1|n\rangle + \langle n'|n\rangle\langle\phi_R|H_1|\phi_R\rangle \qquad (3.18)\\
&\pm \langle n'|H_1|\phi_R\rangle\langle\phi_R|n\rangle \pm \langle n'|\phi_R\rangle\langle\phi_R|H_1|n\rangle\\
&+ \langle n', \phi_R|v_{ee}|n, \phi_R\rangle \pm \langle n', \phi_R|v_{ee}|\phi_R, n\rangle\\
\langle n'|S_{GVB}|n\rangle &= \langle n'|n\rangle \pm \langle n'|\phi_R\rangle\langle\phi_R|n\rangle. \qquad (3.19)
\end{aligned}$$

The iteration continues until self-consistency is reached. For the triplet state, we carry out the reorthonormalization and projection procedure described in Fang *et al.* [45] to resolve the linear-dependence problem in the generalized eigenvalue problem.

3.1.3 The double well model

We model a GNB double-dot system by a double square well potential in the y-direction, as shown in Fig. 3.1. Unless specified, we use the following parameters throughout this work. The physical parameters used in the model are those reported in the experimental study by Liu *et al.* [83] The width of the ribbon is $W = 20(nm) \sim 1q_0^{-1}$, and hence our characteristic energy is $\hbar v q_0 \sim 32.9(meV)$. The length of the ribbon is $L = 800(nm) \sim 40q_0^{-1}$. The width of each dot (i.e., the width of each confining well) is $w = 4q_0^{-1}$. The separation between the dots (i.e., the width of the potential barrier between two dots) is d. The electric potential of the left dot, right dot, barrier, and outside region is given by μ_L, μ_R, μ_b, and μ_{out}, respectively. We use $\mu_{out} = 1.5\hbar v q_0 = 49.4(meV)$ as suggested by previous theoretical work. [13] The potential of the left dot and the right dot are fixed to $\mu_L = \mu_R = 0$, and the Fermi energy is fixed to $E_F/\hbar v q_0 = 1$. The number of sinusoidal basis functions used is 50.

3.2 Results and Discussion

3.2.1 Single particle solutions

We first examine the single-particle behavior of single and double potential wells. Figure 3.2(a) shows the single-particle energy levels as functions of confining potential height μ_{out} for a single confining well, where the width of the well is $q_0 w = 2$ and the length of the ribbon is $q_0 L = 16$. For small confining potentials (the left upper triangle region), the potential is not high enough to confine the electron. Hence this region contains many lines which are the states of the discretized continuous conduction band. The discretization is caused by the finite length (L) of GNB considered. For higher confining potential (the middle region), there are 3 quantized levels, which is in consistent with the results given in Trauzettel *et al.* [13] For higher confining potentials (the right lower triangle region), the energies of conduction band electrons in the well become coincide with the valence band of the barrier, and hence the region contains many lines consisting of the discretized Klein tunneling states.

Figure 3.2(b) shows energy levels as functions of inter-well distance for a double square well potential. The width of the wells is $q_0 w = 4$. This data involves the information of some high energy excited states, so the number of sinusoidal basis functions used in this calculation is 100 for higher accuracy. Above the energy of the valence band maximum (VBM) of the barrier (black dotted line), there are the ground state (blue solid), 1st-excited state (blue dashed), 2nd-excited (green solid), 3rd-excited (green dashed), 4th-excited (red solid), 5th-excited (red dashed) energy levels. The ground state is very close to the barrier VBM, and one expects to see the enhancement of inter-well coupling due to Klein tunneling in this regime.

Figure 3.2(c) shows the energy gaps $\Delta E_m = E_{m+1} - E_m$ as as functions of inter-well distance for the same

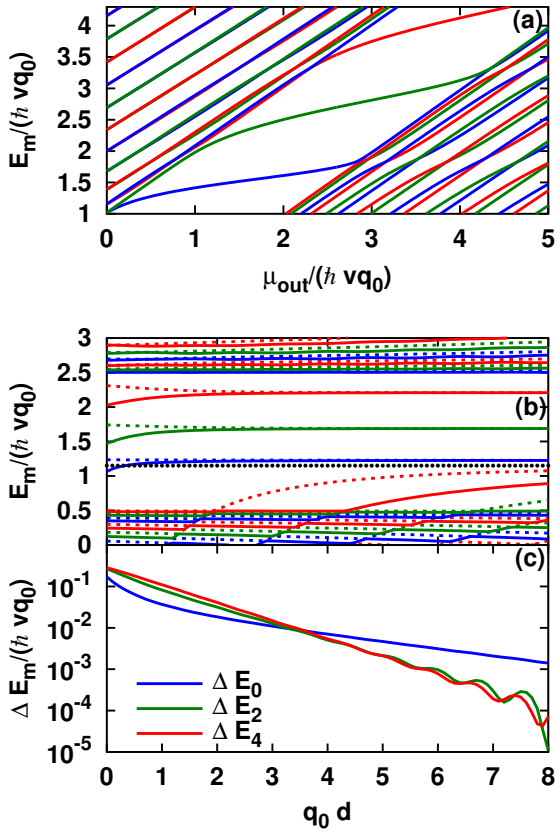

Figure 3.2: (a) Single particle energy levels as functions of confining potential height for a single well. The width of the well is $q_0 w = 2$. The quantized levels in the middle regime are in consistent with the results in Trauzettel *et al.* [13] The conducting states (states forming the left upper triangle) and the Klein tunneling states (states forming the right lower triangle) are also shown in our calculation. (b) Single particle energy levels as functions of inter-well distance for a double well. The width of the wells is $q_0 w = 4$. The ground state (solid blue) is generally above but very close to the top of the barrier valence band (dotted black), and hence is a Klien tunneling assisted localized state. (c) Energy gaps as functions of inter-well distance for a double well. The energy gaps are defined to be $\Delta E_m = E_{m+1} - E_m$. The gap between the ground state and the first-excited state (solid blue) decays slower than the other states. Figure borrowed from Chen and Chang [14].

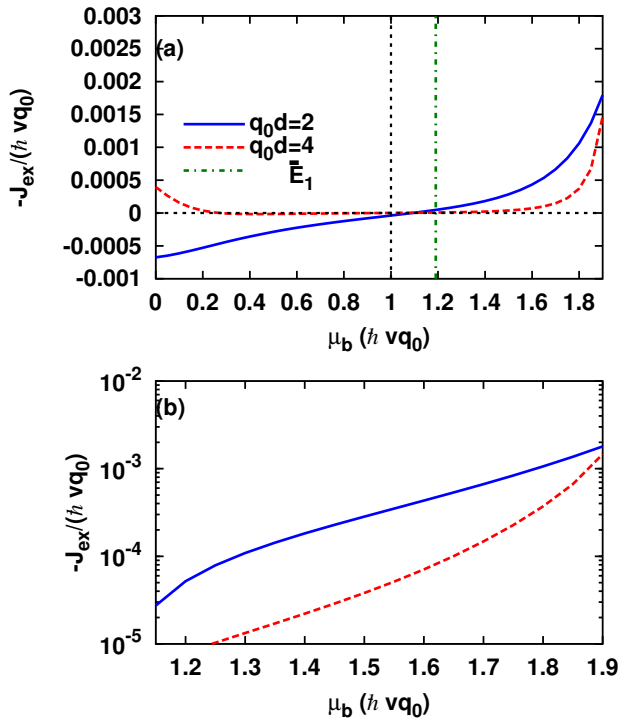

Figure 3.3: Negative exchange coupling $-J_{ex} = E_{singlet} - E_{triplet}$ as a function of the inter-well barrier potential height μ_b for well-to-well distance $q_0 d = 2$ (blue solid) and $q_0 d = 4$ (red dashed). (a) Linear plot. (b) Semi-log plot. Figure borrowed from Chen and Chang [14].

double square well potential in a semi-log scale. E_0 is the ground state energy, E_1 is the 1st-excited state energy ...etc. Linear curves in the semi-log scale indicate that the gaps decay exponentially with the well-to-well distance. For small separation d, the ground state gap ΔE_0 is smaller than the excited state gaps $\Delta E_m, m = 2, 4$, but the decay length increases as d increases. For long distance $q_0 d > 4$, the ground state gap becomes larger than the excited state gaps, indicating the ground state gap has a smaller decay rate comparing to the excited state gaps. This suggests that the long-distance coupling is enhanced by the Klein tunneling for the single-particle wave function, consistent with the prediction in Ref. Trauzettel *et al.* [13].

3.2.2 Effects of barrier height on the exchange coupling between two qubits

Here, we study the effects of barrier height on the exchange coupling between two electrons in the GNB double well. Figure 3.3(a) shows the negative exchange splitting $-J_{ex} = E_{singlet} - E_{triplet}$ as a function of barrier potential height μ_b. For small barrier heights, the negative exchange splitting can be either negative ($q_0 d = 2$, blue solid) or positive ($q_0 d = 4$, red dashed) depending on the well-to-well separation $q_0 d$. For small barrier heights, the potential profile is a single confining well instead of double well. A singlet-triplet ground state transition is expected for barrier

Table 3.1: Singlet total energy $E_{singlet}$, triplet total energy $E_{triplet}$, and triplet single particle energy E_1 for some selected inter-dot distance $q_0 d$ and barrier height $\mu_b/\hbar v q_0$.

$q_0 d$	$\mu_b/\hbar v q_0$	$E_{singlet}/\hbar v q_0$	$E_{triplet}/\hbar v q_0$	$E_1/\hbar v q_0$
2	1.5	2.63897	2.63869	1.20982
2	1.9	2.65891	2.65711	1.21937
4	1.5	2.57493	2.57489	1.20796
4	1.9	2.59815	2.59668	1.21833
8	1.5	2.51309	2.51309	1.20725
8	1.9	2.53504	2.53501	1.21845

heights lower than a critical value, which shall be discussed further in Section 3.2.3. In this section we focus on the regime in which the barrier height is larger than or equal to the critical value. In our model, the critical value can be estimated by comparing the barrier height with both the single-particle ground state energy and the bottom of the conduction bands associated with the wells. In Fig. 3.3(a), the green dashed line marks the point when μ_b crosses $\langle H_1 \rangle$, the expectation value of H_1 in the triplet solution for $q_0 d = 2$, which has a weak dependence on μ_b. We label this point by $\bar{E}_1$. $\bar{E}_1$ happens to be almost the same as the average of $\langle H_1 \rangle$ over μ_b for μ_b from 0 to $2\hbar v q_0$. The black dashed line indicates where the barrier height equals to the bottom of the conduction bands of the wells, which is at $1\hbar v q_0$. The critical value lies somewhere between $1\hbar v q_0$ and $\bar{E}_1$. For μ_b larger than the critical value $\sim 1.1\hbar v q_0$, $-J_{ex}$ is always positive, and increases monotonically up to $\mu_b/\hbar v q_0 = 1.9$.

Figure 3.3(b) shows the negative exchange coupling for $\mu_b > 1.1\hbar v q_0$ on a semi-log scale. The negative exchange coupling grows exponentially for $q_0 d = 2$, and super-exponentially for $q_0 d = 4$. The coupling for $q_0 d = 4$ can be almost as large as $q_0 d = 2$ as μ_b reaches $1.9\hbar v q_0$. The exchange coupling of $q_0 d = 2$ (blue solid) is linear in the semi-log plot, which indicates an exponential growth. For a longer well-to-well separation, $q_0 d = 4$, one can see super-exponential growth of the exchange coupling. For $q_0 d = 4$ and $\mu_b > 1.92\hbar v q_0$, the electrons in the singlet state are in the first-excited single-particle state of both dots, while the electrons in the triplet state are still in the single-particle ground state. The exchange coupling can not be defined in this case.

The super-exponential growth for larger well-to-well distances in Fig. 3.3(b) is a special characteristic of a graphene quantum dot. The overlap between the wave functions of the electrons in the left dot and the right dot is expected to be enhanced by Klein tunnelling of Dirac fermions when the valence band of the barrier region is close to the single-particle energy. [13] This long-distance coupling of Dirac fermions is suggested as a possible advantage of the graphene quantum dot qubit over traditional constructions. In the graphene qubit, the exchange coupling for the long distance case, $q_0 d = 4$, is almost as large as that in the short distance case, $q_0 d = 2$, as the barrier potential approaches $\mu_b/\hbar v q_0 = 2$. This result implies that the top of the valence band in the barrier regions approaches the bottom of the well conduction band at $1\hbar v q_0$. This result supports the proposal in Trauzettel *et al.* [13]

This overlap enhancement is explicitly shown in Fig. 3.4, where the normalized charge density $\rho_{\pm}(y_1) = |\langle y_1 | \psi_{\pm} \rangle|^2$

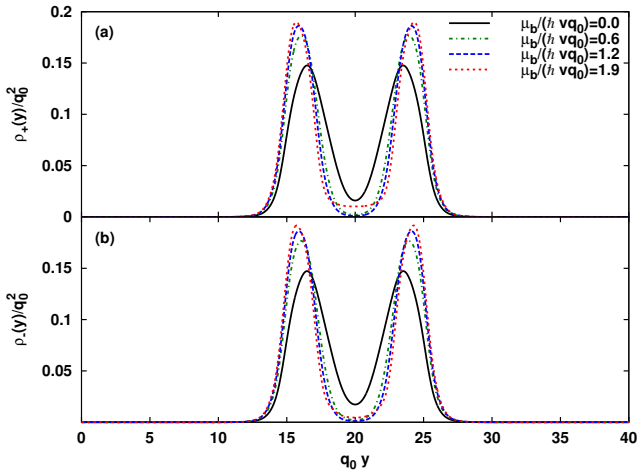

Figure 3.4: Normalized charge density along the ribbon for the case $q_0 d = 4$ for (a) singlet state and (b) triplet state for various barrier potential strengths. $\mu_b/\hbar v q_0 = 0$ (black solid), $\mu_b/\hbar v q_0 = 0.6$ (green dash-dot), $\mu_b/\hbar v q_0 = 1.2$ (blue dashed), $\mu_b/\hbar v q_0 = 1.9$ (red dotted). The density in the barrier region decreases as $\mu_b/\hbar v q_0$ increasing from zero to 0.6 and 1.2, but increases as $\mu_b/\hbar v q_0$ further increasing to a higher value 1.9. The increment of density in the barrier region is larger for the singlet state than that of the triplet state. Figure borrowed from Chen and Chang [14].

is plotted as a function of y-coordinate for singlet and triplet states for various barrier heights. The electron density is mainly localized in the two potential wells. The charge density between two wells decreases as the barrier potential is raised from zero (black solid) to $\mu_b/\hbar v q_0 = 0.6$ (green dash-dot) and $\mu_b/\hbar v q_0 = 1.2$ (blue dashed). However, as the barrier height is raised to a higher value $\mu_b/\hbar v q_0 = 1.9$ (red dotted), the charge density between the wells increases.

This counter-intuitive behavior due to Klein tunnelling is a characteristic of Dirac fermions. As the barrier height approaches $\mu_b/\hbar v q_0 = 2$, the VBM of the barrier is aligned with the conduction band minimum in the well. This leads to an enhancement of the overlap between the two electrons. The enhancement for singlet state is stronger than that for the triplet state, which leads to an increase of the singlet-triplet energy splitting. This result is in agreement with the result shown in Fig. 3.3.

3.2.3 Effects of inter-dot distance on the exchange coupling between two qubits

Figure 3.5(a) shows the negative exchange coupling as a function of inter-dot distance for different barrier heights. In the absence of a barrier (red dash-dot), the negative exchange coupling starts with negative values and increases to positive values for $q_0 d > 3$. For $\mu_b/\hbar v q_0 = 1.5$ and $\mu_b = 1.9 \hbar v q_0$, the negative exchange splitting starts with a positive value, and decays exponentially for $q_0 d > 3$, as shown in Fig. 3.5(b).

For $\mu_b/\hbar v q_0 = 0$, there is no barrier and we only have one confining potential well. For $\mu_b = 0$, increasing d is the same as increasing the width of a single potential well (which equals to d+2w, as shown in Fig. 1). This situation has been studied using various first-principle calculations, as summarized in Rayne and Forest [84] The ground state is a

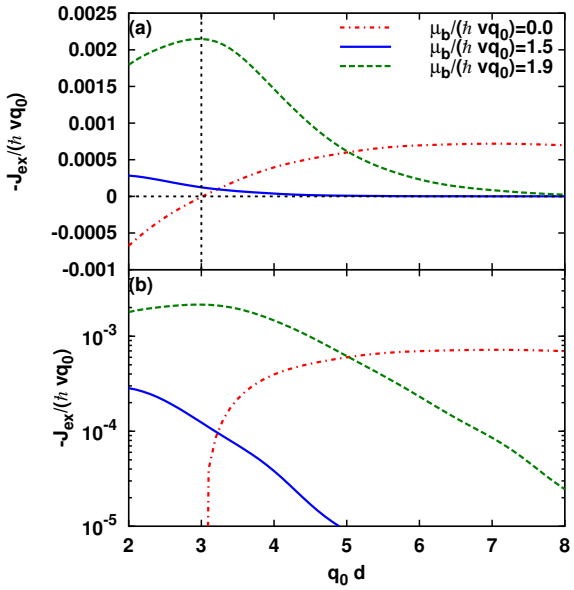

Figure 3.5: Negative exchange coupling $-J_{ex}$ as a function of well-to-well distance d for various barrier heights in (a) linear scale and (b) semi-log scale. $\mu_b/\hbar v q_0 = 0$ (red dash-dot), $\mu_b/\hbar v q_0 = 1.5$ (blue solid), $\mu_b/\hbar v q_0 = 1.9$ (green dashed). For zero barrier, the singlet-triplet ground state transition occurs roughly at critical distance $q_0 d_c \sim 3$ (black vertical dashed). For finite barrier, the negative exchange coupling decays exponentially for $q_0 d > 3$. Figure borrowed from Chen and Chang [14].

singlet for a short ribbon, and a triplet for a long ribbon. Our result is consistent to the previous studies. In particular, the red dash-dot line is similar to Fig. 2(a) in Rayne and Forest [84] In our calculation, the singlet-triplet ground state transition occurs roughly at the critical distance $q_0 d_c \sim 3$, which is labelled by the black vertical dashed line. For larger barrier heights, the singlet state has a larger density at the barrier region and hence has higher energy. This is why the triplet state is the ground state and the negative exchange coupling is always positive for $\mu_b/\hbar v q_0 = 1.5$ and $\mu_b/\hbar v q_0 = 1.9$.

For medium barrier height $\mu_b/\hbar v q_0 = 1.5$, the exchange coupling decreases exponentially when the inter-dot distance increases, as shown in Fig. 3.5. For higher barrier height $\mu_b/\hbar v q_0 = 1.9$, where Klein paradox assisted tunneling occurs, the negative exchange coupling is generally larger than that for $\mu_b/\hbar v q_0 = 1.5$. For small values of $q_0 d$, the negative exchange coupling increases with increasing separation before reaching the singlet-triplet ground state transition point $q_0 d_c \sim 3$. For inter-dot distances longer than the critical distance $q_0 d_c \sim 3$, we see the expected exponential decay. Hence in the Klein tunneling regime, the location of the maximum of the exchanged coupling can be roughly predicted by looking at the zero barrier height solution.

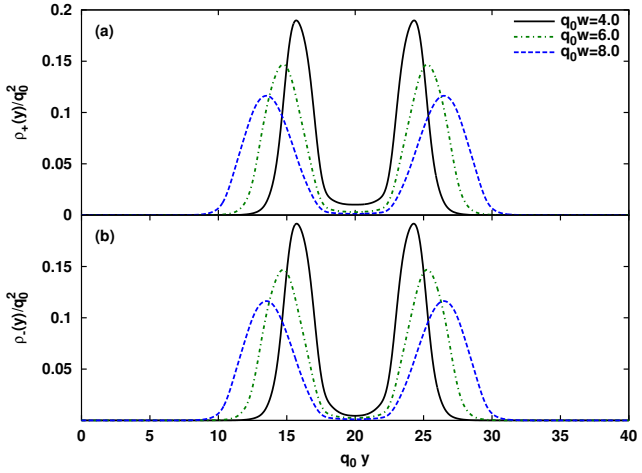

Figure 3.6: Normalized charge density along the ribbon of well-to-well separation $q_0 d = 4$ and $\mu_b/\hbar v q_0 = 1.9$ for (a) singlet state and (b) triplet state for various well widths. $q_0 w = 0$ (black solid), $q_0 w = 4$ (green dash-dot), $q_0 w = 8$ (blue dashed). Figure borrowed from Chen and Chang [14].

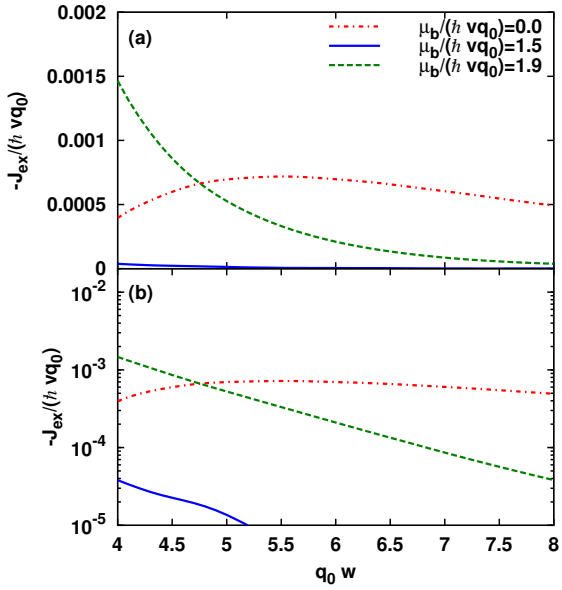

Figure 3.7: Negative exchange coupling $-J_{ex}$ as a function of well width w for various barrier heights in (a) linear scale and (b) semi-log scale. Figure borrowed from Chen and Chang [14].

3.2.4 Effects of well width on two-particle solutions

Figure 3.6 shows the charge density along the y-axis for various well widths for (a) the singlet states and (b) the triplet states. The inter-well distance is $q_0 d = 4$ and the barrier height is $\mu_b/\hbar v q_0 = 1.9$. For small well width $q_0 w = 4$ (black solid), the density in the barrier region for the singlet state is much higher than that of the triplet state. For larger well widths, the charge densities spread out from the center, and the difference of the charge densities between the singlet state and the triplet state in the barrier region is not significant. The absolute value of exchange coupling is hence expected to be large for small well width and small for large well width. This is shown in Fig. 3.7, where the negative exchange coupling is plotted as functions of well width $q_0 w$. For barrier height larger than the critical value $\mu_b/\hbar v q_0 = 1.5$ (blue solid) and $\mu_b/\hbar v q_0 = 1.9$ (green dashed), the exchange splitting decays exponentially, as shown in the semi-log scale in Fig. 3.7(b). The exchange splitting of $\mu_b/\hbar v q_0 = 1.9$ is much larger than that of $\mu_b/\hbar v q_0 = 1.5$ due to the Klein tunneling. For zero barrier height (red dash-dot), there is only a single confining well, and the curve is just the long-distance extension of the same curve (red dash-dot) in Fig. 3.5(a) discussed in the previous section.

Chapter 4

Conclusion

In summary, we use an exterior algebra construction for the equation of motion to solve for many-body fermionic Green's function numerically. This method can be applied to few-impurity Anderson model out of equilibrium. We have obtained full solution to the charge transport through TQDM junction in the presence of electron Coulomb interactions, which includes all n-electron ($n = 1, \cdots, 6$) Green's functions and correlation functions. The destructive and constructive QI behaviors of TQDM are clarified by considering the LDCT effect on the conductance spectrum. The conductance spectrum of TQDM with total occupation number varying from one to six directly reveals the electron-hole asymmetry due to topological effect. The calculated correlation functions also illustrate the charge fluctuation and spin frustration behaviors of TQDM. Our numerical results for charge stability diagram match experimental measurements very well. Finally, we demonstrated that the QI effect in TQDM is robust against temperature variation and it can be utilized to control the charge storage. We also apply this method to high figure of merit thermoelectric quantum dot devices.

We have performed theoretical studies of the electronic structures of graphene nanoribbon quantum dot qubits using the Dirac equation and a double square well potential. The two electron wave functions and exchange splitting are calculated for various potential configurations using a generalized-valence-bond wave function within the unrestricted Hartree-Fock approximation. As the barrier height approaches $2\hbar v q_0$ (the band gap of the nanoribbon), the magnitude of the exchange coupling is enhanced by the Klein tunneling. This enhancement can make the long distance coupling almost as large as the short distance coupling. At zero barrier height, the distance dependence of the exchange coupling is in consistent with the results given by previous first-principle studies. For higher barrier heights, the magnitude of the exchange coupling decays, but can be magnified by the Klein tunneling at higher barrier heights. For small wells size the negative exchange coupling is larger than that of large well sizes.

Appendix A

Details for EOMPACK code

A.1 Derivation of the EOM

Let's derive the exact equation of motion of the many-particle Green's function

$$G^{(n)}_{i_1 i_2 \ldots i_{2n}}(t,t') = -i\langle T[d^\dagger_{i_1}(t)\ldots d^\dagger_{i_{n-1}}(t) d_{i_n}(t)\ldots d_{i_{2n-1}}(t) d^\dagger_{i_{2n}}(t')]\rangle, \tag{A.1}$$

for the general quartic Hamiltonian

$$H_0 \quad = \sum_{ij=1}^{N} t_{ij} d^\dagger_i d_j + \sum_{i<j=1}^{N} U_{ij} n_i n_j. \tag{A.2}$$

The result is

$$\begin{aligned} i\partial_t G^{(n)}_{i_1\ldots i_{2n}}(t,t') = \quad & \delta(t-t') \sum_{\mu=n}^{2n-1} (-1)^{(\mu+1)} \delta_{i_\mu, i_{2n}} \langle d^\dagger_{i_1}\ldots d^\dagger_{i_{n-1}} d_{i_n}\ldots d_{i_{\mu-1}} d_{i_{\mu+1}}\ldots d_{i_{2n-1}}\rangle \\ & + (-\sum_{\mu=1}^{n-1}\sum_{j} \bar{t}_{i_\mu j} + \sum_{\mu=n}^{2n-1}\sum_{j} t_{i_\mu j}) G^{(n)}_{i_1\ldots i_{\mu-1} j i_{\mu+1}\ldots i_{2n-1} i_{2n}}(t,t') \\ & + (-\sum_{\mu=1}^{n-1}\sum_{\nu=\mu+1}^{n-1} U_{i_\mu i_\nu} + \sum_{\mu=n}^{2n-1}\sum_{\nu=n}^{\mu-1} U_{i_\mu i_\nu}) G^{(n)}_{i_1\ldots i_{2n}}(t,t') \\ & + (-\sum_{\mu=1}^{n-1} + \sum_{\mu=n}^{2n-1}) \sum_{j} U_{i_\mu j} G^{(n+1)}_{i_1\ldots i_{n-1} j j i_n\ldots i_{2n-1} i_{2n}}(t,t'). \end{aligned} \tag{A.3}$$

All the definitions are the same as that of Section 2.2.

The derivation is divided into 3 parts:

1. The term generated by the tight-binding (quadratic) Hamiltonian (which should be proportional to t_{ij}, and we call it (t-term)).

2. The term generated by the two-particle interaction (quartic) terms (which gives all the terms proportional to U_{ij}, and we call it (U-term)).

3. The contact term generated by differentiate the time-ordering product (which gives the expectation values, and we call it (c-term)).

We denotes each term such that $i\partial_t G^{(n)}_{i_1\ldots i_{2n}} =$ (t-term) + (U-term) + (c-term).

Differentiation the operators with respect to time generates the commutators with the Hamiltonian. In this part we calculate the commutator with the tight-binding Hamiltonian

$$H_t = \sum_{ij=1}^{N} t_{ij} d_i^\dagger d_j. \tag{A.4}$$

It gives

$$i\partial_t d_k(t) = \sum_{j=1}^{N} t_{kj} d_j(t) \tag{A.5}$$

$$i\partial_t d_k^\dagger(t) = \sum_{j=1}^{N} -\bar{t}_{kj} d_j^\dagger(t). \tag{A.6}$$

So in general,

$$\begin{aligned} i\partial_t(d_{i_1}^\dagger \ldots d_{i_{n-1}}^\dagger d_{i_n}\ldots d_{i_{2n-1}}(t)) &= -\sum_{\mu=1}^{n-1}\sum_j \bar{t}_{i_\mu j}(d_{i_1}^\dagger\ldots d_{i_{\mu-1}}^\dagger d_j^\dagger d_{i_{\mu+1}}^\dagger\ldots d_{i_{n-1}}^\dagger d_{i_n}\ldots d_{i_{2n-1}}(t)) \\ &\quad + \sum_{\mu=n}^{2n-1}\sum_j t_{i_\mu j}(d_{i_1}^\dagger\ldots d_{i_{n-1}}^\dagger d_{i_n}\ldots d_{i_\mu - 1} d_j d_{i_\mu+1}\ldots d_{i_{2n-1}}(t)). \end{aligned} \tag{A.7}$$

This gives the result

$$\text{(t-term)} = (-\sum_{\mu=1}^{n-1}\sum_j \bar{t}_{i_\mu j} + \sum_{\mu=n}^{2n-1}\sum_j t_{i_\mu j}) G^{(n)}_{i_1\ldots i_{\mu-1} j i_{\mu+1}\ldots i_{2n-1} i_{2n}}(t,t'). \tag{A.8}$$

In this part we calculate the commutator with the two-particle interaction Hamiltonian (for simplicity, we assume U is real symmetric and diagonal elements are zeros),

$$H_U = \sum_{i<j=1}^{N} U_{ij} n_i n_j. \tag{A.9}$$

It gives

$$i\partial_t d_k(t) = \sum_{j\neq k} U_{kj} d_k n_j(t) \tag{A.10}$$

$$i\partial_t d_k^\dagger(t) = -\sum_{j\neq k} U_{kj} d_k^\dagger n_j(t), \tag{A.11}$$

So in general,

$$\begin{aligned} i\partial_t(d_{i_1}^\dagger ... d_{i_{n-1}}^\dagger d_{i_n} ... d_{i_{2n-1}}(t)) &= -\sum_{\mu=1}^{n-1}\sum_j U_{i_\mu j}(d_{i_1}^\dagger ... d_{i_\mu}^\dagger d_j^\dagger d_j d_{i_{\mu+1}}^\dagger ... d_{i_{n-1}}^\dagger d_{i_n} ... d_{i_{2n-1}}(t)) \\ &+ \sum_{\mu=n}^{2n-1}\sum_j U_{i_\mu j}(d_{i_1}^\dagger ... d_{i_{n-1}}^\dagger d_{i_n} ... d_{i_\mu} d_j^\dagger d_j d_{i_{\mu+1}} ... d_{i_{2n-1}}(t)). \end{aligned} \tag{A.12}$$

To simplify this, we try to move the operators to keep things normal-ordered. What is going to happen is that the anti-commutation relation generates some n-particle terms, which contribute to the shift of poles in the Green's functions due to two-particle interactions. We focus on the first term, and recursively calculate the anti-commutations,

$$d_j d_{i_{\mu+1}}^\dagger ... d_{i_{n-1}}^\dagger = (\delta_{j,i_{\mu+1}} - d_{i_{\mu+1}}^\dagger d_j) d_{i_{\mu+2}}^\dagger ... d_{i_{n-1}}^\dagger \tag{A.13}$$

$$= \delta_{j,i_{\mu+1}} d_{i_{\mu+2}}^\dagger ... d_{i_{n-1}}^\dagger - d_{i_{\mu+1}}^\dagger (\delta_{j,i_{\mu+2}} - d_{i_{\mu+2}}^\dagger d_j) ... d_{i_{n-1}}^\dagger \tag{A.14}$$

$$= ...$$

$$= (-1)^{n-\mu-1} d_{i_{\mu+1}}^\dagger ... d_{i_{n-1}}^\dagger d_j + \sum_{\nu=\mu+1}^{n-1} (-1)^{\nu-\mu-1} d_{i_{\mu+1}}^\dagger ... d_{i_{\nu-1}}^\dagger \delta_{j,i_\nu} d_{i_{\nu+1}}^\dagger ... d_{i_{n-1}}^\dagger. \tag{A.15}$$

Plug it back to the first term, and we get two parts. The first part is simply

$$-\sum_{\mu=1}^{n-1}\sum_j U_{i_\mu j}(d_{i_1}^\dagger ... d_{i_{n-1}}^\dagger d_j^\dagger d_j d_{i_n} ... d_{i_{2n-1}}(t)). \tag{A.16}$$

The second part is

$$\begin{aligned} &-\sum_{\mu=1}^{n-1}\sum_{\nu=\mu+1}^{n-1}\sum_j (-1)^{\nu-\mu-1} U_{i_\mu j}(d_{i_1}^\dagger ... d_{i_\mu}^\dagger d_j^\dagger d_{i_{\mu+1}}^\dagger ... d_{i_{\nu-1}}^\dagger \delta_{j,i_\nu} d_{i_{\nu+1}}^\dagger ... d_{i_{n-1}}^\dagger d_{i_n} ... d_{i_{2n-1}}(t)) \\ &= -\sum_{\mu=1}^{n-1}\sum_{\nu=\mu+1}^{n-1} (-1)^{\nu-\mu-1} U_{i_\mu i_\nu}(d_{i_1}^\dagger ... d_{i_\mu}^\dagger d_{i_\nu}^\dagger d_{i_{\mu+1}}^\dagger ... d_{i_{\nu-1}}^\dagger d_{i_{\nu+1}}^\dagger ... d_{i_{n-1}}^\dagger d_{i_n} ... d_{i_{2n-1}}(t)) \end{aligned} \tag{A.17}$$

$$= -\sum_{\mu=1}^{n-1}\sum_{\nu=\mu+1}^{n-1} U_{i_\mu i_\nu}(d_{i_1}^\dagger ... d_{i_{n-1}}^\dagger d_{i_n} ... d_{i_{2n-1}}(t)). \tag{A.18}$$

So we finish the calculation for the first term. Now for the second term, we calculate the anti-commutations recursively,

$$
\begin{aligned}
d_{i_n}...d_{i_{\mu-1}}d_j^\dagger &= d_{i_n}...d_{i_{\mu-2}}(\delta_{j,i_{\mu-1}} - d_j^\dagger d_{i_{\mu-1}}) && \text{(A.19)}\\
&= d_{i_n}...d_{i_{\mu-2}}\delta_{j,i_{\mu-1}} - d_{i_n}...d_{i_{\mu-3}}(\delta_{j,i_{\mu-2}} - d_j^\dagger d_{i_{\mu-2}})d_{i_{\mu-1}} && \text{(A.20)}\\
&= ...\\
&= (-1)^{\mu-n}d_j^\dagger d_{i_n}...d_{i_{\mu-1}} + \sum_{\nu=n}^{\mu-1}(-1)^{\mu-1-\nu}d_{i_n}...d_{i_{\nu-1}}\delta_{i_\nu,j}d_{i_{\nu+1}}...d_{i_{\mu-1}}. && \text{(A.21)}
\end{aligned}
$$

Plug this back to the second term, we get two parts. The first part is simply

$$
+\sum_{\mu=n}^{2n-1}\sum_j U_{i_\mu j}(d_{i_1}^\dagger...d_{i_{n-1}}^\dagger d_j^\dagger d_j d_{i_n}...d_{i_{2n-1}}(t)). \tag{A.22}
$$

The second part is

$$
\begin{aligned}
&+\sum_{\mu=n}^{2n-1}\sum_{\nu=n}^{\mu-1}\sum_j(-1)^{\mu-1-\nu}U_{i_\mu j}(d_{i_1}^\dagger...d_{i_{n-1}}^\dagger d_{i_n}...d_{i_{\nu-1}}\delta_{i_\nu,j}d_{i_{\nu+1}}...d_{i_{\mu-1}}d_j d_{i_{\mu+1}}...d_{i_{2n-1}}(t))\\
&= +\sum_{\mu=n}^{2n-1}\sum_{\nu=n}^{\mu-1}(-1)^{\mu-1-\nu}U_{i_\mu i_\nu}(d_{i_1}^\dagger...d_{i_{n-1}}^\dagger d_{i_n}...d_{i_{\nu-1}}d_{i_{\nu+1}}...d_{i_{\mu-1}}d_{i_\nu}d_{i_{\mu+1}}...d_{i_{2n-1}}(t)) && \text{(A.23)}\\
&= +\sum_{\mu=n}^{2n-1}\sum_{\nu=n}^{\mu-1}U_{i_\mu i_\nu}(d_{i_1}^\dagger...d_{i_{n-1}}^\dagger d_{i_n}...d_{i_{2n-1}}(t)). && \text{(A.24)}
\end{aligned}
$$

Putting these together, we get a simple result

$$
\begin{aligned}
i\partial_t(d_{i_1}^\dagger...d_{i_{n-1}}^\dagger d_{i_n}...d_{i_{2n-1}}(t)) &= (-\sum_{\mu=1}^{n-1}\sum_{\nu=\mu+1}^{n-1} + \sum_{\mu=n}^{2n-1}\sum_{\nu=n}^{\mu-1})U_{i_\mu i_\nu}(d_{i_1}^\dagger...d_{i_{n-1}}^\dagger d_{i_n}...d_{i_{2n-1}}(t)) && \text{(A.25)}\\
&\quad +(-\sum_{\mu=1}^{n-1}\sum_j + \sum_{\mu=n}^{2n-1}\sum_j)U_{i_\mu j}(d_{i_1}^\dagger...d_{i_{n-1}}^\dagger d_j^\dagger d_j d_{i_n}...d_{i_{2n-1}}(t)).
\end{aligned}
$$

Finally we get

$$
\begin{aligned}
\text{(U-term)} = &+(-\sum_{\mu=1}^{n-1}\sum_{\nu=\mu+1}^{n-1}U_{i_\mu i_\nu} + \sum_{\mu=n}^{2n-1}\sum_{\nu=n}^{\mu-1}U_{i_\mu i_\nu})G^{(n)}_{i_1...i_{2n}}(t,t') && \text{(A.26)}\\
&+(-\sum_{\mu=1}^{n-1} + \sum_{\mu=n}^{2n-1})\sum_j U_{i_\mu j}G^{(n+1)}_{i_1...i_{n-1}jji_n...i_{2n-1}i_{2n}}(t,t').
\end{aligned}
$$

Differentiating the time-ordering product generates the expectation value of the anti-commutator

$$
\text{(c-term)} = \delta(t-t')\langle\{d_{i_1}^\dagger...d_{i_{n-1}}^\dagger d_{i_n}...d_{i_{2n-1}}, d_{i_{2n}}^\dagger\}(t)\rangle. \tag{A.27}
$$

There are two terms,

$$\{d^\dagger_{i_1}...d^\dagger_{i_{n-1}}d_{i_n}...d_{i_{2n-1}}, d^\dagger_{i_{2n}}\} \quad = d^\dagger_{i_{2n}}d^\dagger_{i_1}...d^\dagger_{i_{n-1}}d_{i_n}...d_{i_{2n-1}} + d^\dagger_{i_1}...d^\dagger_{i_{n-1}}d_{i_n}...d_{i_{2n-1}}d^\dagger_{i_{2n}}. \tag{A.28}$$

The strategy is to move the last creation operator $d^\dagger_{i_{2n}}$ in the second term to the left. This will eventually cancel out the first term. In the process of moving, the anti-commutation relation with the annihilation operators will generate some additional $(n-1)$-particle terms. We do this by applying the anti-commutation relation recursively:

$$\begin{aligned} d_{i_n}...d_{i_{2n-1}}d^\dagger_{i_{2n}} &= d_{i_n}...d_{i_{2n-2}}(\delta_{i_{2n-1},i_{2n}} - d^\dagger_{i_{2n}}d_{i_{2n-1}}) && \text{(A.29)}\\ &= d_{i_n}...d_{i_{2n-2}}\delta_{i_{2n-1},i_{2n}} - d_{i_n}...d_{i_{2n-3}}(\delta_{i_{2n-2},i_{2n}} - d^\dagger_{i_{2n}}d_{i_{2n-2}})d_{i_{2n-1}} && \text{(A.30)}\\ &= ... \\ &= (-1)^n d^\dagger_{i_{2n}}d_{i_n}...d_{i_{2n-1}} + \sum_{\mu=n}^{2n-1}(-1)^{(\mu+1)}d_{i_n}...d_{i_{\mu-1}}\delta_{i_\mu,i_{2n}}d_{i_{\mu+1}}...d_{i_{2n-1}}. && \text{(A.31)} \end{aligned}$$

This means

$$\begin{aligned} d^\dagger_{i_1}...d^\dagger_{i_{n-1}}d_{i_n}...d_{i_{2n-1}}d^\dagger_{i_{2n}} &= (-1)d^\dagger_{i_{2n}}d^\dagger_{i_1}...d^\dagger_{i_{n-1}}d_{i_n}...d_{i_{2n-1}} && \text{(A.32)}\\ &\quad + \sum_{\mu=n}^{2n-1}(-1)^{(\mu+1)}\delta_{i_\mu,i_{2n}}d^\dagger_{i_1}...d^\dagger_{i_{n-1}}d_{i_n}...d_{i_{\mu-1}}d_{i_{\mu+1}}...d_{i_{2n-1}}. \end{aligned}$$

The result is

$$\langle\{d^\dagger_{i_1}...d^\dagger_{i_{n-1}}d_{i_n}...d_{i_{2n-1}}, d^\dagger_{i_{2n}}\}\rangle \quad = \sum_{\mu=n}^{2n-1}(-1)^{(\mu+1)}\delta_{i_\mu,i_{2n}}\langle d^\dagger_{i_1}...d^\dagger_{i_{n-1}}d_{i_n}...d_{i_{\mu-1}}d_{i_{\mu+1}}...d_{i_{2n-1}}\rangle. \tag{A.33}$$

Hence the contact term is

$$\text{(c-term)} \quad = \delta(t-t')\sum_{\mu=n}^{2n-1}(-1)^{(\mu+1)}\delta_{i_\mu,i_{2n}}\langle d^\dagger_{i_1}...d^\dagger_{i_{n-1}}d_{i_n}...d_{i_{\mu-1}}d_{i_{\mu+1}}...d_{i_{2n-1}}\rangle. \tag{A.34}$$

The correlations can be obtained by the integral relation

$$\begin{aligned} \langle d^\dagger_{i_1}...d^\dagger_{i_n}d_{i_{n+1}}...d_{i_{2n}}\rangle &= \int\frac{d\epsilon}{2\pi i}G^{(n)<}_{i_2...i_{2n}i_1}(\epsilon) && \text{(A.35)}\\ &= \frac{1}{n!}\sum_{\mu=1}^{n}(-1)^{\mu+1}\int\frac{d\epsilon}{2\pi i}G^{(n)<}_{i_1...\widehat{i_\mu}...i_n i_{n+1}...i_{2n}i_\mu}(\epsilon)\,. && \text{(A.36)} \end{aligned}$$

In the second line, it is written in the anti-symmetric tensor expression.

A.2 Derivation of the matrix EOM

Given a vector space $V = \text{span}(\{e_1, ..., e_N\})$, we consider antisymmetric n-form spaces $\Lambda^{(n)}(V) = \text{span}(\{w^1 \wedge ... \wedge w^n\})$, where $w^j \in \Lambda^{(1)}(V)$. There are three basic maps associated with Lie derivatives, wedge product and interior product, respectively. For convenience, we will formulate these maps as the following.

For a given matrix f with matrix elements f_{mn}, there is a corresponding map $\hat{f} : \Lambda^{(1)}(V) \mapsto \Lambda^{(1)}(V)$ defined by $\hat{f} = f_{mn} e^m \otimes e_n$. There is a corresponding L-map $\hat{L} : \Lambda^{(n)} \mapsto \Lambda^{(n)}$ defined by the Leibniz rule

$$\hat{L}[f](w^1 \wedge ... \wedge w^n) = \sum_{\mu=1}^{n} w^1 \wedge ... \wedge w^{\mu-1} \wedge \hat{f}(w^\mu) \wedge w^{\mu+1} ... \wedge w^n, \tag{A.37}$$

where $w^j \in \Lambda^{(1)}(V)$ are some one-form. We can also define the wedge product map $\hat{\wedge} : \Lambda^{(n)} \mapsto \Lambda^{(n+1)}$ as

$$\hat{\wedge}_j(\cdot) = e^j \wedge (\cdot), \tag{A.38}$$

and the interior product $\hat{i} : \Lambda^{(n)} \mapsto \Lambda^{(n-1)}$ as

$$\hat{i}_j(w^1 \wedge ... \wedge w^n) = \sum_{\mu=1}^{n} (-1)^{\mu-1} w^1 \wedge ... \wedge w^{\mu-1} \wedge \hat{i}_j(w^\mu) \wedge w^{\mu+1} ... \wedge w^n \tag{A.39}$$

$$\hat{i}_j(e^k) = \delta_{j,k}. \tag{A.40}$$

We also define the associated maps on $\Lambda^{(n-1)} \otimes \Lambda^{(n)}$ tensor space by

$$\hat{K}[\hat{L}_1, \hat{L}_2] \equiv (-\hat{L}_1) \oplus \hat{L}_2 \tag{A.41}$$

$$= -\hat{L}_1 \otimes \mathbb{1} + \mathbb{1} \otimes \hat{L}_2 \tag{A.42}$$

$$\hat{K}[\hat{L}] \equiv \hat{K}[\hat{L}, \hat{L}], \tag{A.43}$$

where $\hat{L}_1$ and $\hat{L}_2$ are L-maps on $\Lambda^{(n-1)}$ and $\Lambda^{(n)}$, respectively. $\oplus$ here denotes the Kronecker sum, not the direct sum. $\mathbb{1}$ denotes an identity map. We will use the same notation for the maps associated with $V = \text{span}(\{e_1, ..., e_N\})$ and $\bar{V} = \text{span}(\{\bar{e}_1, ..., \bar{e}_N)\}$. The space on which they act should be clear from the order of the maps.

On the spaces

$$\Omega^{(n),(n)} \equiv \Lambda^{(n)} \otimes \Lambda^{(n)} \tag{A.44}$$

$$\Theta^{(n)} \equiv \Lambda^{(n-1)} \otimes \Lambda^{(n)} \otimes \Lambda^{(1)}, \tag{A.45}$$

we define the maps

$$\hat{\nabla}_t^{1(n)} \quad : \quad \Lambda^{(n-1)} \otimes \Lambda^{(n)} \otimes \Lambda^{(1)} \mapsto \Lambda^{(n-1)} \otimes \Lambda^{(n)} \otimes \Lambda^{(1)} \tag{A.46}$$

$$\hat{\nabla}_U^{2(n)} \quad : \quad \Lambda^{(n-1)} \otimes \Lambda^{(n)} \otimes \Lambda^{(1)} \mapsto \Lambda^{(n-1)} \otimes \Lambda^{(n)} \otimes \Lambda^{(1)} \tag{A.47}$$

$$\hat{\nabla}_U^{-(n+1)} \quad : \quad \Lambda^{(n)} \otimes \Lambda^{(n+1)} \otimes \Lambda^{(1)} \mapsto \Lambda^{(n-1)} \otimes \Lambda^{(n)} \otimes \Lambda^{(1)} \tag{A.48}$$

$$\hat{\nabla}^{+(n-1)} \quad : \quad \Lambda^{(n-1)} \otimes \Lambda^{(n-1)} \mapsto \Lambda^{(n-1)} \otimes \Lambda^{(n)} \otimes \Lambda^{(1)} \tag{A.49}$$

$$\hat{\nabla}^{<(n)} \quad : \quad \Lambda^{(n-1)} \otimes \Lambda^{(n)} \otimes \Lambda^{(1)} \mapsto \Lambda^{(n)} \otimes \Lambda^{(n)}. \tag{A.50}$$

The goal of this section is to compute the formulae in explicit indices for the following maps:

$$\hat{\nabla}_t^{1(n)} \quad = \quad \hat{K}[\hat{L}[\bar{t}], \hat{L}[t]] \otimes \mathbb{1} \tag{A.51}$$

$$\hat{\nabla}_U^{2(n)} \quad = \quad \sum_{jk} \frac{U_{jk}}{2} \hat{K}[\hat{L}[\eta_j] \cdot \hat{L}[\eta_k]] \otimes \mathbb{1} \tag{A.52}$$

$$\hat{\nabla}_U^{-(n+1)} \quad = \quad (-1)^{(n+1)} \sum_{jk} U_{jk} [\hat{K}[\hat{L}[\eta_j]] \cdot (\hat{i}_k \otimes \hat{i}_k)] \otimes \mathbb{1} \tag{A.53}$$

$$\hat{\nabla}^{+(n-1)} \quad = \quad (-1)^{(n-1)} \sum_j \mathbb{1} \otimes \hat{\wedge}_j \otimes \hat{\wedge}_j \tag{A.54}$$

$$\hat{\nabla}^{<(n)} \quad = \quad \frac{1}{n} \sum_j \hat{\wedge}_j \otimes \mathbb{1} \otimes \hat{i}_j, \tag{A.55}$$

acting on

$$\hat{G}^{(n)} = G^{(n)}_{i_1 \ldots i_{2n}} e^{i_1} \wedge \ldots \wedge e^{i_{n-1}} \otimes \bar{e}^{i_n} \wedge \ldots \wedge \bar{e}^{i_{2n-1}} \otimes e^{i_{2n}}. \tag{A.56}$$

A.2.1 $\hat{\nabla}_t^1$ map

$$\hat{\nabla}_t^1 G^{(n)} \tag{A.57}$$

$$= \frac{1}{(n-1)!n!} \sum_{i_1 \ldots i_{2n}} G^{(n)}_{i_1 \ldots i_{2n}} \hat{\nabla}_t^1 (e^{i_1} \wedge \ldots \wedge e^{i_{n-1}} \otimes \bar{e}^{i_n} \wedge \ldots \wedge \bar{e}^{i_{2n-1}} \otimes e^{i_{2n}}) \tag{A.58}$$

$$= \frac{1}{(n-1)!n!} \sum_{i_1 \ldots i_{2n}} G^{(n)}_{i_1 \ldots i_{2n}} (-\hat{L}[\bar{t}](e^{i_1} \wedge \ldots \wedge e^{i_{n-1}}) \otimes \bar{e}^{i_n} \wedge \ldots \wedge \bar{e}^{i_{2n-1}} \otimes e^{i_{2n}} \tag{A.59}$$

$$+ e^{i_1} \wedge \ldots \wedge e^{i_{n-1}} \otimes \hat{L}[t](\bar{e}^{i_n} \wedge \ldots \wedge \bar{e}^{i_{2n-1}}) \otimes e^{i_{2n}}) \tag{A.60}$$

$$= \frac{1}{(n-1)!n!} \sum_{i_1 \ldots i_{2n}} G^{(n)}_{i_1 \ldots i_{2n}} \tag{A.61}$$

$$\times (-\sum_{\mu=1}^{n-1} (e^{i_1} \wedge \ldots \wedge e^{i_{\mu-1}} \wedge (\sum_j \bar{t}_{j i_\mu} e^j) \wedge e^{i_{\mu+1}} \wedge \ldots \wedge e^{i_{n-1}}) \otimes \bar{e}^{i_n} \wedge \ldots \wedge \bar{e}^{i_{2n-1}} \otimes e^{i_{2n}} \tag{A.62}$$

$$+ \sum_{\mu=n}^{2n-1} e^{i_1} \wedge \ldots \wedge e^{i_{n-1}} \otimes (\bar{e}^{i_n} \wedge \ldots \wedge \bar{e}^{i_{\mu-1}} \wedge (\sum_j t_{j i_\mu} \bar{e}^j) \wedge \bar{e}^{i_{\mu+1}} \wedge \ldots \wedge \bar{e}^{i_{2n-1}}) \otimes e^{i_{2n}}). \tag{A.63}$$

Rename the dummy indices $j \leftrightarrow i_\mu$ to get the result

$$= \frac{1}{(n-1)!n!} \sum_{i_1 \ldots i_{2n}} (-\sum_{\mu=1}^{n-1} \sum_j \bar{t}_{i_\mu j} + \sum_{\mu=n}^{2n-1} \sum_j t_{i_\mu j}) G^{(n)}_{i_1 \ldots i_{\mu-1} j i_{\mu+1} \ldots i_{2n}} \tag{A.64}$$

$$\times e^{i_1} \wedge \ldots \wedge e^{i_{n-1}} \otimes \bar{e}^{i_n} \wedge \ldots \wedge \bar{e}^{i_{2n-1}} \otimes e^{i_{2n}}. \tag{A.65}$$

A.2.2 $\hat{\nabla}^2_U$ map

In the following keep in mind that $U_{jj} = 0$.

$$\hat{\nabla}^2_U G^{(n)} \tag{A.66}$$

$$= \frac{1}{(n-1)!n!} \sum_{i_1 \dots i_{2n}} G^{(n)}_{i_1 \dots i_{2n}} \hat{\nabla}^2_U (e^{i_1} \wedge \dots \wedge e^{i_{n-1}} \otimes \bar{e}^{i_n} \wedge \dots \wedge \bar{e}^{i_{2n-1}} \otimes e^{i_{2n}}) \tag{A.67}$$

$$= \frac{1}{(n-1)!n!} \sum_{i_1 \dots i_{2n}} G^{(n)}_{i_1 \dots i_{2n}} \tag{A.68}$$

$$\times \sum_{jk} \frac{U_{jk}}{2} (-\hat{L}[\eta_j] \cdot \hat{L}[\eta_k] (e^{i_1} \wedge \dots \wedge e^{i_{n-1}}) \otimes \bar{e}^{i_n} \wedge \dots \wedge \bar{e}^{i_{2n-1}} \otimes e^{i_{2n}} \tag{A.69}$$

$$+ e^{i_1} \wedge \dots \wedge e^{i_{n-1}} \otimes \hat{L}[\eta_j] \cdot \hat{L}[\eta_k] (\bar{e}^{i_n} \wedge \dots \wedge \bar{e}^{i_{2n-1}}) \otimes e^{i_{2n}}) \tag{A.70}$$

$$= \frac{1}{(n-1)!n!} \sum_{i_1 \dots i_{2n}} G^{(n)}_{i_1 \dots i_{2n}} \sum_{jk} \frac{U_{jk}}{2} \tag{A.71}$$

$$\times (-\hat{L}[\eta_j] (\sum_{\mu=1}^{n-1} e^{i_1} \wedge \dots \wedge e^{i_{\mu-1}} \wedge (\delta_{i_\mu k} e^k) \wedge e^{i_{\mu+1}} \wedge \dots \wedge e^{i_{n-1}}) \otimes \bar{e}^{i_n} \wedge \dots \wedge \bar{e}^{i_{2n-1}} \otimes e^{i_{2n}} \tag{A.72}$$

$$+ e^{i_1} \wedge \dots \wedge e^{i_{n-1}} \otimes \hat{L}[\eta_j] (\sum_{\mu=n}^{2n-1} \bar{e}^{i_n} \wedge \dots \wedge \bar{e}^{i_{\mu-1}} \wedge (\delta_{i_\mu k} \bar{e}^k) \wedge \bar{e}^{i_{\mu+1}} \wedge \dots \wedge \bar{e}^{i_{2n-1}}) \otimes e^{i_{2n}}) \tag{A.73}$$

$$= \frac{1}{(n-1)!n!} \sum_{i_1 \dots i_{2n}} G^{(n)}_{i_1 \dots i_{2n}} \sum_{j} \tag{A.74}$$

$$\times (-\hat{L}[\eta_j] (\sum_{\mu=1}^{n-1} \frac{U_{j i_\mu}}{2} e^{i_1} \wedge \dots \wedge e^{i_{n-1}}) \otimes \bar{e}^{i_n} \wedge \dots \wedge \bar{e}^{i_{2n-1}} \otimes e^{i_{2n}} \tag{A.75}$$

$$+ e^{i_1} \wedge \dots \wedge e^{i_{n-1}} \otimes \hat{L}[\eta_j] (\sum_{\mu=n}^{2n-1} \frac{U_{j i_\mu}}{2} \bar{e}^{i_n} \wedge \dots \wedge \bar{e}^{i_{2n-1}}) \otimes e^{i_{2n}}) \tag{A.76}$$

$$= \frac{1}{(n-1)!n!} \sum_{i_1 \dots i_{2n}} G^{(n)}_{i_1 \dots i_{2n}} \sum_{j} \tag{A.77}$$

$$\times (-(\sum_{\mu,\nu=1}^{n-1} \frac{U_{j i_\mu}}{2} e^{i_1} \wedge \dots \wedge e^{i_{\nu-1}} \wedge (\delta_{i_\nu j} e^j) \wedge e^{i_{\nu+1}} \wedge \dots \wedge e^{i_{n-1}}) \otimes \bar{e}^{i_n} \wedge \dots \wedge \bar{e}^{i_{2n-1}} \otimes e^{i_{2n}} \tag{A.78}$$

$$+ e^{i_1} \wedge \dots \wedge e^{i_{n-1}} \otimes (\sum_{\mu,\nu=n}^{2n-1} \frac{U_{j i_\mu}}{2} \bar{e}^{i_n} \wedge \dots \wedge \bar{e}^{i_{\nu-1}} \wedge (\delta_{i_\nu j} \bar{e}^j) \wedge \bar{e}^{i_{\nu+1}} \wedge \dots \wedge \bar{e}^{i_{2n-1}}) \otimes e^{i_{2n}}) \tag{A.79}$$

$$= \frac{1}{(n-1)!n!} \sum_{i_1 \dots i_{2n}} G^{(n)}_{i_1 \dots i_{2n}} (-\sum_{\mu,\nu=1}^{n-1} \frac{U_{i_\mu i_\nu}}{2} + \sum_{\mu,\nu=n}^{2n-1} \frac{U_{i_\mu i_\nu}}{2}) \tag{A.80}$$

$$\times e^{i_1} \wedge \dots \wedge e^{i_{n-1}} \otimes \bar{e}^{i_n} \wedge \dots \wedge \bar{e}^{i_{2n-1}} \otimes e^{i_{2n}}. \tag{A.81}$$

A.2.3 $\hat{\nabla}_U^-$ map

$$\nabla_U^- G^{(n+1)} \tag{A.82}$$

$$= \frac{1}{n!(n+1)!} \sum_{i_1 \dots i_{2n+2}} G^{(n+1)}_{i_1 \dots i_{2n+2}} \nabla_U^- (e^{i_1} \wedge \dots \wedge e^{i_n} \otimes \bar{e}^{i_{n+1}} \wedge \dots \wedge \bar{e}^{i_{2n+1}} \otimes e^{i_{2n+2}}) \tag{A.83}$$

$$= \frac{(-1)^{(n+1)}}{n!(n+1)!} \sum_{i_1 \dots i_{2n+2}} G^{(n+1)}_{i_1 \dots i_{2n+2}} \sum_{jk} U_{jk} K[L[\eta_j]]\{ \tag{A.84}$$

$$(\sum_{\mu=1}^{n} (-1)^{\mu-1} e^{i_1} \wedge \dots \wedge e^{i_{\mu-1}} \wedge \hat{i}_k(e^{i_\mu}) \wedge e^{i_{\mu+1}} \wedge \dots \wedge e^{i_n}) \otimes \tag{A.85}$$

$$(\sum_{\nu=n+1}^{2n+1} (-1)^{\nu-n-1} \bar{e}^{i_{n+1}} \wedge \dots \wedge \bar{e}^{i_{\nu-1}} \wedge \hat{i}_k(\bar{e}^{i_\nu}) \wedge \bar{e}^{i_{\nu+1}} \wedge \dots \wedge \bar{e}^{i_{2n+1}} \otimes e^{i_{2n+2}})\} \tag{A.86}$$

$$= \frac{1}{n!(n+1)!} \sum_{i_1 \dots i_{2n+2}} G^{(n+1)}_{i_1 \dots i_{2n+2}} \sum_{jk} \sum_{\mu=1}^{n} \sum_{\nu=n+1}^{2n+1} (-1)^{\mu+\nu+1} \delta_{k i_\mu} \delta_{k i_\nu} U_{jk} K[L[\eta_j]](\tag{A.87}$$

$$e^{i_1} \wedge \dots \wedge e^{i_{\mu-1}} \wedge e^{i_{\mu+1}} \wedge \dots \wedge e^{i_n} \otimes \bar{e}^{i_{n+1}} \wedge \dots \wedge \bar{e}^{i_{\nu-1}} \wedge \bar{e}^{i_{\nu+1}} \wedge \dots \wedge \bar{e}^{i_{2n+1}} \otimes e^{i_{2n+2}}). \tag{A.88}$$

Now rename the dummy indices

$$\begin{pmatrix} i_\mu & i_{\mu+1} & \dots & i_n & i_{n+1} & \dots & i_{\nu-1} & i_\nu & i_{\nu+1} & \dots & i_{2n+2} \\ \downarrow & \downarrow & \dots & \downarrow & \downarrow & \dots & \downarrow & \downarrow & \downarrow & \dots & \downarrow \\ l & i_\mu & \dots & i_{n-1} & i_n & \dots & i_{\nu-2} & s & i_{\nu-1} & \dots & i_{2n} \end{pmatrix}, \tag{A.89}$$

and get

$$= \frac{1}{n!(n+1)!}\sum_{i_1\ldots i_{2n}}\sum_{jkls}\sum_{\mu=1}^{n}\sum_{\nu=n+1}^{2n+1}(-1)^{\mu+\nu+1}\delta_{kl}\delta_{ks}U_{jk}G^{(n+1)}_{i_1\ldots i_{\mu-1}li_\mu\ldots i_{\nu-1}si_\nu\ldots i_{2n}}\times \tag{A.90}$$

$$K[L[\eta_j]](e^{i_1}\wedge\ldots\wedge e^{i_{n-1}}\otimes\bar{e}^{i_n}\wedge\ldots\wedge\bar{e}^{i_{2n-1}}\otimes e^{i_{2n}}) \tag{A.91}$$

$$= \frac{1}{n!(n+1)!}\sum_{i_1\ldots i_{2n}}\sum_{jkls}\sum_{\mu=1}^{n}\sum_{\nu=n+1}^{2n+1}\delta_{kl}\delta_{ks}U_{jk}G^{(n+1)}_{i_1\ldots i_{n-1}lsi_n\ldots i_{2n}}\times \tag{A.92}$$

$$K[L[\eta_j]](e^{i_1}\wedge\ldots\wedge e^{i_{n-1}}\otimes\bar{e}^{i_n}\wedge\ldots\wedge\bar{e}^{i_{2n-1}}\otimes e^{i_{2n}}) \tag{A.93}$$

$$= \frac{1}{(n-1)!n!}\sum_{i_1\ldots i_{2n}}\sum_{jl}U_{jl}G^{(n+1)}_{i_1\ldots i_{n-1}lli_n\ldots i_{2n}}\times \tag{A.94}$$

$$K[L[\eta_j]](e^{i_1}\wedge\ldots\wedge e^{i_{n-1}}\otimes\bar{e}^{i_n}\wedge\ldots\wedge\bar{e}^{i_{2n-1}}\otimes e^{i_{2n}}) \tag{A.95}$$

$$= \frac{1}{(n-1)!n!}\sum_{i_1\ldots i_{2n}}\sum_{jl}U_{jl}G^{(n+1)}_{i_1\ldots i_{n-1}lli_n\ldots i_{2n}}\times \tag{A.96}$$

$$(-\sum_{\mu=1}^{n}\delta_{ji_\mu}+\sum_{\mu=n+1}^{2n-1}\delta_{ji_\mu})(e^{i_1}\wedge\ldots\wedge e^{i_{n-1}}\otimes\bar{e}^{i_n}\wedge\ldots\wedge\bar{e}^{i_{2n-1}}\otimes e^{i_{2n}}) \tag{A.97}$$

$$= \frac{1}{(n-1)!n!}\sum_{i_1\ldots i_{2n}}\sum_{l}(-\sum_{\mu=1}^{n}+\sum_{\mu=n+1}^{2n-1})U_{i_\mu l}G^{(n+1)}_{i_1\ldots i_{n-1}lli_n\ldots i_{2n}}\times \tag{A.98}$$

$$e^{i_1}\wedge\ldots\wedge e^{i_{n-1}}\otimes\bar{e}^{i_n}\wedge\ldots\wedge\bar{e}^{i_{2n-1}}\otimes e^{i_{2n}}. \tag{A.99}$$

A.2.4 ∇^+ map

$$\nabla^{+(n-1)}[\frac{1}{(n-1)!(n-1)!}\sum_{i_1\ldots i_{2n-2}}\langle d^\dagger_{i_1}\ldots d^\dagger_{i_{n-1}}d_{i_n}\ldots d_{i_{2n-2}}\rangle e_{i_1}\wedge\ldots e_{i_{n-1}}\otimes\bar{e}_{i_n}\wedge\ldots\bar{e}_{i_{2n-2}}] \tag{A.100}$$

$$= \frac{(-1)^{(n-1)}}{(n-1)!(n-1)!}\sum_{i_1\ldots i_{2n-2}}\sum_{j}\mathbb{1}\otimes\hat{\wedge}_j\otimes\hat{\wedge}_j[\langle d^\dagger_{i_1}\ldots d^\dagger_{i_{n-1}}d_{i_n}\ldots d_{i_{2n-2}}\rangle e_{i_1}\wedge\ldots e_{i_{n-1}}\otimes\bar{e}_{i_n}\wedge\ldots\bar{e}_{i_{2n-2}}] \tag{A.101}$$

$$= \frac{(-1)^{n-1}}{(n-1)!(n-1)!}\sum_{i_1\ldots i_{2n-2}}\sum_{j}\langle d^\dagger_{i_1}\ldots d^\dagger_{i_{n-1}}d_{i_n}\ldots d_{i_{2n-2}}\rangle e_{i_1}\wedge\ldots e_{i_{n-1}}\otimes\bar{e}_j\wedge\bar{e}_{i_n}\wedge\ldots\bar{e}_{i_{2n-2}}\otimes e_j \tag{A.102}$$

$$= \frac{1}{(n-1)!(n-1)!}\sum_{i_1\ldots i_{2n-2}}\sum_{ij}\delta_{ij}\langle d^\dagger_{i_1}\ldots d^\dagger_{i_{n-1}}d_{i_n}\ldots d_{i_{2n-2}}\rangle e_{i_1}\wedge\ldots e_{i_{n-1}}\otimes\bar{e}_{i_n}\wedge\ldots\bar{e}_{i_{2n-2}}\wedge\bar{e}_i\otimes e_j \tag{A.103}$$

Rename the dummy indices

$$\begin{pmatrix} i_n & i_{n+1} & \ldots & i_{\mu-1} & i_\mu & \ldots & i_{2n-2} & i & j \\ \downarrow & \downarrow & \ldots & \downarrow & \downarrow & \downarrow & \ldots & \downarrow & \downarrow \\ i_n & i_{n+1} & \ldots & i_{\mu-1} & i_{\mu+1} & \ldots & i_{2n-1} & i_\mu & i_{2n} \end{pmatrix}, \tag{A.104}$$

to get

$$= \frac{1}{(n-1)!n!}\sum_{i_1\ldots i_{2n}}\sum_{\mu=n}^{2n-1}\delta_{i_\mu,i_{2n}}\langle d^\dagger_{i_1}...d^\dagger_{i_{n-1}}d_{i_n}...d_{i_{\mu-1}}d_{i_{\mu+1}}...d_{i_{2n-1}}\rangle \tag{A.105}$$

$$e_{i_1}\wedge...e_{i_{n-1}}\otimes\bar{e}_{i_n}\wedge...\wedge\bar{e}_{i_{\mu-1}}\wedge\bar{e}_{i_{\mu+1}}\wedge...\wedge\bar{e}_{i_{2n-2}}\wedge\bar{e}_{i_\mu}\otimes e_{i_{2n}} \tag{A.106}$$

$$= \frac{1}{(n-1)!n!}\sum_{i_1\ldots i_{2n}}\sum_{\mu=n}^{2n-1}(-1)^{(\mu+1)}\delta_{i_\mu,i_{2n}}\langle d^\dagger_{i_1}...d^\dagger_{i_{n-1}}d_{i_n}...d_{i_{\mu-1}}d_{i_{\mu+1}}...d_{i_{2n-1}}\rangle \tag{A.107}$$

$$e_{i_1}\wedge...e_{i_{n-1}}\otimes\bar{e}_{i_n}\wedge...\wedge\bar{e}_{i_{2n-2}}\otimes e_{i_{2n}}. \tag{A.108}$$

A.2.5 $\nabla^{<(n)}$ map

$$\hat{\nabla}^{<(n)}[\frac{1}{(n-1)!n!}\sum_{i_1\ldots i_{2n}}G^{(n)}_{i_1i_2\ldots i_{2n}}e_{i_1}\wedge...\wedge e_{i_{n-1}}\wedge\bar{e}_{i_n}\wedge...\bar{e}_{i_{2n-1}}\otimes e_{i_{2n}}] \tag{A.109}$$

$$= \frac{1}{n}\sum_{i_1\ldots i_{2n}}\sum_j\hat{\wedge}_j\otimes\mathbb{1}\otimes\hat{i}_j[\frac{1}{(n-1)!n!}G^{(n)}_{i_1i_2\ldots i_{2n}}e_{i_1}\wedge...\wedge e_{i_{n-1}}\wedge\bar{e}_{i_n}\wedge...\bar{e}_{i_{2n-1}}\otimes e_{i_{2n}}] \tag{A.110}$$

$$= \frac{1}{n!n!}\sum_{i_1\ldots i_{2n}}\sum_j G^{(n)}_{i_1i_2\ldots i_{2n}}e_j\wedge e_{i_1}\wedge...\wedge e_{i_{n-1}}\wedge\bar{e}_{i_n}\wedge...\bar{e}_{i_{2n-1}}\otimes\delta_{j,i_{2n}} \tag{A.111}$$

$$= \frac{1}{n!n!}\sum_{i_1\ldots i_{2n-1}}\sum_j G^{(n)}_{i_1i_2\ldots i_{2n-1}j}e_j\wedge e_{i_1}\wedge...\wedge e_{i_{n-1}}\wedge\bar{e}_{i_n}\wedge...\bar{e}_{i_{2n-1}}. \tag{A.112}$$

Rename the dummy indices

$$\begin{pmatrix} j & i_1 & ... & i_{n-1} & i_n & ... & i_{2n-1} \\ \downarrow & \downarrow & ... & \downarrow & \downarrow & ... & \downarrow \\ i_1 & i_2 & ... & i_n & i_{n+1} & ... & i_{2n} \end{pmatrix} \tag{A.113}$$

to get

$$= \frac{1}{n!n!}\sum_{i_1\ldots i_{2n}}G^{(n)}_{i_2\ldots i_{2n}i_1}e_{i_1}\wedge...\wedge e_{i_n}\wedge\bar{e}_{i_{n+1}}\wedge...\bar{e}_{i_{2n}}. \tag{A.114}$$

A.3 EOM in the differential form

In this section we show that the matrix operators

$$\hat{\nabla}_t^{1(n)} = \hat{K}[\hat{L}[\bar{t}], \hat{L}[t]] \otimes \mathbb{1} \tag{A.115}$$

$$\hat{\nabla}_U^{2(n)} = \sum_{jk} \frac{U_{jk}}{2} \hat{K}[\hat{L}[\eta_j] \cdot \hat{L}[\eta_k]] \otimes \mathbb{1} \tag{A.116}$$

$$\hat{\nabla}_U^{-(n+1)} = (-1)^{(n+1)} \sum_{jk} U_{jk} [\hat{K}[\hat{L}[\eta_j]] \cdot (\hat{i}_k \otimes \hat{i}_k)] \otimes \mathbb{1} \tag{A.117}$$

$$\hat{\nabla}^{+(n-1)} = (-1)^{(n-1)} \sum_j \mathbb{1} \otimes \hat{\wedge}_j \otimes \hat{\wedge}_j \tag{A.118}$$

$$\hat{\nabla}^{<(n)} = \frac{1}{n} \sum_j \hat{\wedge}_j \otimes \mathbb{1} \otimes \hat{i}_j, \tag{A.119}$$

are equivalent to the geometric mappings

$$\hat{\nabla}_t^1 = i\mathcal{L}_{X[\bar{t}]} \otimes \mathbb{1} \tag{A.120}$$

$$\hat{\nabla}_U^2 = \frac{-i}{2} \sum_{jk} U_{jk} \mathcal{L}_{X[\eta_j]} \mathcal{L}_{JX[\eta_k]} \otimes \mathbb{1} \tag{A.121}$$

$$\hat{\nabla}_U^- = -i \sum_{jk} U_{jk} \mathcal{L}_{X[\eta_j]} \hat{i}_{\partial_k} \hat{i}_{\partial_{\bar{k}}} \otimes \mathbb{1} \tag{A.122}$$

$$\hat{\nabla}^+ = \sum_j d\bar{z}^j \wedge (\cdot) \otimes dz^j \tag{A.123}$$

$$\hat{\nabla}^{<(n)} = \frac{1}{n} \sum_j dz^j \wedge (\cdot) \otimes \hat{i}_{\partial_j}, \tag{A.124}$$

when acting on the differential forms with constant components. It is sufficient to show the equivalence upon basis forms. We perform brute-force computation for $\hat{\nabla}_t^{1(n)}$ and $\hat{\nabla}_U^{2(n)}$. The equivalence of other maps are clear from the definitions.

A.3.1 Lie derivatives

Firstly we prove the equivalence between Lie derivative and L-map. This will simplify the following proofs.

$$\mathcal{L}_{\sum_{j,k} t_{kj} z^j \partial_k}(dz^{i_1} \wedge ... \wedge dz^{i_n}) \tag{A.125}$$

$$= (\sum_{j,k} t_{kj} d\hat{i}_{z^j \partial_k} dz^{i_1} \wedge ... \wedge dz^{i_n}) \tag{A.126}$$

$$= \sum_{\mu=1}^{n} dz^{i_1} \wedge ... \wedge dz^{i_{\mu-1}} \wedge (\sum_{j,k} t_{kj} dz^j \delta_k^{i_\mu}) \wedge dz^{i_{\mu+1}} \wedge ... \wedge dz^{i_n} \tag{A.127}$$

$$= \sum_{\mu=1}^{n} dz^{i_1} \wedge ... \wedge dz^{i_{\mu-1}} \wedge (\sum_{j} t_{i_\mu j} dz^j) \wedge dz^{i_{\mu+1}} \wedge ... \wedge dz^{i_n} \tag{A.128}$$

$$= \hat{L}[t](dz^{i_1} \wedge ... \wedge dz^{i_n}). \tag{A.129}$$

A.3.2 $\hat{\nabla}_t^{1(n)}$ map

$$i\mathcal{L}_{X[\bar{t}]}(dz^{i_1} \wedge ... \wedge dz^{i_{n-1}} \wedge d\bar{z}^{i_n} \wedge ... \wedge d\bar{z}^{i_{2n-1}}) \tag{A.130}$$

$$= (i\mathcal{L}_{\sum_{j,k} i\bar{t}_{kj} z^j \partial_k - i t_{kj} \bar{z}^j \partial_{\bar{k}}})(dz^{i_1} \wedge ... \wedge dz^{i_{n-1}} \wedge d\bar{z}^{i_n} \wedge ... \wedge d\bar{z}^{i_{2n-1}}) \tag{A.131}$$

$$= (\mathcal{L}_{-\sum_{j,k} \bar{t}_{kj} z^j \partial_k} + \mathcal{L}_{\sum_{j,k} t_{kj} \bar{z}^j \partial_{\bar{k}}})(dz^{i_1} \wedge ... \wedge dz^{i_{n-1}} \wedge d\bar{z}^{i_n} \wedge ... \wedge d\bar{z}^{i_{2n-1}}) \tag{A.132}$$

$$= (-\sum_{j,k} \bar{t}_{kj} d\hat{i}_{z^j \partial_k} dz^{i_1} \wedge ... \wedge dz^{i_{n-1}}) \wedge d\bar{z}^{i_n} \wedge ... \wedge d\bar{z}^{i_{2n-1}} \tag{A.133}$$

$$+ dz^{i_1} \wedge ... \wedge dz^{i_{n-1}} \wedge (\sum_{j,k} t_{kj} d\hat{i}_{\bar{z}^j \partial_{\bar{k}}} d\bar{z}^{i_n} \wedge ... \wedge d\bar{z}^{i_{2n-1}}). \tag{A.134}$$

A.3.3 $\hat{\nabla}_U^{2(n)}$ map

$$JX[\eta_k] = (\sum_{l} i dz^l \otimes \partial_l - i d\bar{z}^l \otimes \partial_{\bar{l}})(i z^k \partial_k - i \bar{z}^k \partial_{\bar{k}}) \tag{A.135}$$

$$= -(z^k \partial_k + \bar{z}^k \partial_{\bar{k}}). \tag{A.136}$$

$$-i\mathcal{L}_{X[\eta_j]}\mathcal{L}_{JX[\eta_k]}(dz^{i_1}\wedge ...\wedge dz^{i_{n-1}}\wedge d\bar{z}^{i_n}\wedge ...\wedge d\bar{z}^{i_{2n-1}}) \tag{A.137}$$

$$= \mathcal{L}_{-z^j\partial_j+\bar{z}^j\partial_{\bar{j}}}\mathcal{L}_{z^k\partial_k+\bar{z}^k\partial_{\bar{k}}}(dz^{i_1}\wedge ...\wedge dz^{i_{n-1}}\wedge d\bar{z}^{i_n}\wedge ...\wedge d\bar{z}^{i_{2n-1}}) \tag{A.138}$$

$$= (-d\hat{i}_{z^j\partial_j}+d\hat{i}_{\bar{z}^j\partial_{\bar{j}}})(d\hat{i}_{z^k\partial_k}+d\hat{i}_{\bar{z}^k\partial_{\bar{k}}})(dz^{i_1}\wedge ...\wedge dz^{i_{n-1}}\wedge d\bar{z}^{i_n}\wedge ...\wedge d\bar{z}^{i_{2n-1}}) \tag{A.139}$$

$$= -(d\hat{i}_{z^j\partial_j}d\hat{i}_{z^k\partial_k})(dz^{i_1}\wedge ...\wedge dz^{i_{n-1}})\wedge d\bar{z}^{i_n}\wedge ...\wedge d\bar{z}^{i_{2n-1}} \tag{A.140}$$

$$+dz^{i_1}\wedge ...\wedge dz^{i_{n-1}}\wedge (d\hat{i}_{\bar{z}^j\partial_j}d\hat{i}_{\bar{z}^k\partial_{\bar{k}}})(d\bar{z}^{i_n}\wedge ...\wedge d\bar{z}^{i_{2n-1}}). \tag{A.141}$$

A.4 Numerical Implementation: EOMPACK

A.4.1 Structure of the EOMPACK code

In this section we summarize the process of the EOMPACK code:

1. Generate basis for anti-symmetric tensors (extalgebra.f90).
2. Compute the matrix elements (matelement.f90).
3. Solve the EOM (eom.f90).

In the next section we explain how each step is done, and use $N = 2$ as a practical example. Some discussions about numerical exterior algebra could be found in Allen and Bridges [85].

A.4.2 Generate tensor basis (extalgebra.f90)

Generate anti-symmetric tensor basis

Assume N-dimensional vector space V with ordered basis $\{e_1, e_2, ..., e_N\}$.

The full tensors of rank n is a space with dimension N^n. We want to work in the smaller space consisting of only the anti-symmetric tensors, which is of a smaller dimension $\binom{N}{n}$.

The basis for anti-symmetric tensors is constructed by the wedge product

$$e_{i_1}\wedge e_{i_2}\wedge ...\wedge e_{i_n} \quad = \sum_P sgn(P)e_{i_{P(1)}}\otimes e_{i_{P(2)}}\otimes ...\otimes e_{i_{P(n)}}, \tag{A.142}$$

where P is permutation. A general anti-symmetric tensor can be expressed in the component form

$$A = \sum_{i_1<...<i_n} A_{i_1,...,i_n} e_{i_1} \wedge e_{i_2} \wedge ... \wedge e_{i_n} \tag{A.143}$$

$$= \sum_{i_1,...,i_n} \frac{1}{n!} A_{i_1,...,i_n} e_{i_1} \wedge e_{i_2} \wedge ... \wedge e_{i_n}. \tag{A.144}$$

For $N = 2$, we should generate the following ordered basis:

$$\Lambda^0(V) = \text{span}\{1\} \tag{A.145}$$

$$\Lambda^1(V) = \text{span}\{e_1, e_2\} \tag{A.146}$$

$$\Lambda^2(V) = \text{span}\{e_1 \wedge e_2\}. \tag{A.147}$$

For $N = 3$, we should generate the following ordered basis:

$$\Lambda^0(V) = \text{span}\{1\} \tag{A.148}$$

$$\Lambda^1(V) = \text{span}\{e_1, e_2, e_3\} \tag{A.149}$$

$$\Lambda^2(V) = \text{span}\{e_1 \wedge e_2, e_1 \wedge e_3, e_2 \wedge e_3\} \tag{A.150}$$

$$\Lambda^3(V) = \text{span}\{e_1 \wedge e_2 \wedge e_3\}. \tag{A.151}$$

The dimensions should be $dim(\Lambda^p) = \binom{N}{p}$.

Generate Green's function tensor basis

It is given by the tensor product $\Theta^n(V) = \Lambda^{n-1}(V) \otimes \Lambda^n(V) \otimes \Lambda^1(V)$ (convenient for C-style array) or $\Theta^n(V) = \Lambda^1(V) \otimes \Lambda^{n-1}(V) \otimes \Lambda^n(V)$ (convenient for Fortran-style array). We choose the first convention for the Python code and the second one for the Fortran code. For all the derivations, we use the C-like convention.

For $N = 2$, we should generate the following ordered basis:

$$\Theta^0(V) = \text{span}\{1\} \tag{A.152}$$

$$\Theta^1(V) = \text{span}\{e_1 \otimes e_1, e_1 \otimes e_2, e_2 \otimes e_1, e_2 \otimes e_2\} \tag{A.153}$$

$$\Theta^2(V) = \text{span}\{e_1 \otimes e_1 \wedge e_2 \otimes e_1, e_1 \otimes e_1 \wedge e_2 \otimes e_2, e_2 \otimes e_1 \wedge e_2 \otimes e_1, e_2 \otimes e_1 \wedge e_2 \otimes e_2\} \tag{A.154}$$

A.4.3 Compute the matrix elements (matelement.f90)

For a linear map $\hat{F}$, the matrix element is computed by $F_{ij} = \langle i|\hat{F}|j\rangle$ for all $|i\rangle, |j\rangle$ in the basis. So what we will do is

1. Compute all $\hat{F}|j\rangle$.
2. Take the inner product.

Compute the mappings

The maps can be written explicitly as

$$\hat{\nabla}_t^{1(n)} = \hat{K}[\hat{L}[t], \hat{L}[t]] \otimes \mathbb{1} \tag{A.155}$$

$$\hat{\nabla}_U^{2(n)} = \sum_{jk} \frac{U_{jk}}{2} \hat{K}[\hat{L}[\eta_j] \cdot \hat{L}[\eta_k]] \otimes \mathbb{1} \tag{A.156}$$

$$\hat{\nabla}_U^{-(n+1)} = (-1)^{(n+1)} \sum_{jk} U_{jk} [\hat{K}[\hat{L}[\eta_j]] \cdot (\hat{i}_k \otimes \hat{i}_k)] \otimes \mathbb{1} \tag{A.157}$$

$$\hat{\nabla}^{+(n-1)} = (-1)^{(n-1)} \sum_j \mathbb{1} \otimes \hat{\wedge}_j \otimes \hat{\wedge}_j \tag{A.158}$$

$$\hat{\nabla}^{<(n)} = \frac{1}{n} \sum_j \hat{\wedge}_j \otimes \mathbb{1} \otimes \hat{i}_j. \tag{A.159}$$

So we can construct the matrices by evaluating these matrix elements first:

$$\langle \beta(\Lambda^{(n)}) | \hat{L}[t] | \beta(\Lambda^{(n)}) \rangle \tag{A.160}$$

$$\langle \beta(\Lambda^{(n-1)}) | \hat{i}_j | \beta(\Lambda^{(n)}) \rangle \tag{A.161}$$

$$\langle \beta(\Lambda^{(n+1)}) | \hat{\wedge}_j | \beta(\Lambda^{(n)}) \rangle. \tag{A.162}$$

Then the full matrices can then be calculated efficiently by sparse matrix arithmetic.

Compute the inner product

The inner product between two alternating tensors is mathematically defined by the Hodge star operator. It could be generally computed by determinants ($O(n^3)$) which is super slow. A better way to do this is to sort (in worst case $O(n^2)$) and then do a comparison ($O(n)$). This is what we do in the Python code. However, with carefully surgery in the maps, we can actually do the sorting by a binary search ($O(\ln(n))$) and then an insertion ($O(1)$). This algorithm is implemented in our Fortran code. The algorithm is very fast and hence the computational time for constructing the matrices is negligible comparing to the time for solving the equations up to $N = 12$.

A.4.4 Sparse matrix arithmetic (spmatrix.f90)

There are several standard sparse matrix formats. In our code we use minimal amount of formats: coordinate format(COO), compressed sparse row format(CSR), and linked list format(LIL). Notice that Intel has its own CSR format (so called 3-array variation, or CSR3) which differs from the NIST standard CSR format. See the Intel MKL manual for further information.

Each of these matrix type has its own advantage. The following list shows the most efficient format to do the tasks (and this is how we implement our code):

1. LILmatrix: append new matrix element.
2. COOmatrix: Kronecker product.
3. CSRmatrix: matrix addtion, matrix multiplication, sparse solver.

Intel MKL provides subroutines to do the following tasks:

1. Transformation between COO and CSR .
2. Matrix-matrix addition and multiplication for CSR.
3. Matrix-vector and matrix-dense matrix multiplication for CSR.
4. Sparse solver for CSR.

We write the codes to do all the other operations and wrappers in the file spmatrix.f90.

A.4.5 Linear and non-linear solvers and numerical quadrature (eom.f90)

For the linear solver, we have a direct solver and an iterative solver. The user can choose the direct solver INTEL PARDISO [86], or the conjugate gradient(CG) iterative solver [87–89].

Other possible methods are Krylov subspace method for shifted linear systems [90] and various model order reduction methods [91] like PRIMA [92]. To apply these methods, one needs to rewrite the EOM in the form described in section A.6. But we found that the CG implementation is simpler and more reliable.

For the non-linear solver, I write a limited-memory Broyden solver based on the restart algorithm described in van de Rotten and Lunel [93]. The memory cost is $O(kD)$, where k is a constant parameter. This is much better than the standard Broyden method ($O(D^2)$).

Several options for the numerical quadrature are Simpson's method, Gaussian quadrature and adaptive Cash-Karp-Runge-Kutta. [94]

A.5 Step-by-step example to construct the matrix EOM for $N = 2$

Here we type up the case for $N = 2$. In this section, we simplify the notation by substituting V for $\beta(V)$.

A.5.1 Generate tensor basis

Dimensions for $\Lambda^{(n)}$ should be $1, 2, 1$ for $n = 0, 1, 2$.

$$\Lambda^{(0)}(V) = \{1\} \tag{A.163}$$

$$\Lambda^{(1)}(V) = \{e_1, e_2\} \tag{A.164}$$

$$\Lambda^{(2)}(V) = \{e_1 \wedge e_2\}. \tag{A.165}$$

Dimensions for $\Theta^{(n)}$ should be $1, 4, 4$ for $n = 0, 1, 2$.

$$\Theta^{(0)}(V) = \{1\} \tag{A.166}$$

$$\Theta^{(1)}(V) = \{e_1 \otimes e_1, e_1 \otimes e_2, e_2 \otimes e_1, e_2 \otimes e_2\} \tag{A.167}$$

$$\Theta^{(2)}(V) = \{e_1 \otimes e_1 \wedge e_2 \otimes e_1, e_1 \otimes e_1 \wedge e_2 \otimes e_2, e_2 \otimes e_1 \wedge e_2 \otimes e_1, e_2 \otimes e_1 \wedge e_2 \otimes e_2\}. \tag{A.168}$$

A.5.2 Matrix element

L-map

For $n = 0$,

$$1 \mapsto 0. \tag{A.169}$$

The matrix is,

$$L^{(0)}[t] = \langle \Lambda^{(0)} | \hat{L}[t] | \Lambda^{(0)} \rangle = \begin{pmatrix} 0 \end{pmatrix}. \tag{A.170}$$

For $n = 1$,

$$e_1 \mapsto t_{11} e_1 + t_{21} e_2 \tag{A.171}$$

$$e_2 \mapsto t_{12} e_1 + t_{22} e_2 \tag{A.172}$$

The matrix is,

$$L^{(1)}[t] \quad = \quad \langle \Lambda^{(1)} | \hat{L}[t] | \Lambda^{(1)} \rangle = \begin{pmatrix} t_{11} & t_{12} \\ t_{21} & t_{22} \end{pmatrix} \tag{A.173}$$

For $n = 2$,

$$e_1 \wedge e_2 \mapsto (t_{11} + t_{22}) e_1 \wedge e_2. \tag{A.174}$$

The matrix is,

$$L^{(2)}[t] \quad = \quad \langle \Lambda^{(2)} | \hat{L}[t] | \Lambda^{(2)} \rangle = \begin{pmatrix} t_{11} + t_{22} \end{pmatrix}. \tag{A.175}$$

Prepare some other matrices

$$L^{(0)}[\eta_i] \cdot L^{(0)}[\eta_j] \quad = 0 \tag{A.176}$$

$$L^{(1)}[\eta_1] \cdot L^{(1)}[\eta_1] \quad = \begin{pmatrix} 1 & 0 \\ 0 & 0 \end{pmatrix} \tag{A.177}$$

$$L^{(1)}[\eta_2] \cdot L^{(1)}[\eta_2] \quad = \begin{pmatrix} 0 & 0 \\ 0 & 1 \end{pmatrix} \tag{A.178}$$

$$L^{(1)}[\eta_1] \cdot L^{(1)}[\eta_2] \quad = \begin{pmatrix} 0 & 0 \\ 0 & 0 \end{pmatrix} \tag{A.179}$$

$$L^{(2)}[\eta_i] \cdot L^{(2)}[\eta_j] \quad = \begin{pmatrix} 1 \end{pmatrix} \tag{A.180}$$

1-particle Kronecker sum:

$$K^{(1)}[L[\eta_1]\cdot L[\eta_1]] = -0\otimes\begin{pmatrix}1&0\\0&1\end{pmatrix}+1\otimes\begin{pmatrix}1&0\\0&0\end{pmatrix} \tag{A.181}$$

$$= \begin{pmatrix}1&0\\0&0\end{pmatrix} \tag{A.182}$$

$$K^{(1)}[L[\eta_2]\cdot L[\eta_2]] = -0\otimes\begin{pmatrix}1&0\\0&1\end{pmatrix}\otimes 1+\begin{pmatrix}0&0\\0&1\end{pmatrix}\otimes 1 \tag{A.183}$$

$$= \begin{pmatrix}0&0\\0&1\end{pmatrix} \tag{A.184}$$

$$K^{(1)}[L[\eta_1]\cdot L[\eta_2]] = -0\otimes\begin{pmatrix}1&0\\0&1\end{pmatrix}\otimes 1+\begin{pmatrix}0&0\\0&0\end{pmatrix}\otimes 1 \tag{A.185}$$

$$= \begin{pmatrix}0&0\\0&0\end{pmatrix} \tag{A.186}$$

2-particle Kronecker sum:

$$K^{(2)}[L[\eta_1]\cdot L[\eta_1]] = -\begin{pmatrix}1&0\\0&0\end{pmatrix}\otimes 1+\begin{pmatrix}1&0\\0&1\end{pmatrix}\otimes 1 \tag{A.187}$$

$$= \begin{pmatrix}0&0\\0&1\end{pmatrix} \tag{A.188}$$

$$K^{(2)}[L[\eta_2]\cdot L[\eta_2]] = -\begin{pmatrix}0&0\\0&1\end{pmatrix}\otimes 1+\begin{pmatrix}1&0\\0&1\end{pmatrix}\otimes 1 \tag{A.189}$$

$$= \begin{pmatrix}1&0\\0&0\end{pmatrix} \tag{A.190}$$

$$K^{(2)}[L[\eta_1]\cdot L[\eta_2]] = -\begin{pmatrix}0&0\\0&0\end{pmatrix}\otimes 1+\begin{pmatrix}1&0\\0&1\end{pmatrix}\otimes 1 \tag{A.191}$$

$$= \begin{pmatrix}1&0\\0&1\end{pmatrix} \tag{A.192}$$

$\hat{\nabla}_t^1$ map

The map is

$$\hat{\nabla}_t^{1(n)} = \hat{K}[\hat{L}[\bar{t}], \hat{L}[t]] \otimes \mathbb{1}. \tag{A.193}$$

1-particle matrix is

$$\nabla_t^{1(1)} = \langle \Theta^{(1)} | \hat{\nabla}_t^1 | \Theta^{(1)} \rangle = \begin{pmatrix} t_{11} & t_{12} \\ t_{21} & t_{22} \end{pmatrix}. \tag{A.194}$$

2-particle matrix is

$$\nabla_t^{1(2)} = \langle \Theta^{(2)} | \hat{\nabla}_t^1 | \Theta^{(2)} \rangle = -\begin{pmatrix} \bar{t}_{11} & \bar{t}_{12} \\ \bar{t}_{21} & \bar{t}_{22} \end{pmatrix} \otimes 1 + \begin{pmatrix} 1 & 0 \\ 0 & 1 \end{pmatrix} \otimes \Big(t_{11} + t_{22} \Big) \tag{A.195}$$

$$= \begin{pmatrix} -\bar{t}_{11} + t_{11} + t_{22} & -\bar{t}_{12} \\ -\bar{t}_{21} & -\bar{t}_{22} + t_{11} + t_{22} \end{pmatrix}. \tag{A.196}$$

$\hat{\nabla}_U^2$ map

The map is

$$\hat{\nabla}_U^{2(n)} = \sum_{jk} \frac{U_{jk}}{2} \hat{K}[\hat{L}[\eta_j] \cdot \hat{L}[\eta_k]] \otimes \mathbb{1}. \tag{A.197}$$

The matrices are

$$\nabla_U^{2(1)} = \langle \Theta^{(1)} | \hat{\nabla}_U^2 | \Theta^{(1)} \rangle = U_{12} K^{(1)}[L[\eta_1] \cdot L[\eta_2]] \tag{A.198}$$

$$= \begin{pmatrix} 0 & 0 \\ 0 & 0 \end{pmatrix} \tag{A.199}$$

$$\nabla_U^{2(2)} = \langle \Theta^{(2)} | \hat{\nabla}_U^2 | \Theta^{(2)} \rangle = U_{12} K^{(2)}[L[\eta_1] \cdot L[\eta_2]] \tag{A.200}$$

$$= \begin{pmatrix} U_{12} & 0 \\ 0 & U_{12} \end{pmatrix}. \tag{A.201}$$

$\hat{i}_j$ map

For $n = 1$, $j = 1$,

$$e_1 \mapsto 1 \tag{A.202}$$

$$e_2 \mapsto 0. \tag{A.203}$$

For $n = 1$, $j = 2$,

$$e_1 \mapsto 0 \tag{A.204}$$

$$e_2 \mapsto 1. \tag{A.205}$$

The matrices are

$$i_1^{(1)} = \langle \Lambda^{(0)} | \hat{i}_1 | \Lambda^{(1)} \rangle = \begin{pmatrix} 1 & 0 \end{pmatrix} \tag{A.206}$$

$$i_2^{(1)} = \langle \Lambda^{(0)} | \hat{i}_2 | \Lambda^{(1)} \rangle = \begin{pmatrix} 0 & 1 \end{pmatrix}. \tag{A.207}$$

For $n = 2$, $j = 1$,

$$e_1 \wedge e_2 \mapsto e_2. \tag{A.208}$$

For $n = 2$, $j = 2$,

$$e_1 \wedge e_2 \mapsto -e_1. \tag{A.209}$$

The matrices are

$$i_1^{(2)} = \langle \Lambda^{(1)} | \hat{i}_1 | \Lambda^{(2)} \rangle = \begin{pmatrix} 0 \\ 1 \end{pmatrix} \tag{A.210}$$

$$i_2^{(2)} = \langle \Lambda^{(1)} | \hat{i}_2 | \Lambda^{(2)} \rangle = \begin{pmatrix} -1 \\ 0 \end{pmatrix}. \tag{A.211}$$

$\hat{\nabla}_U^-$ map

The map is

$$\hat{\nabla}_U^{-(n+1)} = (-1)^{(n+1)} \sum_{jk} U_{jk}[\hat{K}[\hat{L}[\eta_j]] \cdot (\hat{i}_k \otimes \hat{i}_k)] \otimes \mathbb{1}. \tag{A.212}$$

The interior matrices are

$$i_1^{(1)} \otimes i_1^{(2)} = \begin{pmatrix} 1 & 0 \end{pmatrix} \otimes \begin{pmatrix} 0 \\ 1 \end{pmatrix} \tag{A.213}$$

$$= \begin{pmatrix} 0 & 0 \\ 1 & 0 \end{pmatrix} \tag{A.214}$$

$$i_2^{(1)} \otimes i_2^{(2)} = \begin{pmatrix} 0 & 1 \end{pmatrix} \otimes \begin{pmatrix} -1 \\ 0 \end{pmatrix} \tag{A.215}$$

$$= \begin{pmatrix} 0 & -1 \\ 0 & 0 \end{pmatrix}. \tag{A.216}$$

The matrix is

$$\nabla_U^{-(2)} = \langle \Theta^{(1)} | \hat{\nabla}_U^- | \Theta^{(2)} \rangle \tag{A.217}$$

$$= U_{12} K^{(1)}[L[\eta_1] \cdot L[\eta_1]] \cdot (i_2^{(1)} \otimes i_2^{(2)}) + U_{21} K^{(1)}[L[\eta_2] \cdot L[\eta_2]] \cdot (i_1^{(1)} \otimes i_1^{(2)}) \tag{A.218}$$

$$= U_{12}(\begin{pmatrix} 1 & 0 \\ 0 & 0 \end{pmatrix} \cdot \begin{pmatrix} 0 & -1 \\ 0 & 0 \end{pmatrix} + \begin{pmatrix} 0 & 0 \\ 0 & 1 \end{pmatrix} \cdot \begin{pmatrix} 0 & 0 \\ 1 & 0 \end{pmatrix}) \tag{A.219}$$

$$= \begin{pmatrix} 0 & -U_{12} \\ U_{12} & 0 \end{pmatrix}. \tag{A.220}$$

$\hat{\wedge}_j$ map

For $n = 0$, $j = 1$,

$$1 \mapsto e_1. \tag{A.221}$$

For $n = 0$, $j = 2$,

$$1 \mapsto e_2. \tag{A.222}$$

The matrices are

$$\wedge_1^{(0)} = \langle \Lambda^{(1)} | \hat{\wedge}_1 | \Lambda^{(0)} \rangle = \begin{pmatrix} 1 \\ 0 \end{pmatrix} \tag{A.223}$$

$$\wedge_2^{(0)} = \langle \Lambda^{(1)} | \hat{\wedge}_2 | \Lambda^{(0)} \rangle = \begin{pmatrix} 0 \\ 1 \end{pmatrix}. \tag{A.224}$$

For $n = 1$, $j = 1$,

$$e_1 \mapsto 0 \tag{A.225}$$

$$e_2 \mapsto e_1 \wedge e_2. \tag{A.226}$$

For $n = 1$, $j = 2$,

$$e_1 \mapsto -e_1 \wedge e_2 \tag{A.227}$$

$$e_2 \mapsto 0. \tag{A.228}$$

The matrices are

$$\wedge_1^{(1)} = \langle \Lambda^{(2)} | \hat{\wedge}_1 | \Lambda^{(1)} \rangle = \begin{pmatrix} 0 & 1 \end{pmatrix} \tag{A.229}$$

$$\wedge_2^{(1)} = \langle \Lambda^{(2)} | \hat{\wedge}_2 | \Lambda^{(1)} \rangle = \begin{pmatrix} -1 & 0 \end{pmatrix}. \tag{A.230}$$

$\hat{\nabla}_+$ map

The map is

$$\hat{\nabla}^{+(n-1)} = (-1)^{(n-1)} \sum_j \mathbb{1} \otimes \hat{\wedge}_j \otimes \hat{\wedge}_j. \tag{A.231}$$

The matrices are

$$\nabla^{+(0)} = \langle\Theta^{(1)}|\nabla^{+(0)}|\Omega^{(0),(0)}\rangle \tag{A.232}$$

$$= (-1)^{(0)}\sum_j \langle\Lambda^{(0)}|\mathbb{1}|\Lambda^{(0)}\rangle \otimes \langle\Lambda^{(1)}|\hat{\wedge}_j|\Lambda^{(0)}\rangle \otimes \langle\Lambda^{(1)}|\hat{\wedge}_j|\Lambda^{(0)}\rangle \tag{A.233}$$

$$= 1 \otimes \begin{pmatrix} 1 \\ 0 \end{pmatrix} \otimes \begin{pmatrix} 1 \\ 0 \end{pmatrix} + 1 \otimes \begin{pmatrix} 0 \\ 1 \end{pmatrix} \otimes \begin{pmatrix} 0 \\ 1 \end{pmatrix} \tag{A.234}$$

$$= \begin{pmatrix} 1 \\ 0 \\ 0 \\ 1 \end{pmatrix}, \tag{A.235}$$

and

$$\nabla^{+(1)} = \langle\Theta^{(2)}|\nabla^{+(1)}|\Omega^{(1),(1)}\rangle \tag{A.236}$$

$$= (-1)^{(1)}\sum_j \langle\Lambda^{(1)}|\mathbb{1}|\Lambda^{(1)}\rangle \otimes \langle\Lambda^{(2)}|\hat{\wedge}_j|\Lambda^{(1)}\rangle \otimes \langle\Lambda^{(1)}|\hat{\wedge}_j|\Lambda^{(0)}\rangle \tag{A.237}$$

$$= (-1)\begin{pmatrix} 1 & 0 \\ 0 & 1 \end{pmatrix} \otimes \begin{pmatrix} 0 & 1 \end{pmatrix} \otimes \begin{pmatrix} 1 \\ 0 \end{pmatrix} + (-1)\begin{pmatrix} 1 & 0 \\ 0 & 1 \end{pmatrix} \otimes \begin{pmatrix} -1 & 0 \end{pmatrix} \otimes \begin{pmatrix} 0 \\ 1 \end{pmatrix} \tag{A.238}$$

$$= \begin{pmatrix} 0 & -1 & 0 & 0 \\ 1 & 0 & 0 & 0 \\ 0 & 0 & 0 & -1 \\ 0 & 0 & 1 & 0 \end{pmatrix}. \tag{A.239}$$

$\hat{\nabla}^{<(n)}$ map

The map is

$$\hat{\nabla}^{<(n)} = \frac{1}{n}\sum_j \hat{\wedge}_j \otimes \mathbb{1} \otimes \hat{i}_j. \tag{A.240}$$

The matrices are

$$\nabla^{<(1)} = \langle\Omega^{(1),(1)}|\hat{\nabla}^{<(1)}|\Theta^{(1)}\rangle \tag{A.241}$$

$$= \sum_j \langle\Lambda^{(1)}|\hat{\wedge}_j|\Lambda^{(0)}\rangle \otimes \langle\Lambda^{(1)}|\mathbb{1}|\Lambda^{(1)}\rangle \otimes \langle\Lambda^{(0)}|\hat{i}_j|\Lambda^{(1)}\rangle \tag{A.242}$$

$$= \begin{pmatrix}1\\0\end{pmatrix} \otimes \begin{pmatrix}1 & 0\\0 & 1\end{pmatrix} \otimes \begin{pmatrix}1 & 0\end{pmatrix} + \begin{pmatrix}0\\1\end{pmatrix} \otimes \begin{pmatrix}1 & 0\\0 & 1\end{pmatrix} \otimes \begin{pmatrix}0 & 1\end{pmatrix} \tag{A.243}$$

$$= \begin{pmatrix}1 & 0 & 0 & 0\\0 & 0 & 1 & 0\\0 & 1 & 0 & 0\\0 & 0 & 0 & 1\end{pmatrix}, \tag{A.244}$$

and

$$\nabla^{<(2)} = \langle\Omega^{(2),(2)}|\hat{\nabla}^{<(2)}|\Theta^{(2)}\rangle \tag{A.245}$$

$$= \frac{1}{2}\sum_j \langle\Lambda^{(2)}|\hat{\wedge}_j|\Lambda^{(1)}\rangle \otimes \langle\Lambda^{(2)}|\mathbb{1}|\Lambda^{(2)}\rangle \otimes \langle\Lambda^{(0)}|\hat{i}_j|\Lambda^{(1)}\rangle \tag{A.246}$$

$$= \frac{1}{2}\begin{pmatrix}0 & 1\end{pmatrix} \otimes \begin{pmatrix}1\end{pmatrix} \otimes \begin{pmatrix}1 & 0\end{pmatrix} + \frac{1}{2}\begin{pmatrix}-1 & 0\end{pmatrix} \otimes \begin{pmatrix}1\end{pmatrix} \otimes \begin{pmatrix}0 & 1\end{pmatrix} \tag{A.247}$$

$$= \frac{1}{2}\begin{pmatrix}0 & -1 & 1 & 0\end{pmatrix}. \tag{A.248}$$

A.5.3 Results

For the case of a single QD

$$H = \sum_\sigma E_\sigma d_\sigma^\dagger d_\sigma + t(d_\sigma^\dagger d_{\bar{\sigma}} + h.c.) + U n_\sigma n_{\bar{\sigma}} + \sum_{\sigma k}(V_{k\sigma} c_k^\dagger d_\sigma + h.c.) + \sum_k \epsilon_k c_k^\dagger c_k, \tag{A.249}$$

the procedure directly generates the following eom, which is the same as the known results. We assume t and U to be the real number for simplicity. Level $1 = \sigma$, level $2 = \bar{\sigma}$. We write the expectation values in vector form and the Green's functions in the matrix form, so reshaping steps (rs) between vector and matrix form is required. All the vector-matrix reshaping here should be done in row-major, since we are using C-like array convention throughout this work.

EOM for 1-particle retarded Green's function:

$$(\epsilon - \begin{pmatrix} E_\sigma + \Sigma^r_\sigma & t \\ t & E_{\bar\sigma} + \Sigma^r_{\bar\sigma} \end{pmatrix}) \begin{pmatrix} G^{(1)r}_{\sigma\sigma} & G^{(1)r}_{\sigma\bar\sigma} \\ G^{(1)r}_{\bar\sigma\sigma} & G^{(1)r}_{\bar\sigma\bar\sigma} \end{pmatrix} = (\mathrm{rs}) \begin{pmatrix} 1 \\ 0 \\ 0 \\ 1 \end{pmatrix} + \begin{pmatrix} 0 & -U \\ U & 0 \end{pmatrix} \begin{pmatrix} G^{(2)r}_{\sigma\sigma\bar\sigma\sigma} & G^{(2)r}_{\sigma\sigma\bar\sigma\bar\sigma} \\ G^{(2)r}_{\bar\sigma\sigma\bar\sigma\sigma} & G^{(2)r}_{\bar\sigma\sigma\bar\sigma\bar\sigma} \end{pmatrix} \tag{A.250}$$

EOM for 2-particle retarded Green's function:

$$(\epsilon - \begin{pmatrix} E_{\bar\sigma} + U - \bar\Sigma^r_\sigma + \Sigma^r_\sigma + \Sigma^r_{\bar\sigma} & -t \\ -t & E_\sigma + U - \bar\Sigma^r_{\bar\sigma} + \Sigma^r_\sigma + \Sigma^r_{\bar\sigma} \end{pmatrix}) \begin{pmatrix} G^{(2)r}_{\sigma\sigma\bar\sigma\sigma} & G^{(2)r}_{\sigma\sigma\bar\sigma\bar\sigma} \\ G^{(2)r}_{\bar\sigma\sigma\bar\sigma\sigma} & G^{(2)r}_{\bar\sigma\sigma\bar\sigma\bar\sigma} \end{pmatrix} \tag{A.251}$$

$$= (\mathrm{rs}) \begin{pmatrix} 0 & -1 & 0 & 0 \\ 1 & 0 & 0 & 0 \\ 0 & 0 & 0 & -1 \\ 0 & 0 & 1 & 0 \end{pmatrix} \begin{pmatrix} \langle d^\dagger_\sigma d_\sigma \rangle \\ \langle d^\dagger_\sigma d_{\bar\sigma} \rangle \\ \langle d^\dagger_{\bar\sigma} d_\sigma \rangle \\ \langle d^\dagger_{\bar\sigma} d_{\bar\sigma} \rangle \end{pmatrix}. \tag{A.252}$$

EOM for 1-particle lessor Green's function:

$$(\epsilon - \begin{pmatrix} E_\sigma + \Sigma^r_\sigma & t \\ t & E_{\bar\sigma} + \Sigma^r_{\bar\sigma} \end{pmatrix}) \begin{pmatrix} G^{(1)<}_{\sigma\sigma} & G^{(1)<}_{\sigma\bar\sigma} \\ G^{(1)<}_{\bar\sigma\sigma} & G^{(1)<}_{\bar\sigma\bar\sigma} \end{pmatrix} \tag{A.253}$$

$$= \begin{pmatrix} \Sigma^<_\sigma & 0 \\ 0 & \Sigma^<_{\bar\sigma} \end{pmatrix} \begin{pmatrix} G^{(1)a}_{\sigma\sigma} & G^{(1)a}_{\sigma\bar\sigma} \\ G^{(1)a}_{\bar\sigma\sigma} & G^{(1)a}_{\bar\sigma\bar\sigma} \end{pmatrix} + \begin{pmatrix} 0 & -U \\ U & 0 \end{pmatrix} \begin{pmatrix} G^{(2)<}_{\sigma\sigma\bar\sigma\sigma} & G^{(2)<}_{\sigma\sigma\bar\sigma\bar\sigma} \\ G^{(2)<}_{\bar\sigma\sigma\bar\sigma\sigma} & G^{(2)<}_{\bar\sigma\sigma\bar\sigma\bar\sigma} \end{pmatrix} \tag{A.254}$$

EOM for 2-particle lessor Green's function:

$$(\epsilon - \begin{pmatrix} E_{\bar\sigma} + U - \bar\Sigma^r_\sigma + \Sigma^r_\sigma + \Sigma^r_{\bar\sigma} & -t \\ -t & E_\sigma + U - \bar\Sigma^r_{\bar\sigma} + \Sigma^r_\sigma + \Sigma^r_{\bar\sigma} \end{pmatrix}) \begin{pmatrix} G^{(2)<}_{\sigma\sigma\bar\sigma\sigma} & G^{(2)<}_{\sigma\sigma\bar\sigma\bar\sigma} \\ G^{(2)<}_{\bar\sigma\sigma\bar\sigma\sigma} & G^{(2)<}_{\bar\sigma\sigma\bar\sigma\bar\sigma} \end{pmatrix} \tag{A.255}$$

$$= \begin{pmatrix} -\bar\Sigma^<_\sigma + \Sigma^<_\sigma + \Sigma^<_{\bar\sigma} & 0 \\ 0 & -\bar\Sigma^<_{\bar\sigma} + \Sigma^<_\sigma + \Sigma^<_{\bar\sigma} \end{pmatrix} \begin{pmatrix} G^{(2)a}_{\sigma\sigma\bar\sigma\sigma} & G^{(2)a}_{\sigma\sigma\bar\sigma\bar\sigma} \\ G^{(2)a}_{\bar\sigma\sigma\bar\sigma\sigma} & G^{(2)a}_{\bar\sigma\sigma\bar\sigma\bar\sigma} \end{pmatrix} \tag{A.256}$$

1-particle expectation values:

$$\begin{pmatrix} \langle d_\sigma^\dagger d_\sigma \rangle \\ \langle d_\sigma^\dagger d_{\bar{\sigma}} \rangle \\ \langle d_{\bar{\sigma}}^\dagger d_\sigma \rangle \\ \langle d_{\bar{\sigma}}^\dagger d_{\bar{\sigma}} \rangle \end{pmatrix} = \begin{pmatrix} 1 & 0 & 0 & 0 \\ 0 & 0 & 1 & 0 \\ 0 & 1 & 0 & 0 \\ 0 & 0 & 0 & 1 \end{pmatrix} (\mathrm{rs}) \int \frac{d\epsilon}{2\pi i} \begin{pmatrix} G_{\sigma\sigma}^{(1)<}(\epsilon) & G_{\sigma\bar{\sigma}}^{(1)<}(\epsilon) \\ G_{\bar{\sigma}\sigma}^{(1)<}(\epsilon) & G_{\bar{\sigma}\bar{\sigma}}^{(1)<}(\epsilon) \end{pmatrix}. \tag{A.257}$$

2-particle expectation values:

$$\left(\langle d_\sigma^\dagger d_{\bar{\sigma}}^\dagger d_\sigma d_{\bar{\sigma}} \rangle \right) = \frac{1}{2} \begin{pmatrix} 0 & -1 & 1 & 0 \end{pmatrix} (\mathrm{rs}) \int \frac{d\epsilon}{2\pi i} \begin{pmatrix} G_{\sigma\sigma\bar{\sigma}\sigma}^{(2)<} & G_{\sigma\sigma\bar{\sigma}\bar{\sigma}}^{(2)<} \\ G_{\bar{\sigma}\sigma\bar{\sigma}\sigma}^{(2)<} & G_{\bar{\sigma}\sigma\bar{\sigma}\bar{\sigma}}^{(2)<} \end{pmatrix}. \tag{A.258}$$

A.6 EOM in the direct sum space

In the model order reduction method and the proof for fluctuation-dissipation theory, it is convenient to write the EOM in the direct sum space $\bigoplus_n \Theta^{(n)}$. For example, the non-equilibrium EOM

$$\begin{aligned} (\epsilon - \nabla_t^{1(n)} - \nabla_U^{2(n)} - \nabla_{\Sigma^r}^{s(n)}) G^{r(n)}(\epsilon) &= \nabla^{+(n-1)} C^{(n-1)} + \nabla_U^{-(n+1)} G^{r(n+1)}(\epsilon) && \text{(A.259)} \\ (\epsilon - \nabla_t^{1(n)} - \nabla_U^{2(n)} - \nabla_{\Sigma^r}^{s(n)}) G^{<(n)}(\epsilon) &= \nabla_{\Sigma^<}^{s(n)} G^{a(n)}(\epsilon) + \nabla_U^{-(n+1)} G^{r(n+1)}(\epsilon) && \text{(A.260)} \\ C^{(n)} &= \frac{1}{2\pi i} \nabla^{<(n)} \int d\epsilon G^{<(n)}(\epsilon), && \text{(A.261)} \end{aligned}$$

can be written as

$$\begin{aligned} (\epsilon - \nabla_t^1 - \nabla_U^2 - \nabla_U^- - \nabla_{\Sigma^r}^s) G^r(\epsilon) &= \nabla^+ C && \text{(A.262)} \\ (\epsilon - \nabla_t^1 - \nabla_U^2 - \nabla_U^- - \nabla_{\Sigma^r}^s) G^<(\epsilon) &= \nabla_{\Sigma^<}^s G^a(\epsilon) && \text{(A.263)} \\ C &= \frac{1}{2\pi i} \nabla^< \int d\epsilon G^<(\epsilon), && \text{(A.264)} \end{aligned}$$

where

$$G = \begin{pmatrix} G^{(1)} \\ \vdots \\ G^{(N)} \end{pmatrix} \tag{A.265}$$

$$C = \begin{pmatrix} C^{(1)} \\ \vdots \\ C^{(N)} \end{pmatrix} \tag{A.266}$$

$$\nabla_X^x = \begin{pmatrix} \nabla_X^{x(1)} & 0 & \cdots & 0 \\ 0 & \nabla_X^{x(2)} & \ddots & \vdots \\ \vdots & \ddots & \ddots & 0 \\ 0 & \cdots & 0 & \nabla_X^{x(N)} \end{pmatrix} \tag{A.267}$$

$$\nabla_U^- = \begin{pmatrix} 0 & \nabla_U^{-(2)} & 0 & \cdots & 0 \\ & \ddots & \ddots & \ddots & \vdots \\ & & \ddots & \ddots & 0 \\ & & & \ddots & \nabla_U^{-(N)} \\ & & & & 0 \end{pmatrix} \tag{A.268}$$

$$\nabla^+ = \begin{pmatrix} 0 & & & & \\ \nabla^{+(1)} & \ddots & & & \\ 0 & \ddots & \ddots & & \\ \vdots & \ddots & \ddots & \ddots & \\ 0 & \cdots & 0 & \nabla^{+(N-1)} & 0 \end{pmatrix}, \tag{A.269}$$

and $x = 1, 2, s, <$, $X = t, U, \Sigma$. The empty part of the matrices are zeros. The solution is

$$G^r(\epsilon) = (\mathcal{G}^{-1}(\epsilon) - \nabla_{\Sigma^r}^s)^{-1} \nabla^+ C \tag{A.270}$$

$$G^<(\epsilon) = (\mathcal{G}^{-1}(\epsilon) - \nabla_{\Sigma^r}^s)^{-1} \nabla_{\Sigma^<}^s G^a(\epsilon) \tag{A.271}$$

$$C = \frac{1}{2\pi i} \nabla^< \int d\epsilon G^<(\epsilon), \tag{A.272}$$

where $\mathcal{G}(\epsilon) = (\epsilon - \nabla_t^1 - \nabla_U^2 - \nabla_U^-)^{-1}$. The equations take the form of Dyson and Keldysh equation, since these are the many-particle generalizations.

A.7 Fluctuation-dissipation theorem

A.7.1 Equilibrium theory

For fermionic operators A, B, where A maps from $(N+1)$-particle subspace to N-particle subspace and B maps from N-particle subspace to $(N+1)$-particle subspace, then the equilibrium Green's function satisfies

$$G^<(\epsilon) \quad = -2if(\epsilon)\Im G^r(\epsilon), \tag{A.273}$$

where $G^<(\epsilon) = \int dt e^{i\epsilon t} i\langle BA(t)\rangle$ and $G^r(\epsilon) = \int dt e^{i\epsilon t} - i\theta(t)\langle\{A(t), B\}\rangle$ and $f(\epsilon) = \frac{1}{1+e^{\beta(\epsilon-\mu)}}$ is the Fermi distribution. Notice that the formula can be applied to general n-particle Green's function, not just the 1-particle Green's function. For example A can be $A = d^\dagger_{i_1} d_{i_2} d_{i_3}$, or linear combinations of different operators like $A = \alpha d^\dagger_{i_1} d_{i_2} d_{i_3} + \beta d_{i_4}$. This fact is shown in the following derivation. [95]

Derivation:

$$\begin{aligned}
G^r(\epsilon) &= \int dt e^{i\epsilon t} - i\theta(t)\langle\{A(t), B\}\rangle && \text{(A.274)}\\
&= -i\int_0^\infty dt e^{i\epsilon t} Tr(e^{-\beta(H-\mu N)}\{e^{iHt}Ae^{-iHt}, B\}) && \text{(A.275)}\\
&= -i\int_0^\infty dt e^{i\epsilon t}(Tr(e^{-\beta(H-\mu N)}e^{iHt}Ae^{-iHt}B) + Tr(e^{-\beta(H-\mu N)}Be^{iHt}Ae^{-iHt})) && \text{(A.276)}\\
&= -i\int_0^\infty dt e^{i\epsilon t}\sum_{mn}(e^{-\beta(E_m-\mu N_m)}e^{iE_m t}A_{mn}e^{-iE_n t}B_{nm} && \text{(A.277)}\\
&\quad + e^{-\beta(E_n-\mu N_n)}B_{nm}e^{iE_m t}A_{mn}e^{-iE_n t}) && \text{(A.278)}\\
&= -i\int_0^\infty dt e^{i\epsilon t}\sum_{mn}(e^{-\beta(E_m-\mu N_m)} + e^{-\beta(E_n-\mu N_n)})e^{i(E_m-E_n)t}A_{mn}B_{nm} && \text{(A.279)}\\
&= -i\int_0^\infty dt e^{i\epsilon t}\sum_{mn}(1 + e^{-\beta((E_m-E_n)-\mu(N_m-N_n))})e^{-\beta(E_n-\mu N_n)}e^{i(E_m-E_n)t}A_{mn}B_{nm} && \text{(A.280)}\\
&= \sum_{mn}(1 + e^{-\beta((E_m-E_n)-\mu(N_m-N_n))})e^{-\beta(E_n-\mu N_n)}\frac{A_{mn}B_{nm}}{\epsilon + (E_m-E_n) + i\delta}. && \text{(A.281)}
\end{aligned}$$

Use the fact $N_m - N_n = -1$ to get

$$\begin{aligned}
\Im G^r(\epsilon) &= -\pi\sum_{mn}(1 + e^{-\beta((E_m-E_n)-\mu(N_m-N_n))})e^{-\beta(E_n-\mu N_n)}A_{mn}B_{nm}\delta(\epsilon + (E_m-E_n)) && \text{(A.282)}\\
&= -\pi(1 + e^{\beta(\epsilon-\mu)})\sum_{mn}e^{-\beta(E_n-\mu N_n)}A_{mn}B_{nm}\delta(\epsilon + E_m - E_n). && \text{(A.283)}
\end{aligned}$$

So we get the result

$$
\begin{aligned}
G^<(\epsilon) &= \int dt e^{i\epsilon t} i\langle BA(t)\rangle && \text{(A.284)}\\
&= \int dt e^{i\epsilon t} iTr(Be^{iHt}Ae^{-iHt}) && \text{(A.285)}\\
&= i\int dt e^{i\epsilon t}\sum_{mn} B_{nm}A_{mn}e^{i(E_m-E_n)t}e^{-\beta(E_n-\mu N_n)} && \text{(A.286)}\\
&= 2\pi i\sum_{mn} A_{mn}B_{nm}\delta(\epsilon+E_m-E_n)e^{-\beta(E_n-\mu N_n)} && \text{(A.287)}\\
&= -2i\frac{1}{1+e^{\beta(\epsilon-\mu)}}\Im G^r(\epsilon). && \text{(A.288)}
\end{aligned}
$$

A.7.2 Non-equilibrium theory

As a consistent check, we prove that under the equilibrium condition $f_\alpha = f$ our non-equilibrium equation of motion gives the correct fluctuation-dissipation relation. In this section we work in the direct sum space $\bigoplus_n \Theta^{(n)}$ described in section A.6.

Proof:

$$
\begin{aligned}
-2if\Im G^r &= f(G^a - G^r) && \text{(A.289)}\\
&= f[(\mathcal{G}^{-1}-\nabla^s_{\Sigma^a})^{-1} - (\mathcal{G}^{-1}-\nabla^s_{\Sigma^r})^{-1}]\nabla^+ C && \text{(A.290)}\\
&= f(\mathcal{G}^{-1}-\nabla^s_{\Sigma^r})^{-1}[(\mathcal{G}^{-1}-\nabla^s_{\Sigma^r}) - (\mathcal{G}^{-1}-\nabla^s_{\Sigma^a})](\mathcal{G}^{-1}-\nabla^s_{\Sigma^a})^{-1}\nabla^+ C && \text{(A.291)}\\
&= f(\mathcal{G}^{-1}-\nabla^s_{\Sigma^r})^{-1}[\nabla^s_{\Sigma^a} - \nabla^s_{\Sigma^r}]G^a && \text{(A.292)}\\
&= (\mathcal{G}^{-1}-\nabla^s_{\Sigma^r})^{-1}\nabla^s_{f(\Sigma^a-\Sigma^r)}G^a && \text{(A.293)}\\
&= G^<, && \text{(A.294)}
\end{aligned}
$$

since the equilibrium condition $f_\alpha = f$ implies $\Sigma^< = f(\Sigma^a - \Sigma^r)$. Notice that for finite bias $f_L \neq f_R$ and the relation breaks down. Also notice that the self-energy is not required to be small. The requirements for the fluctuation-dissipation theory to hold are $f_\alpha = f$ and the real linearity of ∇^s. Also notice that if there is $1 - f_\alpha$, then the relation also breaks down.

A.8 Transport properties

In this section bold text implies matrix. For example, $\mathbf{G}$ means the matrix G_{ij}. The non-equilibrium current tunnelling through the electrode α can be obtained by the Meir-Wingreen formula[28, 46]

$$J^\alpha = \frac{ie}{h}\int d\epsilon \mathrm{Tr}\{\mathbf{\Gamma}^\alpha[\mathbf{G}^< + f_\alpha(\mathbf{G}^\mathbf{r} - \mathbf{G}^\mathbf{a})]\} \tag{A.295}$$

$$= \frac{e}{h}\int d\epsilon I^\alpha. \tag{A.296}$$

The unit for the current is $[\frac{e}{h}][energy]$. The integrand is

$$I^\alpha = -\mathrm{Tr}\{\mathbf{\Gamma}^\alpha[\Im\mathbf{G}^< + f_\alpha(2\Im\mathbf{G}^\mathbf{r})]\}. \tag{A.297}$$

We can define some moments coefficients

$$L_n^\alpha = \frac{1}{h}\int d\epsilon(\frac{\epsilon-\mu}{T})^n\frac{\delta I^\alpha}{\delta f_\alpha}\frac{\partial f_\alpha}{\partial \mu_\alpha}. \tag{A.298}$$

Then we can calculate some transport properties:

$$\text{Differential conductance} : G_e^\alpha = e\frac{\partial J^\alpha}{\partial \mu_\alpha} = e^2 L_0^\alpha \tag{A.299}$$

$$\text{Seebeck coefficient} : S^\alpha = -\frac{\partial V}{\partial T}|_{J=0} = -\frac{L_1^\alpha}{eL_0^\alpha} \tag{A.300}$$

$$\text{Thermal current} : Q^\alpha = \frac{1}{h}\int d\epsilon(\epsilon-\mu_\alpha)I^\alpha \tag{A.301}$$

$$\text{Electron thermal conductance} : \kappa_e^\alpha = \frac{\partial Q^\alpha}{\partial T^\alpha} + \frac{\partial Q^\alpha}{\partial V^\alpha}S^\alpha = T^\alpha(L_2^\alpha - \frac{(L_1^\alpha)^2}{L_0^\alpha}). \tag{A.302}$$

A.8.1 Derivation for the thermal transport coefficients

In this section we ignore α for brevity. The derivatives of Fermi function is

$$\frac{df}{d\mu} = \frac{1}{2T(1+\cosh(\frac{\epsilon-\mu}{T}))} \tag{A.303}$$

$$\frac{df}{dT} = \frac{\epsilon-\mu}{T}\frac{df}{d\mu}. \tag{A.304}$$

For zero temperature we have

$$\frac{df}{d\mu} = \delta(\epsilon - \mu). \tag{A.305}$$

Derivation for Seebeck coefficient:

$$\frac{\partial J}{\partial T} = \frac{e}{h}\int d\epsilon \frac{\partial I}{\partial f}\frac{\partial f}{\partial T} \tag{A.306}$$

$$= eL_1. \tag{A.307}$$

So we have

$$S = -\frac{\partial V}{\partial T}|_{J=0} \tag{A.308}$$

$$= -\frac{\partial J}{\partial T}/\frac{\partial J}{\partial V} \tag{A.309}$$

$$= -\frac{eL_1}{e^2 L_0} \tag{A.310}$$

$$= -\frac{L_1}{eL_0}. \tag{A.311}$$

Derivation for thermal conductivity :

$$\frac{\partial Q}{\partial T} = \frac{1}{h}\int d\epsilon(\epsilon - \mu)\frac{\partial I}{\partial f}\frac{\partial f}{\partial T} \tag{A.312}$$

$$= \frac{T}{h}\int d\epsilon(\frac{\epsilon - \mu}{T})^2\frac{\partial I}{\partial f}\frac{\partial f}{\partial \mu} \tag{A.313}$$

$$= TL_2. \tag{A.314}$$

$$\frac{\partial Q}{\partial V} = \frac{e}{h}\int d\epsilon[-I + (\epsilon - \mu)\frac{\partial I}{\partial f}\frac{\partial f}{\partial \mu}] \tag{A.315}$$

$$= -\frac{e}{h}\int d\epsilon I + \frac{eT}{h}\int d\epsilon(\frac{\epsilon - \mu}{T})\frac{\partial I}{\partial f}\frac{\partial f}{\partial \mu} \tag{A.316}$$

$$= -J + eTL_1. \tag{A.317}$$

The first term proportional to the electric current J is called Joule heating term [12] and is ignored in the linear

response regime. So we have

$$\kappa_e = \frac{\partial Q}{\partial T} + \frac{\partial Q}{\partial V} S \tag{A.318}$$

$$= TL_2 + eTL_1 S \tag{A.319}$$

$$= T(L_2 - \frac{(L_1)^2}{L_0}). \tag{A.320}$$

A.8.2 Linear response

For the linear-response differential conductance, we use the equilibrium relations $\mathbf{G}^< = -2if\Im\mathbf{G}^\mathbf{r}$ and $f_{L/R} = f \pm \frac{\partial f}{\partial x}\frac{\delta x}{2}$. For diagonal tunnelling matrix $\mathbf{\Gamma}$ we also have $\mathbf{G}^\mathbf{r} - \mathbf{G}^\mathbf{a} = 2i\Im\mathbf{G}^\mathbf{r}$, and hence

$$\frac{\partial J}{\partial x} = \frac{-e}{2h}\int d\epsilon \mathrm{Tr}[(\mathbf{\Gamma}^\mathbf{L} + \mathbf{\Gamma}^\mathbf{R})(\Im\mathbf{G}^\mathbf{r})](\frac{\partial f}{\partial x}). \tag{A.321}$$

This formula works for both electric and thermal conductance. The unit for the electric conductance is $[\frac{e}{h}][\frac{energy}{V}] = [\frac{e^2}{h}]$. Notice that $\frac{\partial f}{\partial \mu} = (4T\cosh^2(\frac{\epsilon-\mu}{2T}))^{-1}$, and at zero-temperature $\frac{\partial f}{\partial \mu} = \delta(\epsilon - \mu)$, so

$$\frac{\partial J}{\partial \mu} = \frac{-e}{2h}\mathrm{Tr}[(\mathbf{\Gamma}^\mathbf{L} + \mathbf{\Gamma}^\mathbf{R})(\Im\mathbf{G}^\mathbf{r})]|_\mu. \tag{A.322}$$

Hence the linear response electric conductance is a probe for the local density of states.

Appendix B

Details for the study of graphene nanoribbon quantum dot qubits

B.1 Graphene nanoribbon QD

B.1.1 The Problem

Consider a graphene nanoribbon with width W and length L. To solve the Dirac equation[13, 39, 96, 97]

$$(\frac{-i}{q_0}\begin{pmatrix}\sigma_x\partial_x+\sigma_y\partial_y & 0\\ 0 & -\sigma_x\partial_x+\sigma_y\partial_y\end{pmatrix}+\frac{V(y)}{\hbar v q_0})\langle x,y|\psi\rangle=\frac{\epsilon}{\hbar v q_0}\langle x,y|\psi\rangle, \tag{B.1}$$

where $q_0=\frac{\pi}{3W}$ is some momentum scale to be explained later. The 4-components spinor in this representation is

$$\begin{pmatrix}\psi(\text{valley=K, sublattice=A})\\ \psi(\text{valley=K, sublattice=B})\\ -\psi(\text{valley=K', sublattice=A})\\ -\psi(\text{valley=K', sublattice=B})\end{pmatrix}. \tag{B.2}$$

We need the four-component spinor here, because the valley degrees of freedom are coupled by the semiconducting armchair boundary condition of the nanoribbon. Without this boundary condition, the wavefunction for two valleys are decoupled, and we only need the two-component spinor (for example, gate-defined quantum dot.[98])

We use the basis expansion

$$|\psi\rangle = \sum_{m,s,n}\phi_s^{m,n}|\psi_s^{m,n}\rangle \tag{B.3}$$

$$\langle x,y|\psi_s^{m,n}\rangle = \frac{1}{\sqrt{2WL}}\begin{pmatrix}\chi_s e^{iq_n x}\\ \chi_s e^{-iq_n x}\end{pmatrix}f_m(y), \tag{B.4}$$

where $\{f_m(y)\}$ is a set of basis functions, $s=A,B$ denotes the two sublattices, and the constant two-component

spinors are

$$\chi_A = \begin{pmatrix} 1 \\ 0 \end{pmatrix} \tag{B.5}$$

$$\chi_B = \begin{pmatrix} 0 \\ 1 \end{pmatrix}. \tag{B.6}$$

The overlap matrix is

$$\langle \psi_{s'}^{m',n'} | \psi_s^{m,n} \rangle = \delta_{s',s} \delta_{n',n} a_{m',m}, \tag{B.7}$$

where the integral is defined as

$$a_{m',m} = \int_0^L \frac{dy}{L} f_{m'}(y) f_m(y). \tag{B.8}$$

Our goal is to solve for the generalized eigenvalue problem

$$\sum_{ms} \langle \psi_{s'}^{m'n} | H_1 | \psi_s^{m,n} \rangle \phi_s^{m,n} = \frac{\epsilon}{\hbar v q_0} \sum_{ms} \langle \psi_{s'}^{m'n} | \psi_s^{m,n} \rangle \phi_s^{m,n}. \tag{B.9}$$

B.1.2 Boundary condition

The armchair boundary condition is

$$\langle x, y|\psi\rangle|_{x=0} = \begin{pmatrix} 0 & 1 \\ 1 & 0 \end{pmatrix} \langle x, y|\psi\rangle_{x=0} \tag{B.10}$$

$$\langle x, y|\psi\rangle|_{x=W} = \begin{pmatrix} 0 & e^{+i\frac{2\pi\mu}{3}} \\ e^{-i\frac{2\pi\mu}{3}} & 0 \end{pmatrix} \langle x, y|\psi\rangle|_{x=W}, \tag{B.11}$$

where $\mu = \pm 1, 0$ is a constant determined by the width of the ribbon. $\mu = \pm 1$ gives the semiconducting boundary condition

$$e^{iq_n W} \chi_s = e^{+i\frac{2\pi\mu}{3}} e^{-iq_n W} \chi_s, \tag{B.12}$$

so

$$q_n = \frac{\pi}{W}(n + \frac{\mu}{3}), n \in \mathbb{Z} \tag{B.13}$$

$$= (3n + \mu)q_0, \tag{B.14}$$

where we define the momentum scale to be $q_0 = \frac{\pi}{3W}$.

B.1.3 Single-particle Matrix elements

Single-particle Hamiltonian is $H_1 = H_K + H_V$. The kinetic part of the Hamiltonian is

$$H_K = \int_0^W dx \int_0^L dy |x, y\rangle \frac{-i}{q_0} \begin{pmatrix} \sigma_x\partial_x + \sigma_y\partial_y & 0 \\ 0 & -\sigma_x\partial_x + \sigma_y\partial_y \end{pmatrix} \langle x, y|. \tag{B.15}$$

The matrix elements are

$$\begin{aligned} \langle \psi_{s'}^{m',n'} | H_K | \psi_s^{m,n} \rangle &= \frac{-i}{2q_0} \int_0^W \frac{dx}{W} \int \frac{dy}{L} \begin{pmatrix} \chi_{s'} e^{-iq_{n'}x} \\ \chi_{s'} e^{iq_{n'}x} \end{pmatrix}^T f_{m'}(y) \begin{pmatrix} (\sigma_x\partial_x + \sigma_y\partial_y)\chi_s e^{iq_n x} \\ (-\sigma_x\partial_x + \sigma_y\partial_y)\chi_s e^{-iq_n x} \end{pmatrix} f_m(y) \\ &= \begin{cases} \delta_{nn'}(\frac{q_n}{q_0}a_{m',m} - b_{m',m}) & s' = A, s = B \\ \delta_{nn'}(\frac{q_n}{q_0}a_{m',m} + b_{m',m}) & s' = B, s = A \\ 0 & s' = s \end{cases}, \end{aligned} \tag{B.16}$$

where the integral is defined as

$$b_{m',m} = \int_0^L \frac{dy}{L} f_{m'}(y) \frac{\partial y}{q_0} f_m(y). \tag{B.17}$$

The potential energy part of the Hamiltonian is

$$H_V = \int_0^W dx \int_0^L dy |x, y\rangle \frac{V(y)}{\hbar v q_0} \langle x, y|, \tag{B.18}$$

so the matrix element is

$$\langle \psi_{s'}^{m',n'} | H_V | \psi_s^{m,n} \rangle = \delta_{s',s}\delta_{n',n}c_{m',m}, \tag{B.19}$$

where the integral is defined as

$$c_{m',m} = \int_0^L \frac{dy}{L} f_{m'}(y) \frac{V(y)}{\hbar v q_0} f_m(y). \tag{B.20}$$

B.1.4 Plot the charge density

The expansion is

$$|\psi\rangle = \sum_{m,s,n} \phi_s^{m,n} |\psi_s^{m,n}\rangle \tag{B.21}$$

$$\langle x,y|\psi_s^{m,n}\rangle = \frac{1}{\sqrt{2WL}} \begin{pmatrix} \chi_s e^{iq_n x} \\ \chi_s e^{-iq_n x} \end{pmatrix} f_m(y). \tag{B.22}$$

For a fixed n, we make plot for charge density as a function of y-coordinate

$$\rho(y) = \int_0^W dx \langle\psi|x,y\rangle\langle x,y|\psi\rangle \tag{B.23}$$

$$= \int_0^W dx \sum_{m',m,s',s} \phi_{s'}^{m',n} \phi_s^{m,n} \langle\psi_{s'}^{m',n}|x,y\rangle\langle x,y|\psi_s^{m,n}\rangle \tag{B.24}$$

$$= \int_0^W dx \frac{1}{2WL} \sum_{m's'ms} \phi_{s'}^{m',n} \phi_s^{m,n} \begin{pmatrix} \chi_{s'}^T e^{-iq_n x} & \chi_{s'}^T e^{iq_n x} \end{pmatrix} \begin{pmatrix} \chi_s e^{iq_n x} \\ \chi_s e^{-iq_n x} \end{pmatrix} f_{m'}(y) f_m(y) \tag{B.25}$$

$$= \frac{1}{L} \sum_{m'ms} \phi_s^{m',n} \phi_s^{m,n} f_{m'}(y) f_m(y) \tag{B.26}$$

$$= \frac{1}{L} \sum_s [\sum_m \phi_s^{m,n} f_m(y)]^2. \tag{B.27}$$

B.1.5 One-particle Integrals for Sinusoidal basis

In this section we record the single particle integrals in the sinusoidal basis.

$$f_m(y) = \sqrt{2}\sin(\frac{\pi m y}{L}) \tag{B.28}$$

$$a_{m',m} = \delta_{m',m} \tag{B.29}$$

$$b_{m',m} = \begin{cases} 0 & m = m' \\ \frac{m}{q_0 L}[\frac{1-(-1)^{m'+m}}{m'+m} + \frac{1-(-1)^{m'-m}}{m'-m}] & m \neq m' \end{cases} \tag{B.30}$$

$$c_{m'm}(u,l) = -\frac{\sin[\pi(m'+m)y]|_{l/L}^{u/L}}{\pi(m'+m)} + \begin{cases} \frac{u-l}{L} & (m = m') \\ \frac{\sin[\pi(m'-m)y]|_{l/L}^{u/L}}{\pi(m'-m)} & (m \neq m') \end{cases} \tag{B.31}$$

$$c_{m',m} = \sum_{i=0}^{N_{seg}-1} \mu_{i+1} c_{m'm}(h_{i+1}, h_i)\ , (h_0 = 0, h_{N_{seg}} = L). \tag{B.32}$$

B.1.6 Coulomb Matrix elements for Sinusoidal Basis

The basis vectors are

$$\langle x, y|\psi_s^{m,n}\rangle = \frac{1}{\sqrt{2WL}} \begin{pmatrix} \chi_s e^{iq_n x} \\ \chi_s e^{-iq_n x} \end{pmatrix} f_m(y). \tag{B.33}$$

The Coulomb interaction operator is

$$v_{ee} = \frac{e^2}{4\pi\epsilon\hbar v}\frac{1}{q_0}\int dx_1 dy_1 dx_2 dy_2 \frac{1}{\sqrt{(x_1-x_2)^2+(y_1-y_2)^2}}|x_1, y_1, x_2, y_2\rangle\langle x_1, y_1, x_2, y_2|, \tag{B.34}$$

where $\frac{e^2}{4\pi\epsilon\hbar v}$ is the dimensionless Coulomb parameter, or so-called fine-structure constant of graphene[80]. $\frac{e^2}{4\pi\epsilon\hbar v} = 2.2$ for suspended graphene, $\frac{e^2}{4\pi\epsilon\hbar v} = 1.43$ for graphene on quartz substrate (which is a popular choice for graphene nanoribbon QD.) . Use

$$\langle\psi_{s'}^{m',n'}|x,y\rangle\langle x,y|\psi_s^{m,n}\rangle = (\frac{2}{WL})\delta_{ss'}\cos(\frac{\pi(n-n')x}{W})\sin(\frac{\pi m' y}{L})\sin(\frac{\pi m y}{L}), \tag{B.35}$$

to get

$$\langle\psi_{s_1'}^{m_1',n_1'}, \psi_{s_2'}^{m_2',n_2'}|v_{ee}|\psi_{s_1}^{m_1,n_1}, \psi_{s_2}^{m_2,n_2}\rangle = \frac{e^2}{4\pi\epsilon\hbar v}\delta_{s_1',s_1}\delta_{s_2',s_2}u_{m_1',n_1',m_2',n_2';m_1,n_1,m_2,n_2}, \tag{B.36}$$

where the two-particle integral is

$$u_{m_1',n_1',m_2',n_2';m_1,n_1,m_2,n_2} = \int_0^W \frac{dx_1 dx_2}{W^2} \int_0^L \frac{dy_1 dy_2}{L^2} \frac{4}{\sqrt{[(q_0 W)(\frac{x_1-x_2}{W})]^2 + [(q_0 L)(\frac{y_1-y_2}{L})]^2}} \quad \text{(B.37)}$$

$$\times \cos(\frac{\pi(n_1-n_1')x_1}{W}) \sin(\frac{\pi m_1' y_1}{L}) \sin(\frac{\pi m_1 y_1}{L}) \cos(\frac{\pi(n_2-n_2')x_2}{W}) \sin(\frac{\pi m_2' y_2}{L}) \sin(\frac{\pi m_2 y_2}{L}). \quad \text{(B.38)}$$

B.1.7 Two-particle Integral for Sinusoidal Basis

Use $\frac{1}{\sqrt{s}} = \frac{2}{\sqrt{\pi}} \int_0^\infty dt e^{-st^2}$ and $\int_0^\infty dt f(t) = \int_0^1 [f(t) + \frac{1}{t^2} f(\frac{1}{t})]$ to decouple the integral and get

$$u_{m_1',n_1',m_2',n_2';m_1,n_1,m_2,n_2} = \frac{8}{\sqrt{\pi}} \int_0^1 dt [I^x_{n_1',n_2';n_1,n_2}(t) I^y_{m_1',m_2';m_1,m_2}(t) + \frac{1}{t^2} I^x_{n_1',n_2';n_1,n_2}(\frac{1}{t}) I^y_{m_1',m_2';m_1,m_2}(\frac{1}{t})] \quad \text{(B.39)}$$

where

$$I^x_{n_1',n_2';n_1,n_2}(t) = \int_0^1 dx_1 dx_2 e^{-[t(q_0 W)(x_1-x_2)]^2} \cos(\pi(n_1-n_1')x_1) \cos(\pi(n_2-n_2')x_2) \quad \text{(B.40)}$$

$$I^y_{m_1',m_2';m_1,m_2}(t) = \int_0^1 dy_1 dy_2 e^{-[t(q_0 L)(y_1-y_2)]^2} \sin(\pi m_1' y_1) \sin(\pi m_1 y_1) \sin(\pi m_2' y_2) \sin(\pi m_2 y_2). \quad \text{(B.41)}$$

B.1.8 Generalized Valence Bound Method

We apply the unrestricted Hartree-Fock method[99] to the generalized valence bound wave function for $(1,1)$-particle sector.[45] The spatial part of the singlet$(+)$ and triplet$(-)$ wave functions

$$|\psi_\pm\rangle = \frac{1}{\sqrt{2(1 \pm S^2)}} (|\phi_L, \phi_R\rangle \pm |\phi_R, \phi_L\rangle), \quad \text{(B.42)}$$

where $S = |\langle \phi_L | \phi_R \rangle|$. The Hamiltonian is

$$H = H_1 \otimes 1 + 1 \otimes H_1 + v_{ee}. \quad \text{(B.43)}$$

The Schrodinger equation is

$$H|\psi_\pm\rangle = E|\psi_\pm\rangle. \quad \text{(B.44)}$$

Given ϕ_R, we solve for

$$\langle n', \phi_R | H | \psi_\pm \rangle = E \langle n', \phi_R | \psi_\pm \rangle. \quad \text{(B.45)}$$

We need a non-orthonormal basis set $\{|n\rangle\}$. Assuming $|\phi_R\rangle$ is normalized, the left-hand side is

$$\begin{aligned}
\sqrt{2(1\pm S^2)}\langle n',\phi_R|H|\psi_\pm\rangle &= \langle n',\phi_R|(H_1\otimes 1+1\otimes H_1+v_{ee})(|\phi_L,\phi_R\rangle\pm|\phi_R,\phi_L\rangle) && \text{(B.46)}\\
&= \langle n'|H_1|\phi_L\rangle\langle\phi_R|\phi_R\rangle+\langle n'|\phi_L\rangle\langle\phi_R|H_1|\phi_R\rangle\pm\langle n'|H_1|\phi_R\rangle\langle\phi_R|\phi_L\rangle && \text{(B.47)}\\
&\quad \pm\langle n'|\phi_R\rangle\langle\phi_R|H_1|\phi_L\rangle+\langle n',\phi_R|v_{ee}|\phi_L,\phi_R\rangle\pm\langle n',\phi_R|v_{ee}|\phi_R,\phi_L\rangle && \text{(B.48)}\\
&= \sum_n\langle n'|H_1|n\rangle\langle n|\phi_L\rangle+\langle n'|n\rangle\langle n|\phi_L\rangle\langle\phi_R|H_1|\phi_R\rangle\pm\langle n'|H_1|\phi_R\rangle\langle\phi_R|n\rangle\langle n|\phi_L\rangle && \text{(B.49)}\\
&\quad \pm\langle n'|\phi_R\rangle\langle\phi_R|H_1|n\rangle\langle n|\phi_L\rangle+\langle n',\phi_R|v_{ee}|n,\phi_R\rangle\langle n|\phi_L\rangle\pm\langle n',\phi_R|v_{ee}|\phi_R,n\rangle\langle n|\phi_L\rangle\\
&= \sum_n(\langle n'|H_1|n\rangle+\langle n'|n\rangle\langle\phi_R|H_1|\phi_R\rangle\pm\langle n'|H_1|\phi_R\rangle\langle\phi_R|n\rangle && \text{(B.50)}\\
&\quad \pm\langle n'|\phi_R\rangle\langle\phi_R|H_1|n\rangle+\langle n',\phi_R|v_{ee}|n,\phi_R\rangle\pm\langle n',\phi_R|v_{ee}|\phi_R,n\rangle)\langle n|\phi_L\rangle. && \text{(B.51)}
\end{aligned}$$

The right-hand side is

$$\begin{aligned}
\sqrt{2(1\pm S^2)}\langle n',\phi_R|\psi_\pm\rangle &= \langle n',\phi_R|(|\phi_L,\phi_R\rangle\pm|\phi_R,\phi_L\rangle) && \text{(B.52)}\\
&= \langle n'|\phi_L\rangle\langle\phi_R|\phi_R\rangle\pm\langle n'|\phi_R\rangle\langle\phi_R|\phi_L\rangle && \text{(B.53)}\\
&= \sum_n\langle n'|n\rangle\langle n|\phi_L\rangle\pm\langle n'|\phi_R\rangle\langle\phi_R|n\rangle\langle n|\phi_L\rangle && \text{(B.54)}\\
&= \sum_n(\langle n'|n\rangle\pm\langle n'|\phi_R\rangle\langle\phi_R|n\rangle)\langle n|\phi_L\rangle. && \text{(B.55)}
\end{aligned}$$

Hence the generalized eigen problem to be solved is

$$\langle n'|H_{GVB}|n\rangle\langle n|\phi_L\rangle=E\langle n'|S_{GVB}|n\rangle\langle n|\phi_L\rangle, \tag{B.56}$$

where the Hamiltonian and overlap matrices elements are

$$\begin{aligned}
\langle n'|H_{GVB}|n\rangle &= \langle n'|H_1|n\rangle+\langle n'|n\rangle\langle\phi_R|H_1|\phi_R\rangle\pm\langle n'|H_1|\phi_R\rangle\langle\phi_R|n\rangle\pm\langle n'|\phi_R\rangle\langle\phi_R|H_1|n\rangle && \text{(B.57)}\\
&\quad +\langle n',\phi_R|v_{ee}|n,\phi_R\rangle\pm\langle n',\phi_R|v_{ee}|\phi_R,n\rangle\\
\langle n'|S_{GVB}|n\rangle &= \langle n'|n\rangle\pm\langle n'|\phi_R\rangle\langle\phi_R|n\rangle. && \text{(B.58)}
\end{aligned}$$

To check the correctness, let the basis be orthonormal and coefficients be $L_n = \langle n|\phi_L\rangle, R_n = \langle n|\phi_R\rangle$, then

$$\begin{aligned}
\langle n'|H_{GVB}|n\rangle &= \langle n'|H_1|n\rangle + \delta_{n'n}\langle\phi_R|H_1|\phi_R\rangle \pm \langle n'|H_1|\phi_R\rangle R_n \pm R_{n'}\langle\phi_R|H_1|n\rangle \qquad \text{(B.59)}\\
&\quad +\langle n', \phi_R|v_{ee}|n, \phi_R\rangle \pm \langle n', \phi_R|v_{ee}|\phi_R, n\rangle\\
\langle n'|S_{GVB}|n\rangle &= \delta_{n'n} \pm R_{n'}R_n, \qquad \text{(B.60)}
\end{aligned}$$

which is the same as Fang *et al.* [45]. The set of equations is

$$\begin{aligned}
\langle n'|H_{GVB}|n\rangle &= \langle n'|H_1|n\rangle + \langle n'|n\rangle\langle\phi_L|H_1|\phi_L\rangle \pm \langle n'|H_1|\phi_L\rangle\langle\phi_L|n\rangle \pm \langle n'|\phi_L\rangle\langle\phi_L|H_1|n\rangle \qquad \text{(B.61)}\\
&\quad +\langle\phi_L, n'|v_{ee}|\phi_L, n\rangle \pm \langle\phi_L, n'|v_{ee}|n, \phi_L\rangle\\
\langle n'|S_{GVB}|n\rangle &= \langle n'|n\rangle \pm \langle n'|\phi_L\rangle\langle\phi_L|n\rangle \qquad \text{(B.62)}\\
\langle n'|H_{GVB}|n\rangle &= \langle n'|H_1|n\rangle + \langle n'|n\rangle\langle\phi_R|H_1|\phi_R\rangle \pm \langle n'|H_1|\phi_R\rangle\langle\phi_R|n\rangle \pm \langle n'|\phi_R\rangle\langle\phi_R|H_1|n\rangle \qquad \text{(B.63)}\\
&\quad +\langle n', \phi_R|v_{ee}|n, \phi_R\rangle \pm \langle n', \phi_R|v_{ee}|\phi_R, n\rangle\\
\langle n'|S_{GVB}|n\rangle &= \langle n'|n\rangle \pm \langle n'|\phi_R\rangle\langle\phi_R|n\rangle. \qquad \text{(B.64)}
\end{aligned}$$

B.1.9 Evaluating Two-particle Integrals

To evaluate

$$\begin{aligned}
I^x_{n'_1,n'_2;n_1,n_2}(t) &= \int_0^1 dx_1dx_2e^{-[t(q_0W)(x_1-x_2)]^2}\cos(\pi(n_1-n'_1)x_1)\cos(\pi(n_2-n'_2)x_2) \qquad \text{(B.65)}\\
&= I^{xy}(tq_0W, (n_1-n'_1), (n_2-n'_2)) \qquad \text{(B.66)}\\
I^y_{m'_1,m'_2;m_1,m_2}(t) &= \int_0^1 dy_1dy_2e^{-[t(q_0L)(y_1-y_2)]^2}\sin(\pi m'_1y_1)\sin(\pi m_1y_1)\sin(\pi m'_2y_2)\sin(\pi m_2y_2) \qquad \text{(B.67)}\\
&= \frac{1}{4}\int_0^1 dy_1dy_2e^{-[t(q_0L)(y_1-y_2)]^2} \qquad \text{(B.68)}\\
&\quad \times[\cos(\pi(m'_1+m_1)y_1)\cos(\pi(m'_2+m_2)y_2) + \cos(\pi(m'_1-m_1)y_1)\cos(\pi(m'_2-m_2)y_2)\\
&\quad -\cos(\pi(m'_1+m_1)y_1)\cos(\pi(m'_2-m_2)y_2) - \cos(\pi(m'_1-m_1)y_1)\cos(\pi(m'_2+m_2)y_2)]\\
&= \frac{1}{4}[I^{xy}(tq_0L, (m'_1+m_1), (m'_2+m_2)) + I^{xy}(tq_0L, (m'_1-m_1), (m'_2-m_2)) \qquad \text{(B.69)}\\
&\quad -I^{xy}(tq_0L, (m'_1+m_1), (m'_2-m_2)) - I^{xy}(tq_0L, (m'_1-m_1), (m'_2+m_2))] \qquad \text{(B.70)}\\
I^{xy}(tl, j_1, j_2) &= \int_0^1 dx_1dx_2e^{-[tl(x_1-x_2)]^2}\cos(\pi j_1x_1)\cos(\pi j_2x_2), \qquad \text{(B.71)}
\end{aligned}$$

we use Fourier transform

$$f(x) = \frac{1}{\sqrt{2\pi}}\int_{-\infty}^{\infty} dk e^{ikx} f(k) \tag{B.72}$$

$$\int_{-\infty}^{\infty} dx dx' \bar{f}(x) K(x-x') g(x') = \sqrt{2\pi}\int_{-\infty}^{\infty} dk \bar{f}(k) K(k) g(k). \tag{B.73}$$

The transformations needed are

$$F_g(a,k) = F\{e^{-(ax)^2}\} = \frac{1}{\sqrt{2}a} e^{-(\frac{k}{2a})^2} \tag{B.74}$$

$$F_c(\pi j,k) = F\{[\Theta(x)-\Theta(x-1)]\cos(\pi j x)\} = \begin{cases} \frac{ik}{\sqrt{2\pi}}\frac{1-e^{-ik}\cos(\pi j)}{(\pi j-k)(\pi j+k)} & k \neq \pm\pi j \\ \frac{i}{2\sqrt{2\pi}}\frac{1-i\pi j-e^{i\pi j}\cos(\pi j)}{\pi j} & k \to -\pi j \\ (k\to -\pi j)^\dagger & k \to \pi j \\ \frac{1}{\sqrt{2\pi}} & k \to \pm\pi j \to 0 \end{cases}. \tag{B.75}$$

Then the integral is

$$I^{xy}(tl,j_1,j_2) = \sqrt{2\pi}\int_{-\infty}^{\infty} dk \bar{F}_c(\pi j_1,k)\frac{1}{\sqrt{2tl}} e^{-(\frac{k}{2tl})^2} F_c(\pi j_2,k) \tag{B.76}$$

$$= 2\sqrt{\pi}\int_{-\infty}^{\infty} dK e^{-K^2} \bar{F}_c(\pi j_1, 2tlK) F_c(\pi j_2, 2tlK). \tag{B.77}$$

The last line is the form of Gauss-Hermite quadrature.

To summarize, the following expressions are all we need:

$$u_{m_1',n_1',m_2',n_2';m_1,n_1,m_2,n_2} = \frac{8}{\sqrt{\pi}}\int_0^1 dt [I^x_{n_1',n_2';n_1,n_2}(t) I^y_{m_1',m_2';m_1,m_2}(t) \tag{B.78}$$

$$+\frac{1}{t^2} I^x_{n_1',n_2';n_1,n_2}(\frac{1}{t}) I^y_{m_1',m_2';m_1,m_2}(\frac{1}{t})] \tag{B.79}$$

$$I^x_{n_1',n_2';n_1,n_2}(t) = I^{xy}(tq_0 W, (n_1-n_1'), (n_2-n_2')) \tag{B.80}$$

$$I^y_{m_1',m_2';m_1,m_2}(t) = \frac{1}{4}[I^{xy}(tq_0 L, (m_1'+m_1), (m_2'+m_2)) \tag{B.81}$$

$$+I^{xy}(tq_0 L, (m_1'-m_1), (m_2'-m_2)) \tag{B.82}$$

$$-I^{xy}(tq_0 L, (m_1'+m_1), (m_2'-m_2)) \tag{B.83}$$

$$-I^{xy}(tq_0 L, (m_1'-m_1), (m_2'+m_2))] \tag{B.84}$$

$$I^{xy}(tl,j_1,j_2) = \frac{1}{\sqrt{\pi}}\int_{-\infty}^{\infty} dk e^{-k^2} F_{xy}(j_1,j_2,2tlk) \tag{B.85}$$

$$F_{xy}(j_1,j_2,k) = \frac{k^2[1+(-1)^{j_1+j_2}-\cos(k)((-1)^{j_1}+(-1)^{j_2})]}{(\pi j_1-k)(\pi j_1+k)(\pi j_2-k)(\pi j_2+k)} \tag{B.86}$$

Various limits of the integrand ($j \equiv (j_1 + j_2)$):

$$F_{xy}(j_1, j_2, k) \tag{B.87}$$
$$= \begin{cases} 1 & j_1 = j_2 = 0, k = 0 \\ \frac{2}{k^2}(1 - \cos(k)) & j_1 = j_2 = 0, k \neq 0 \\ \frac{2[1-(-1)^{j_1}\cos(k)]}{(\pi j_1 - k)^2 - 4(\pi j_1 - k)(\pi j_1 + k) + (\pi j_1 + k)^2} & j_1 = j_2 \neq 0, k = \pm\pi j_1 \\ \frac{2k^2[1-(-1)^{j_1}\cos(k)]}{(\pi j_1 - k)^2(\pi j_1 + k)^2} & j_1 = j_2 \neq 0, k \neq \pm\pi j_1 \\ 0 & j_1 \; xor \; j_2 = 0, k = \pm\pi j \\ \frac{(1+(-1)^j)(\cos(k)-1)}{(\pi j - k)(\pi j + k)} & j_1 \; xor \; j_2 = 0, k \neq \pm\pi j \\ \frac{2k\{1+(-1)^j - \cos(k)[(-1)^{j_1} + (-1)^{j_2}]\} + k^2 \sin(k)[(-1)^{j_1} + (-1)^{j_2}]}{D} & j_1 \neq j_2, j_1 \neq 0, j_2 \neq 0, \\ & k = \pm\pi j_1 \; or \; \pm\pi j_2 \end{cases}$$

,where $D = -(\pi j_1 + k)(\pi j_2 - k)(\pi j_2 + k) + (\pi j_1 - k)(\pi j_2 - k)(\pi j_2 + k) - (\pi j_1 - k)(\pi j_1 + k)(\pi j_2 + k) + (\pi j_1 - k)(\pi j_1 + k)(\pi j_2 - k)$.

B.2 Analytic solution for single potential well

B.2.1 Introduction

Here we follow Trauzettel *et al.* [13], Brey and Fertig [39] to obtain analytical solution for a single potential well on graphene nanoribbon. In the x-direction the semiconducting armchair boundary condition is imposed , while the confining potential is applied in the y-direction.

B.2.2 Plane wave solution

The low energy effective Hamiltonian for the electron in graphene gives the Dirac equation

$$-i \begin{pmatrix} \sigma_x \partial_x + \sigma_y \partial_y & 0 \\ 0 & -\sigma_x \partial_x + \sigma_y \partial_y \end{pmatrix} \psi = \frac{\epsilon - \mu(y)}{\hbar v} \psi \tag{B.88}$$

$$\psi = \begin{pmatrix} \psi_{AK} \\ \psi_{BK} \\ -\psi_{AK'} \\ -\psi_{BK'} \end{pmatrix}. \tag{B.89}$$

$\psi_{\alpha\beta}$ denotes the components of the spinor, where $\alpha = A, B$ is the index for the two sublattices and $\beta = K, K'$ is the index for the two valleys. In the y-direction it is a potential well $\mu(y) = \mu_{gate}, y \in [0, L]$ and $\mu(y) = \mu_{barrier}, y \in (-\infty, 0) \cup (L, \infty)$ where L is the length of the quantum dot. The boundary condition in the x-direction will be explained later.

Since $(\pm\sigma_x\partial_x + \sigma_y\partial_y)^2 = \partial_x^2 + \partial_y^2$, we get

$$-(\partial_x^2 + \partial_y^2)\psi = (\frac{\epsilon - \mu}{\hbar v})^2\psi. \tag{B.90}$$

Consider the Fourier components

$$\chi_{nk}^{\pm\pm}(x, y) \quad = e^{\pm iq_n x}e^{\pm iky}c^{\pm\pm}(n, k) \tag{B.91}$$

$$c^{\pm\pm}(n, k) = \begin{pmatrix} c_{AK}^{\pm\pm}(n, k) \\ c_{BK}^{\pm\pm}(n, k) \\ -c_{AK'}^{\pm\pm}(n, k) \\ -c_{BK'}^{\pm\pm}(n, k) \end{pmatrix} \tag{B.92}$$

to get the eigen energy

$$\frac{\epsilon_{nk} - \mu}{\hbar v} = \pm\sqrt{q_n^2 + k^2}. \tag{B.93}$$

The positive sign is the conduction band and the negative sign is the valence band. In the following we consider only the conduction band. The valence band solution can be obtained by the particle-hole conjugation partner $(\psi_{AK}, -\psi_{BK}, -\psi_{AK'}, \psi_{BK'})$ with eigen value $\frac{\epsilon_{nk}-\mu}{\hbar v} = -\sqrt{q_n^2 + k^2}$. The above is what we can get from H^2. There is some extra information we can get from H, which is about the relation between different spinor components.

$$\begin{pmatrix} \sigma_x(\pm q_n) + \sigma_y(\pm k) & 0 \\ 0 & -\sigma_x(\pm q_n) + \sigma_y(\pm k) \end{pmatrix} c^{\pm\pm}(n, k) = \sqrt{q_n^2 + k^2}c^{\pm\pm}(n, k), \tag{B.94}$$

which gives

$$(\pm q_n \mp ik)c^{\pm\pm}_{BK}(n,k) = \sqrt{q_n^2+k^2}c^{\pm\pm}_{AK}(n,k) \tag{B.95}$$

$$(\pm q_n \pm ik)c^{\pm\pm}_{AK}(n,k) = \sqrt{q_n^2+k^2}c^{\pm\pm}_{BK}(n,k) \tag{B.96}$$

$$(\mp q_n \mp ik)c^{\pm\pm}_{BK'}(n,k) = \sqrt{q_n^2+k^2}c^{\pm\pm}_{AK'}(n,k) \tag{B.97}$$

$$(\mp q_n \pm ik)c^{\pm\pm}_{AK'}(n,k) = \sqrt{q_n^2+k^2}c^{\pm\pm}_{BK'}(n,k). \tag{B.98}$$

For convenience we define $z_{nk} = \frac{(q_n+ik)}{\sqrt{q_n^2+k^2}}$, which satisfies $z_{nk}^{-1} = \bar{z}_{nk}$. The first two equations imply

$$c^{++}_{BK}(n,k) = +z_{nk}c^{++}_{AK}(n,k) \tag{B.99}$$

$$c^{--}_{BK}(n,k) = -z_{nk}c^{--}_{AK}(n,k) \tag{B.100}$$

$$c^{+-}_{AK}(n,k) = +z_{nk}c^{+-}_{BK}(n,k) \tag{B.101}$$

$$c^{-+}_{AK}(n,k) = -z_{nk}c^{-+}_{BK}(n,k), \tag{B.102}$$

while the other two equations gives

$$c^{++}_{AK'}(n,k) = -z_{nk}c^{++}_{BK'}(n,k) \tag{B.103}$$

$$c^{--}_{AK'}(n,k) = +z_{nk}c^{--}_{BK'}(n,k) \tag{B.104}$$

$$c^{+-}_{BK'}(n,k) = -z_{nk}c^{+-}_{AK'}(n,k) \tag{B.105}$$

$$c^{-+}_{BK'}(n,k) = +z_{nk}c^{-+}_{AK'}(n,k). \tag{B.106}$$

So we can write

$$c^{++}(n,k) = c^{++}_{AK}(n,k)\begin{pmatrix}1\\ z_{nk}\\ 0\\ 0\end{pmatrix} + (-c^{++}_{BK'}(n,k))\begin{pmatrix}0\\ 0\\ -z_{nk}\\ 1\end{pmatrix} \tag{B.107}$$

$$c^{-+}(n,k) = c^{-+}_{BK}(n,k)\begin{pmatrix} -z_{nk} \\ 1 \\ 0 \\ 0 \end{pmatrix} + (-c^{-+}_{AK'}(n,k))\begin{pmatrix} 0 \\ 0 \\ 1 \\ z_{nk} \end{pmatrix} \tag{B.108}$$

$$c^{+-}(n,k) = c^{+-}_{BK}(n,k)\begin{pmatrix} z_{nk} \\ 1 \\ 0 \\ 0 \end{pmatrix} + (-c^{+-}_{AK'}(n,k))\begin{pmatrix} 0 \\ 0 \\ 1 \\ -z_{nk} \end{pmatrix} \tag{B.109}$$

$$c^{--}(n,k) = c^{--}_{AK}(n,k)\begin{pmatrix} 1 \\ -z_{nk} \\ 0 \\ 0 \end{pmatrix} + (-c^{--}_{BK'}(n,k))\begin{pmatrix} 0 \\ 0 \\ z_{nk} \\ 1 \end{pmatrix} \tag{B.110}$$

Comparing to the equation (A3) (A4) (A5) in the arxiv version of the reference[13], we can identify the coefficients

$$a_{n+} = c^{++}_{AK}(n,k) \tag{B.111}$$

$$a'_{n+} = -c^{++}_{BK'}(n,k) \tag{B.112}$$

$$b_{n+} = c^{-+}_{BK}(n,k) \tag{B.113}$$

$$b'_{n+} = -c^{-+}_{AK'}(n,k) \tag{B.114}$$

$$a_{n-} = c^{+-}_{BK}(n,k) \tag{B.115}$$

$$a'_{n-} = -c^{+-}_{AK'}(n,k) \tag{B.116}$$

$$b_{n-} = c^{--}_{AK}(n,k) \tag{B.117}$$

$$b'_{n-} = -c^{--}_{BK'}(n,k). \tag{B.118}$$

In the left-hand-side the coefficients are independent of k. It is OK since in the y-direction we know the answer will be the plane wave solution, so only the sign of k is important. This independence of k is important in the following process of matching the boundary conditions.

So we can now move to the notations in (A3) (A4) (A5) in reference[13].

B.2.3 Semiconducting armchair boundary condition

In the x-direction the boundary condition is the semiconducting armchair boundary condition:

$$\psi(x=0) = \begin{pmatrix} 0 & 1 \\ 1 & 0 \end{pmatrix} \psi(x=0) \tag{B.119}$$

$$\psi(x=W) = \begin{pmatrix} 0 & e^{-i\frac{2\pi\mu}{3}} \\ e^{i\frac{2\pi\mu}{3}} & 0 \end{pmatrix} \psi(x=W), \tag{B.120}$$

where W is the width of the graphene ribbon, $\mu = \pm 1$ is a number determined by W, $\frac{W}{a_0} = 3M + \mu$ for some integer M. $a_0 = 0.246nm$ is the lattice constant of the graphene. The $\mu = 0$ case is metallic (no gap) and we are not interested in it.

Imposing the boundary condition gives the equations for the plane wave travelling in the +y-direction χ^+

$$\begin{pmatrix} a_{n+} \\ z_{nk}a_{n+} \\ -z_{nk}a'_{n+} \\ a'_{n+} \end{pmatrix} + \begin{pmatrix} -z_{nk}b_{n+} \\ b_{n+} \\ b'_{n+} \\ z_{nk}b'_{n+} \end{pmatrix} = \begin{pmatrix} -z_{nk}a'_{n+} \\ a'_{n+} \\ a_{n+} \\ z_{nk}a_{n+} \end{pmatrix} + \begin{pmatrix} b'_{n+} \\ z_{nk}b'_{n+} \\ -z_{nk}b_{n+} \\ b_{n+} \end{pmatrix} \tag{B.121}$$

$$e^{iq_nW}\begin{pmatrix} a_{n+} \\ z_{nk}a_{n+} \\ -z_{nk}a'_{n+} \\ a'_{n+} \end{pmatrix} + e^{-iq_nW}\begin{pmatrix} -z_{nk}b_{n+} \\ b_{n+} \\ b'_{n+} \\ z_{nk}b'_{n+} \end{pmatrix} = e^{iq_nW}\begin{pmatrix} -e^{-i\frac{2\pi\mu}{3}}z_{nk}a'_{n+} \\ e^{-i\frac{2\pi\mu}{3}}a'_{n+} \\ e^{i\frac{2\pi\mu}{3}}a_{n+} \\ e^{i\frac{2\pi\mu}{3}}z_{nk}a_{n+} \end{pmatrix} + e^{-iq_nW}\begin{pmatrix} e^{-i\frac{2\pi\mu}{3}}b'_{n+} \\ e^{-i\frac{2\pi\mu}{3}}z_{nk}b'_{n+} \\ -e^{i\frac{2\pi\mu}{3}}z_{nk}b_{n+} \\ e^{i\frac{2\pi\mu}{3}}b_{n+} \end{pmatrix} \tag{B.122}$$

There are 4 variables and 8 equations. There are only 4 independent equations since the equations for two different valleys are the same, so we only need to look at the equations for the valley K. The independent equations are

$$\begin{pmatrix} 1 \\ z_{nk} \end{pmatrix} a_{n+} + \begin{pmatrix} -z_{nk} \\ 1 \end{pmatrix} b_{n+} = \begin{pmatrix} -z_{nk} \\ 1 \end{pmatrix} a'_{n+} + \begin{pmatrix} 1 \\ z_{nk} \end{pmatrix} b'_{n+} \tag{B.123}$$

$$e^{iq_nW}\begin{pmatrix}1\\ z_{nk}\end{pmatrix}a_{n+}+e^{-iq_nW}\begin{pmatrix}-z_{nk}\\ 1\end{pmatrix}b_{n+}=e^{iq_nW}e^{-i\frac{2\pi\mu}{3}}\begin{pmatrix}-z_{nk}\\ 1\end{pmatrix}a'_{n+}+e^{-iq_nW}e^{-i\frac{2\pi\mu}{3}}\begin{pmatrix}1\\ z_{nk}\end{pmatrix}b'_{n+} \tag{B.124}$$

This is a system of linear equations

$$\begin{pmatrix}1 & -z_{nk} & z_{nk} & -1\\ z_{nk} & 1 & -1 & -z_{nk}\\ u & -z_{nk}/u & uvz_{nk} & -v/u\\ uz_{nk} & 1/u & -uv & -vz_{nk}/u\end{pmatrix}\begin{pmatrix}a_{n+}\\ b_{n+}\\ a'_{n+}\\ b'_{n+}\end{pmatrix}=0, \tag{B.125}$$

where $u=e^{iq_nW}$ and $v=e^{-i\frac{2\pi}{3}}$. The condition for non-zero solution is

$$det=(1+z_{nk}^2)^2(uv-1/u)(u-v/u)=0. \tag{B.126}$$

There are two possible solutions $uv=1/u$ and $u=v/u$. The two solutions give the quantization condition

$$q_n = \frac{\pi}{W}(n+\frac{\mu}{3}), n\in\mathbb{Z} \tag{B.127}$$

$$q_n = \frac{\pi}{W}(n-\frac{\mu}{3}), n\in\mathbb{Z}, \tag{B.128}$$

respectively.

Performing the Gaussian elimination for two steps gives

$$\begin{pmatrix}1 & 0 & 0 & -1\\ 0 & 1 & -1 & 0\\ 0 & z_{nk}(u-1/u) & z_{nk}u(v-1) & u-v/u\\ 0 & z_{nk}^2u+1/u & -u(v+z_{nk}^2) & z_{nk}(u-v/u)\end{pmatrix}, \tag{B.129}$$

which imply $a_{n+}=b'_{n+}$ and $b_{n+}=a'_{n+}$.

For the first solution $uv = 1/u$, we can continue the Gaussian elimination to get

$$\begin{pmatrix} 1 & 0 & 0 & -1 \\ 0 & 1 & -1 & 0 \\ 0 & 0 & 0 & 1 \\ 0 & 0 & 0 & 0 \end{pmatrix}, \tag{B.130}$$

so $a_{n+} = b'_{n+} = 0$. For the second solution $u = v/u$, we can continue the Gaussian elimination to get

$$\begin{pmatrix} 1 & 0 & 0 & -1 \\ 0 & 1 & -1 & 0 \\ 0 & 0 & 1 & 0 \\ 0 & 0 & 0 & 0 \end{pmatrix}, \tag{B.131}$$

so $b_{n+} = a'_{n+} = 0$.

Imposing the boundary condition gives the equations for the plane wave travelling in the -y-direction χ^-,

$$\begin{pmatrix} z_{nk} \\ 1 \end{pmatrix} a_{n-} + \begin{pmatrix} 1 \\ -z_{nk} \end{pmatrix} b_{n-} = \begin{pmatrix} 1 \\ -z_{nk} \end{pmatrix} a'_{n-} + \begin{pmatrix} z_{nk} \\ 1 \end{pmatrix} b'_{n-} \tag{B.132}$$

$$e^{iq_nW} \begin{pmatrix} z_{nk} \\ 1 \end{pmatrix} a_{n-} + e^{-iq_nW} \begin{pmatrix} 1 \\ -z_{nk} \end{pmatrix} b_{n-} = e^{iq_nW} e^{-i\frac{2\pi\mu}{3}} \begin{pmatrix} 1 \\ -z_{nk} \end{pmatrix} a'_{n-} + e^{-iq_nW} e^{-i\frac{2\pi\mu}{3}} \begin{pmatrix} z_{nk} \\ 1 \end{pmatrix} b'_{n-} \tag{B.133}$$

This is a system of linear equations

$$\begin{pmatrix} z_{nk} & 1 & -1 & -z_{nk} \\ 1 & -z_{nk} & z_{nk} & -1 \\ uz_{nk} & 1/u & -uv & -vz_{nk}/u \\ u & -z_{nk}/u & uvz_{nk} & -v/u \end{pmatrix} \begin{pmatrix} a_{n-} \\ b_{n-} \\ a'_{n-} \\ b'_{n-} \end{pmatrix} = 0, \tag{B.134}$$

which is the same as the previous one if we interchange the 1st row with the 2nd row, and interchange the 3rd row with the 4th row.

For the first solution $uv = 1/u$, we should get

$$\begin{pmatrix} 0 & 1 & -1 & 0 \\ 1 & 0 & 0 & -1 \\ 0 & 0 & 0 & 0 \\ 0 & 0 & 0 & 1 \end{pmatrix} \tag{B.135}$$

, so $a_{n-} = b'_{n-} = 0$. For the second solution $u = v/u$ we get

$$\begin{pmatrix} 0 & 1 & -1 & 0 \\ 1 & 0 & 0 & -1 \\ 0 & 0 & 0 & 0 \\ 0 & 0 & 1 & 0 \end{pmatrix}, \tag{B.136}$$

so $b_{n-} = a'_{n-} = 0$.

We have finished the boundary condition in the x-direction. The following is a short summary of the solution we have:

$$\chi^+_{nk}(x) = a_{n+} \begin{pmatrix} e^{iq_n x} \\ z_{nk} e^{iq_n x} \\ e^{-iq_n x} \\ z_{nk} e^{-iq_n x} \end{pmatrix} + a'_{n+} \begin{pmatrix} -z_{nk} e^{-iq_n x} \\ e^{-iq_n x} \\ -z_{nk} e^{iq_n x} \\ e^{iq_n x} \end{pmatrix} \tag{B.137}$$

$$\chi^-_{nk}(x) = a_{n-} \begin{pmatrix} z_{nk} e^{iq_n x} \\ e^{iq_n x} \\ z_{nk} e^{-iq_n x} \\ e^{-iq_n x} \end{pmatrix} + a'_{n-} \begin{pmatrix} e^{-iq_n x} \\ -z_{nk} e^{-iq_n x} \\ e^{iq_n x} \\ -z_{nk} e^{iq_n x} \end{pmatrix} \tag{B.138}$$

with

$$q_n = \frac{\pi}{W}(n + \frac{\mu}{3}), n \in \mathbb{Z} \tag{B.139}$$

$$a_{n\pm} = 0 \tag{B.140}$$

or

$$q_n = \frac{\pi}{W}(n - \frac{\mu}{3}), n \in \mathbb{Z} \tag{B.141}$$

$$a'_{n\pm} = 0. \tag{B.142}$$

There are two possible sets of solutions depending on the boundary condition. We will continue with

$$\chi^+_{nk}(x) = a_{n+} \begin{pmatrix} e^{iq_n x} \\ z_{nk} e^{iq_n x} \\ e^{-iq_n x} \\ z_{nk} e^{-iq_n x} \end{pmatrix} \tag{B.143}$$

$$\chi^-_{nk}(x) = a_{n-} \begin{pmatrix} z_{nk} e^{iq_n x} \\ e^{iq_n x} \\ z_{nk} e^{-iq_n x} \\ e^{-iq_n x} \end{pmatrix} \tag{B.144}$$

$$q_n = \frac{\pi}{W}(n + \frac{1}{3}), n \in \mathbb{Z}. \tag{B.145}$$

B.2.4 Boundary of the potential well

In the y-direction the boundary condition is the potential well. We are interesting in the solution where it is a travelling wave inside the well and exponentially decaying outside the well. So with the requirement

$$(\frac{\epsilon - \mu_{gate}}{\hbar v})^2 > q_n^2 > (\frac{\epsilon - \mu_{barrier}}{\hbar v})^2 \tag{B.146}$$

we can define the momentum outside and inside the well as

$$k = i\sqrt{q_n^2 - (\frac{\epsilon - \mu_{barrier}}{\hbar v})^2} \tag{B.147}$$

$$\tilde{k} = \sqrt{-q_n^2 + (\frac{\epsilon - \mu_{gate}}{\hbar v})^2}. \tag{B.148}$$

The solution is

$$\psi = \begin{cases} \alpha'_n \chi^-_{nk}(x) e^{-iky} & y < 0 \\ \beta'_n \chi^+_{n\tilde{k}}(x) e^{i\tilde{k}y} + \gamma'_n \chi^-_{n\tilde{k}} e^{-i\tilde{k}y} & y \in (0, L) \\ \delta'_n \chi^+_{nk}(x) e^{ik(y-L)} & y > L \end{cases}, \tag{B.149}$$

or equivalently,

$$\psi = \begin{cases} \alpha_n \begin{pmatrix} z_{nk} e^{iq_n x} \\ e^{iq_n x} \\ z_{nk} e^{-iq_n x} \\ e^{-iq_n x} \end{pmatrix} e^{-iky} & y < 0 \\ \beta_n \begin{pmatrix} e^{iq_n x} \\ z_{n\tilde{k}} e^{iq_n x} \\ e^{-iq_n x} \\ z_{n\tilde{k}} e^{-iq_n x} \end{pmatrix} e^{i\tilde{k}y} + \gamma_n \begin{pmatrix} z_{n\tilde{k}} e^{iq_n x} \\ e^{iq_n x} \\ z_{n\tilde{k}} e^{-iq_n x} \\ e^{-iq_n x} \end{pmatrix} e^{-i\tilde{k}y} & y \in (0, L) \\ \delta_n \begin{pmatrix} e^{iq_n x} \\ z_{nk} e^{iq_n x} \\ e^{-iq_n x} \\ z_{nk} e^{-iq_n x} \end{pmatrix} e^{ik(y-L)} & y > L \end{cases}. \tag{B.150}$$

Plug into the boundary condition, the first two components of the spinor give the same equations as the last two components, which is

$$\alpha_n \begin{pmatrix} z_{nk} \\ 1 \end{pmatrix} = \beta_n \begin{pmatrix} 1 \\ z_{n\tilde{k}} \end{pmatrix} + \gamma_n \begin{pmatrix} z_{n\tilde{k}} \\ 1 \end{pmatrix} \tag{B.151}$$

$$\delta_n \begin{pmatrix} 1 \\ z_{nk} \end{pmatrix} = \beta_n e^S \begin{pmatrix} 1 \\ z_{n\tilde{k}} \end{pmatrix} + \gamma_n e^{-S} \begin{pmatrix} z_{n\tilde{k}} \\ 1 \end{pmatrix}, \tag{B.152}$$

where $S = i\tilde{k}L$. Writing as a set of linear equations

$$\begin{pmatrix} z_{nk} & -1 & -z_{n\tilde{k}} & 0 \\ 1 & -z_{n\tilde{k}} & -1 & 0 \\ 0 & -e^S & -z_{n\tilde{k}}e^{-S} & 1 \\ 0 & -z_{n\tilde{k}}e^S & -e^{-S} & z_{nk} \end{pmatrix} \begin{pmatrix} \alpha_n \\ \beta_n \\ \gamma_n \\ \delta_n \end{pmatrix} = 0. \tag{B.153}$$

For nonzero solution, the determinant should be zero

$$\begin{aligned} \det &= z_{nk}[-z_{n\tilde{k}} det \begin{pmatrix} -z_{n\tilde{k}}e^{-S} & 1 \\ -e^{-S} & z_{nk} \end{pmatrix} + det \begin{pmatrix} -e^S & 1 \\ -z_{n\tilde{k}}e^S & z_{nk} \end{pmatrix}] && \text{(B.154)} \\ &-[-det \begin{pmatrix} -z_{n\tilde{k}}e^{-S} & 1 \\ -e^{-S} & z_{nk} \end{pmatrix} + z_{n\tilde{k}} det \begin{pmatrix} -e^S & 1 \\ -z_{n\tilde{k}}e^S & z_{nk} \end{pmatrix}] && \text{(B.155)} \\ &= (1 - z_{nk}z_{n\tilde{k}}) det \begin{pmatrix} -z_{n\tilde{k}}e^{-S} & 1 \\ -e^{-S} & z_{nk} \end{pmatrix} + (z_{nk} - z_{n\tilde{k}}) det \begin{pmatrix} -e^S & 1 \\ -z_{n\tilde{k}}e^S & z_{nk} \end{pmatrix} && \text{(B.156)} \\ &= e^{-S}(1 - z_{nk}z_{n\tilde{k}})^2 - e^S(z_{nk} - z_{n\tilde{k}})^2 && \text{(B.157)} \\ &= 0 && \text{(B.158)} \end{aligned}$$

with the solution

$$e^S = \frac{1 - z_{nk}z_{n\tilde{k}}}{z_{nk} - z_{n\tilde{k}}} \tag{B.159}$$

Recall the definitions $z_{nk} = \frac{(q_n + ik)}{\sqrt{q_n^2 + k^2}}$, $k = i\sqrt{q_n^2 - (\frac{\epsilon - \mu_{barrier}}{\hbar v})^2}$, $\tilde{k} = \sqrt{-q_n^2 + (\frac{\epsilon - \mu_{gate}}{\hbar v})^2}$, $S = i\tilde{k}L$. In the energy window k is purely imaginary and $\tilde{k}$ is purely real. Hence the right-hand side is

$$\begin{aligned} \text{r.h.s.} &= \frac{1 - z_{nk}\cos\theta_n - iz_{nk}\sin\theta_n}{z_{nk} - \cos\theta_n - i\sin\theta_n} && \text{(B.160)} \\ &= \frac{(1 - z_{nk}\cos\theta_n - iz_{nk}\sin\theta_n)(z_{nk} - \cos\theta_n + i\sin\theta_n)}{(z_{nk} - \cos\theta_n)^2 + (\sin\theta_n)^2} && \text{(B.161)} \\ &= \frac{1}{(z_{nk} - \cos\theta_n)^2 + (\sin\theta_n)^2}[(2z_{nk} - (1 + z_{nk}^2)\cos\theta_n) + i(\sin\theta_n(1 - z_{nk}^2))], && \text{(B.162)} \end{aligned}$$

where $z_{n\tilde{k}} = e^{i\theta_n} = \frac{(q_n + i\tilde{k})}{\sqrt{q_n^2 + \tilde{k}^2}}$. Remember $\frac{\epsilon - \mu_{barrier}}{\hbar v} = \sqrt{q_n^2 + k^2}$ and $\frac{\epsilon - \mu_{gate}}{\hbar v} = \sqrt{q_n^2 + \tilde{k}^2}$. So we have

$$\tan(\tilde{k}L) = \frac{\sin\theta_n(1-z_{nk}^2)}{2z_{nk}-(1+z_{nk}^2)\cos\theta_n} \tag{B.163}$$

$$= \frac{\frac{(\tilde{k})}{\sqrt{q_n^2+\tilde{k}^2}}(1-(\frac{(q_n+ik)}{\sqrt{q_n^2+k^2}})^2)}{2(\frac{(q_n+ik)}{\sqrt{q_n^2+k^2}})-(1+(\frac{(q_n+ik)}{\sqrt{q_n^2+k^2}})^2)\frac{(q_n)}{\sqrt{q_n^2+\tilde{k}^2}}} \tag{B.164}$$

$$= \frac{\tilde{k}(q_n^2+k^2-(q_n+ik)^2)}{2(q_n+ik)\sqrt{q_n^2+k^2}\sqrt{q_n^2+\tilde{k}^2}-q_n(q_n^2+k^2+(q_n+ik)^2)} \tag{B.165}$$

$$= \frac{-2ik\tilde{k}(q_n+ik)}{2(q_n+ik)\sqrt{q_n^2+k^2}\sqrt{q_n^2+\tilde{k}^2}-2q_n^2(q_n+ik)} \tag{B.166}$$

$$= \frac{-ik\tilde{k}}{\sqrt{q_n^2+k^2}\sqrt{q_n^2+\tilde{k}^2}-q_n^2} \tag{B.167}$$

$$= \frac{\tilde{k}(\sqrt{q_n^2-(\frac{\epsilon-\mu_{barrier}}{\hbar v})^2})}{(\frac{\epsilon-\mu_{barrier}}{\hbar v})(\frac{\epsilon-\mu_{gate}}{\hbar v})-q_n^2}. \tag{B.168}$$

So the non-linear equation to be solved is

$$\tan(\tilde{k}L) = \frac{\tilde{k}(\sqrt{q_n^2-(\frac{\epsilon-\mu_{barrier}}{\hbar v})^2})}{(\frac{\epsilon-\mu_{barrier}}{\hbar v})(\frac{\epsilon-\mu_{gate}}{\hbar v})-q_n^2}. \tag{B.169}$$

For a fixed n, the momentum in the x-direction is fixed, but there can be more than one solution for the momentum $\tilde{k}$ in the y-direction.

References

[1] T. A. Fulton and G. J. Dolan, Phys. Rev. Lett. **59**, 109 (1987).

[2] L. L. Sohn, L. P. Kouwenhoven, *et al.*, *Mesoscopic Electron Transport: Proceedings of the NATO Advanced Study Institute, 25 June-5 July 1996, Curacao, Netherlands Antilles*, Vol. 345 (Springer Science & Business Media, 1997).

[3] W. G. van der Wiel, S. De Franceschi, J. M. Elzerman, T. Fujisawa, S. Tarucha, and L. P. Kouwenhoven, Rev. Mod. Phys. **75**, 1 (2002).

[4] R. Hanson, L. P. Kouwenhoven, J. R. Petta, S. Tarucha, and L. M. K. Vandersypen, Rev. Mod. Phys. **79**, 1217 (2007).

[5] S. Datta, *Electronic transport in mesoscopic systems* (Cambridge university press, 1997).

[6] M. Baldo, *Introduction to Nanoelectronics* (MIT OpenCourseWare, License, 2011).

[7] I. Žutić, J. Fabian, and S. Das Sarma, Rev. Mod. Phys. **76**, 323 (2004).

[8] T. C. Harman, P. J. Taylor, M. P. Walsh, and B. E. LaForge, Science **297**, 2229 (2002).

[9] B. Sothmann, R. Snchez, and A. N. Jordan, Nanotechnology **26**, 032001 (2015).

[10] F. A. Zwanenburg, A. S. Dzurak, A. Morello, M. Y. Simmons, L. C. L. Hollenberg, G. Klimeck, S. Rogge, S. N. Coppersmith, and M. A. Eriksson, Rev. Mod. Phys. **85**, 961 (2013).

[11] C.-C. Chen, Y.-c. Chang, and D. M. T. Kuo, Phys. Chem. Chem. Phys. **17**, 6606 (2015).

[12] C.-C. Chen, D. M. T. Kuo, and Y.-C. Chang, Phys. Chem. Chem. Phys. **17**, 19386 (2015).

[13] B. Trauzettel, D. V. Bulaev, D. Loss, and G. Burkard, Nature Physics **3**, 192 (2007).

[14] C.-C. Chen and Y.-C. Chang, Submitted to PRB .

[15] M. A. Reed, C. Zhou, C. J. Muller, T. P. Burgin, and J. M. Tour, Science **278**, 252 (1997).

[16] C. Joachim, J. Gimzewski, and A. Aviram, Nature **408**, 541 (2000).

[17] J. P. Bergfield and C. A. Stafford, Phys. Rev. B **79**, 245125 (2009).

[18] M. Busl, G. Granger, L. Gaudreau, R. Sánchez, A. Kam, M. Pioro-Ladrière, S. A. Studenikin, P. Zawadzki, Z. R. Wasilewski, A. S. Sachrajda, and G. Platero, Nature nanotechnology **8**, 261 (2013).

[19] F. R. Braakman, P. Barthelemy, C. Reichl, W. Wegscheider, and L. M. Vandersypen, Nature nanotechnology **8**, 432 (2013).

[20] S. Amaha, W. Izumida, T. Hatano, S. Teraoka, S. Tarucha, J. A. Gupta, and D. G. Austing, Phys. Rev. Lett. **110**, 016803 (2013).

[21] A. Nitzan and M. A. Ratner, Science **300**, 1384 (2003).

[22] C. A. Stafford, D. M. Cardamone, and S. Mazumdar, Nanotechnology **18**, 424014 (2007).

[23] C. Pöltl, C. Emary, and T. Brandes, Phys. Rev. B **87**, 045416 (2013).

[24] M. Seo, H. K. Choi, S.-Y. Lee, N. Kim, Y. Chung, H.-S. Sim, V. Umansky, and D. Mahalu, Phys. Rev. Lett. **110**, 046803 (2013).

[25] C. M. Guédon, H. Valkenier, T. Markussen, K. S. Thygesen, J. C. Hummelen, and S. J. van der Molen, Nature nanotechnology **7**, 304 (2012).

[26] M. Korkusinski, I. P. Gimenez, P. Hawrylak, L. Gaudreau, S. A. Studenikin, and A. S. Sachrajda, Phys. Rev. B **75**, 115301 (2007).

[27] C.-Y. Hsieh, Y.-P. Shim, and P. Hawrylak, Phys. Rev. B **85**, 085309 (2012).

[28] Y. Meir and N. S. Wingreen, Phys. Rev. Lett. **68**, 2512 (1992).

[29] D. M.-T. Kuo and Y.-C. Chang, Phys. Rev. Lett. **99**, 086803 (2007).

[30] B. R. Bułka and T. Kostyrko, Phys. Rev. B **70**, 205333 (2004).

[31] D. M.-T. Kuo, S.-Y. Shiau, and Y.-C. Chang, Phys. Rev. B **84**, 245303 (2011).

[32] D. Loss and D. P. DiVincenzo, Phys. Rev. A **57**, 120 (1998).

[33] I. Weymann, B. Bułka, and J. Barnaś, Phys. Rev. B **83**, 195302 (2011).

[34] D. Deutsch, Proceedings of the Royal Society of London A: Mathematical, Physical and Engineering Sciences **400**, 97 (1985).

[35] M. A. Nielsen and I. L. Chuang, *Quantum computation and quantum information* (Cambridge university press, 2010).

[36] P. Shor, SIAM Journal on Computing **26**, 1484 (1997).

[37] D. Loss and D. P. DiVincenzo, Phys. Rev. A **57**, 120 (1998).

[38] A. H. Castro Neto, F. Guinea, N. M. R. Peres, K. S. Novoselov, and A. K. Geim, Rev. Mod. Phys. **81**, 109 (2009).

[39] L. Brey and H. A. Fertig, Phys. Rev. B **73**, 235411 (2006).

[40] M. Y. Han, B. Özyilmaz, Y. Zhang, and P. Kim, Phys. Rev. Lett. **98**, 206805 (2007).

[41] X. Li, X. Wang, L. Zhang, S. Lee, and H. Dai, Science **319**, 1229 (2008).

[42] C. Stampfer, J. Güttinger, S. Hellmüller, F. Molitor, K. Ensslin, and T. Ihn, Phys. Rev. Lett. **102**, 056403 (2009).

[43] X. L. Liu, D. Hug, and L. M. K. Vandersypen, Nano Letters **10**, 1623 (2010).

[44] D. Wei, H.-O. Li, G. Cao, G. Luo, Z.-X. Zheng, T. Tu, M. Xiao, G.-C. Guo, H.-W. Jiang, and G.-P. Guo, Scientific reports **3** (2013).

[45] A. Fang, Y. C. Chang, and J. R. Tucker, Phys. Rev. B **66**, 155331 (2002).

[46] H. Haug and A.-P. Jauho, *Quantum kinetics in transport and optics of semiconductors* (Springer, 2008).

[47] P. W. Anderson, Phys. Rev. **124**, 41 (1961).

[48] K. G. Wilson, Rev. Mod. Phys. **47**, 773 (1975).

[49] A. C. Hewson, *The Kondo problem to heavy fermions*, Vol. 2 (Cambridge university press, 1997).

[50] R. M. Noack and S. R. Manmana, arXiv preprint cond-mat/0510321 (2005).

[51] R. Bulla, T. A. Costi, and T. Pruschke, Rev. Mod. Phys. **80**, 395 (2008).

[52] P. Pals and A. MacKinnon, Journal of Physics: Condensed Matter **8**, 5401 (1996).

[53] C. Lacroix, Journal of Physics F: Metal Physics **11**, 2389 (1981).

[54] Y. Meir, N. S. Wingreen, and P. A. Lee, Phys. Rev. Lett. **66**, 3048 (1991).

[55] Y. Meir, N. S. Wingreen, and P. A. Lee, Phys. Rev. Lett. **70**, 2601 (1993).

[56] V. Kashcheyevs, A. Aharony, and O. Entin-Wohlman, Phys. Rev. B **73**, 125338 (2006).

[57] S.-y. Shiau, S. Chutia, and R. Joynt, Phys. Rev. B **75**, 195345 (2007).

[58] T. J. Levy and E. Rabani, The Journal of Chemical Physics **138**, 164125 (2013).

[59] X. Xin and D. Zhou, Phys. Rev. B **91**, 165120 (2015).

[60] N. S. Wingreen and Y. Meir, Phys. Rev. B **49**, 11040 (1994).

[61] Y.-C. Chang and D. M.-T. Kuo, Phys. Rev. B **77**, 245412 (2008).

[62] D. N. Zubarev, Soviet Physics Uspekhi **3**, 320 (1960).

[63] A.-P. Jauho, N. S. Wingreen, and Y. Meir, Phys. Rev. B **50**, 5528 (1994).

[64] J. Maciejko, J. Wang, and H. Guo, Phys. Rev. B **74**, 085324 (2006).

[65] J. Maciejko, *An introduction to nonequilibrium many-body theory* (2007).

[66] C. Timm, Phys. Rev. B **77**, 195416 (2008).

[67] M. Nakahara, *Geometry, topology and physics* (CRC Press, 2003).

[68] M. Stone and P. Goldbart, *Mathematics for physics: a guided tour for graduate students* (Cambridge University Press, 2009).

[69] S. Weinberg, *The quantum theory of fields*, Vol. 1 (Cambridge university press, 2005).

[70] M. E. Peskin and D. V. Schroeder, *An introduction to quantum field theory* (Westview, 1995).

[71] "Pointer bounds remapping problem," `https://software.intel.com/en-us/forums/topic/271350` (2012).

[72] "Intel composer xe 2013 compilers fixes list," `https://software.intel.com/en-us/articles/intel-composer-xe-2013-compilers-fixes-list` (2012).

[73] D. Goldhaber-Gordon, H. Shtrikman, D. Mahalu, D. Abusch-Magder, U. Meirav, and M. A. Kastner, Nature **391**, 156 (1998).

[74] T. Numata, Y. Nisikawa, A. Oguri, and A. C. Hewson, Phys. Rev. B **80**, 155330 (2009).

[75] B. Michaelis, C. Emary, and C. Beenakker, EPL (Europhysics Letters) **73**, 677 (2006).

[76] C. Emary, Phys. Rev. B **76**, 245319 (2007).

[77] D. M. T. Kuo and Y.-C. Chang, Phys. Rev. B **89**, 115416 (2014).

[78] F. Bauer, J. Heyder, E. Schubert, D. Borowsky, D. Taubert, B. Bruognolo, D. Schuh, W. Wegscheider, J. von Delft, and S. Ludwig, Nature **501**, 73 (2013).

[79] S. Andergassen, Nature **495**, 321 (2013).

[80] C. Hwang, D. A. Siegel, S.-K. Mo, W. Regan, A. Ismach, Y. Zhang, A. Zettl, and A. Lanzara, Scientific Reports **2** (2012), 10.1038/srep00590.

[81] J. P. Reed, B. Uchoa, Y. I. Joe, Y. Gan, D. Casa, E. Fradkin, and P. Abbamonte, Science **330**, 805 (2010).

[82] V. N. Kotov, B. Uchoa, V. M. Pereira, F. Guinea, and A. H. Castro Neto, Rev. Mod. Phys. **84**, 1067 (2012).

[83] J. Liu, Q.-f. Sun, and X. C. Xie, Phys. Rev. B **81**, 245323 (2010).

[84] S. Rayne and K. Forest, Computational and Theoretical Chemistry **977**, 163 (2011).

[85] L. Allen and T. J. Bridges, Numerische Mathematik **92**, 197 (2002).

[86] O. Schenk and K. Grtner, Future Generation Computer Systems **20**, 475 (2004).

[87] H. Van der Vorst and J. B. M. Melissen, Magnetics, IEEE Transactions on **26**, 706 (1990).

[88] R. Barrett, M. Berry, T. F. Chan, J. Demmel, J. Donato, J. Dongarra, V. Eijkhout, R. Pozo, C. Romine, and H. V. der Vorst, *Templates for the Solution of Linear Systems: Building Blocks for Iterative Methods, 2nd Edition* (SIAM, Philadelphia, PA, 1994).

[89] Y. Saad, *Iterative methods for sparse linear systems* (Siam, 2003).

[90] B. Jegerlehner, arXiv preprint hep-lat/9612014 (1996).

[91] W. H. Schilders, H. A. Van der Vorst, and J. Rommes, *Model order reduction: theory, research aspects and applications*, Vol. 13 (Springer, 2008).

[92] A. Odabasioglu, M. Celik, and L. T. Pileggi, in *Proceedings of the 1997 IEEE/ACM international conference on Computer-aided design* (IEEE Computer Society, 1997) pp. 58–65.

[93] B. A. van de Rotten and S. V. Lunel, *A limited memory Broyden method to solve high-dimensional systems of nonlinear equations* (Thomas Stieltjes Institute for Mathematica, 2003).

[94] W. H. Press, S. A. Teukolsky, W. T. Vetterling, and B. P. Flannery, *Numerical recipes in FORTRAN (Cambridge* (Cambridge Univ. Press, 1992).

[95] "Condensed matter physics ii," `http://eduardo.physics.illinois.edu/phys561/physics561.html` (2015).

[96] G. W. Semenoff, Phys. Rev. Lett. **53**, 2449 (1984).

[97] D. P. DiVincenzo and E. J. Mele, Phys. Rev. B **29**, 1685 (1984).

[98] P. Recher and B. Trauzettel, Nanotechnology **21**, 302001 (2010).

[99] A. Szabo and N. S. Ostlund, *Modern quantum chemistry: introduction to advanced electronic structure theory* (Dover Publications, 1996).